

MAR 10 1981

AFWAL-TR-80-3062

SEP 28 1990

CA

HYPERSONIC BOUNDARY LAYER TRANSITION EXPERIMENTS

Kenneth F. Stetson
High Speed Aero Performance Branch
Aeromechanics Division

October 1980

TECHNICAL REPORT AFWAL-TR-80-3062

Final Report for the Period September 1976 through September 1979

Approved for public release; distribution unlimited.

TECHNICAL REPORTS
FILE COPY

FLIGHT DYNAMICS LABORATORY
~~AIR FORCE WRIGHT AERONAUTICAL LABORATORIES~~
AIR FORCE SYSTEMS COMMAND
WRIGHT-PATTERSON AIR FORCE BASE, OHIO 45433

PROPERTY OF U.S. AIR FORCE
AEDC TECHNICAL LIBRARY
PROPERTY OF U.S. AIR FORCE
AEDC TECHNICAL LIBRARY
ARNOLD AFB, TN 37389

REPORT DOCUMENTATION PAGE		READ INSTRUCTIONS BEFORE COMPLETING FORM												
1. REPORT NUMBER AFWAL-TR-80-3062	2. GOVT ACCESSION NO.	3. RECIPIENT'S CATALOG NUMBER												
4. TITLE (and Subtitle) HYPERSONIC BOUNDARY LAYER TRANSITION EXPERIMENTS		5. TYPE OF REPORT & PERIOD COVERED Final Report Sept 1976 - Sept 1979												
		6. PERFORMING ORG. REPORT NUMBER												
7. AUTHOR(s) Kenneth F. Stetson		8. CONTRACT OR GRANT NUMBER(s)												
9. PERFORMING ORGANIZATION NAME AND ADDRESS Flight Dynamics Laboratory AF Wright Aeronautical Laboratories, AFSC Wright-Patterson Air Force Base, Ohio 45433		10. PROGRAM ELEMENT, PROJECT, TASK AREA & WORK UNIT NUMBERS Project 2307 Task 2307N4 Work Unit 2307N423												
11. CONTROLLING OFFICE NAME AND ADDRESS Flight Dynamics Laboratory Air Force Wright Aeronautical Laboratories Wright-Patterson Air Force Base, Ohio 45433		12. REPORT DATE October 1980												
		13. NUMBER OF PAGES 85												
14. MONITORING AGENCY NAME & ADDRESS (if different from Controlling Office)		15. SECURITY CLASS. (of this report) UNCLASSIFIED												
		15a. DECLASSIFICATION/DOWNGRADING SCHEDULE												
16. DISTRIBUTION STATEMENT (of this Report) Approved for public release; distribution unlimited.														
17. DISTRIBUTION STATEMENT (of the abstract entered in Block 20, if different from Report)														
18. SUPPLEMENTARY NOTES														
19. KEY WORDS (Continue on reverse side if necessary and identify by block number)														
<table border="0"> <tr> <td>boundary layer</td> <td>angle of attack</td> <td>camphor ablation</td> </tr> <tr> <td>boundary layer transition</td> <td>cone</td> <td></td> </tr> <tr> <td>hypersonic flow</td> <td>biconic configuration</td> <td></td> </tr> <tr> <td>bluntness</td> <td>flared nozzle</td> <td></td> </tr> </table>			boundary layer	angle of attack	camphor ablation	boundary layer transition	cone		hypersonic flow	biconic configuration		bluntness	flared nozzle	
boundary layer	angle of attack	camphor ablation												
boundary layer transition	cone													
hypersonic flow	biconic configuration													
bluntness	flared nozzle													
20. ABSTRACT (Continue on reverse side if necessary and identify by block number)														
<p>New hypersonic wind tunnel data have been obtained to investigate boundary layer transition, with primary emphasis given to tip bluntness and angle of attack effects. The rearward displacement of transition on the cone frustum due to tip bluntness was found to be quite sensitive to free stream Mach number as well as the entropy layer swallowing by the boundary layer. At the highest Mach number obtained in these experiments ($M_{\infty}=9.3$), the length of laminar flow could be extended to about nine times the length of laminar flow of a sharp cone at identical conditions. The sensitivity of the maximum rearward</p>														

FHRIV

displacement of transition with free stream Mach number appeared to be primarily related to local Reynolds number reduction because of pressure losses across the bow shock. Low transition Reynolds numbers, typically found on nosetips, extended onto the front portion of the cone frustum. It appears that the still unexplained low transition Reynolds numbers associated with blunt bodies in hypersonic flow (the so-called blunt body paradox or a transition by-pass referred to by Morkovin) includes not only the nosetip region, but the forward portion of the cone frustum.

Transition location was found to be sensitive to small changes in angle of attack, and both the sharp and blunt tips produced a rearward movement of transition on the windward ray at small angles of attack.

Exploratory transition tests were made on a biconic configuration with a 14-degree half angle fore cone and an 8-degree half angle aft cone, with both a sharp and blunt tip configuration. The answer to the question of whether or not boundary layer transition was delayed on the biconic configuration depends upon the manner in which the data are interpreted. In terms of local Reynolds number, there was no significant delay since the local transition Reynolds numbers found on the biconic configuration were essentially the same as found previously on the 8-degree cone. However, when considering the location of transition and the length of laminar run before transition, transition moved rearward on the biconic configuration (the transition location on the sharp 8-degree cone was approximately 5.4 inches back from the tip and the transition location for the sharp biconic configuration was approximately 6.6 inches back from the tip; when both configurations were tested at $M_\infty=5.9$ and $Re_\infty/ft=9.7 \times 10^6$).

A low supersonic flared nozzle closely duplicated the hypersonic pressure and heat transfer distributions over the nose region of a blunt body. Sphere-cone camphor models were tested in a Mach 6 parallel flow field and in a Mach 1.8 flared nozzle flow field. For identical model stagnation conditions which produced transition on the nosetip, a general similarity of ablated shapes was observed for both nozzle flows.

FOREWORD

This document presents the results of an experimental investigation on boundary layer transition. The study was conducted by the High Speed Aero Performance Branch (AFWAL/FIMG), Aeromechanics Division, Flight Dynamics Laboratory, Air Force Wright Aeronautical Laboratories, Wright-Patterson Air Force Base, Ohio. This report is the final report for Work Unit 2307N423 "Boundary Layer Transition on Strategic Missiles", and was performed under Task 2307N4 "Aeromechanics Basic Research".

TABLE OF CONTENTS

SECTION		PAGE
I	INTRODUCTION	1
II	EXPERIMENTAL APPARATUS AND PROCEDURES	3
	1. Checks on Generality of Transition Data	4
III	BOUNDARY LAYER TRANSITION EXPERIMENTS OFF TUNNEL CENTERLINE	11
	1. Results	12
	2. Conclusions	14
IV	BLUNTNESS EFFECTS ($\alpha = 0^\circ$)	21
	1. Results	23
	2. Conclusions	29
V	ANGLE OF ATTACK EFFECTS	38
	1. Results	38
	2. Conclusions	41
VI	TRANSITION ON A BICONIC CONFIGURATION	51
	1. Results	51
	2. Conclusions	52
VII	EXPERIMENTAL STUDIES OF THE FDL FLARED-NOZZLE ABLATION SIMULATION TECHNIQUE	58
	1. Experimental Apparatus	58
	2. Results	60
	3. Conclusions	62
	REFERENCES	73

LIST OF ILLUSTRATIONS

FIGURE		PAGE
1	M=6 Wind Tunnel Nozzle, Jet and Collector Configuration	7
2	Effect of Mach Number and Unit Reynolds Number on Sharp Cone Transition for Small Size Wind Tunnels (Re_x is the End of Transition)	8
3	A Comparison of Bluntness Effects in Three Facilities	9
4	A Comparison of the Movement of Transition on the Windward Ray of a Sharp Cone	10
5	Lateral Mach Number Distribution at $X = 2.5$ Inches	15
6	Sharp Cone Positions for $\alpha = 0^\circ$ and $\alpha = 4^\circ$	16
7	Transition Location for Different Model Positions, Sharp Tip, $\alpha = 0^\circ$ (Recovery Factor of One)	17
8	Transition Location for Different Model Positions, Sharp Tip, $\alpha = 4^\circ$ (Recovery Factor of One)	18
9	Transition Location for Different Model Positions, 10% Bluntness, $\alpha = 4^\circ$ (Recovery Factor of One)	19
10	Surface Temperature History for the Sharp Cone At $\alpha = 0^\circ$	20
11	A Schematic Illustration of Flow Over a Slender, Blunt Cone	30
12	Entropy Layer Swallowing Distance Parameter	31
13	Calculations of Local Flow Properties on an 8-Degree Half Angle Cone with 2% Bluntness at $M_\infty = 5.9$	32
14	Effect of Nose Bluntness on Transition Location	33
15	Transition Movement from Cone Frustum to Nostip on a 7-Degree Half Angle Cone at $M_\infty \approx 9.1$	34
16	Transition Location and Local Mach Number and Reynolds Number on an 8-Degree Half Angle Cone with a 0.60 Inch Nose Radius at $M_\infty = 5.9$ and 9.2 ; $Re_\infty/Ft = 18.5 \times 10^6$ in Both Cases	35
17	Transition Displacement Trend with Mach Number (Data Points from Figure 14)	36
18	Local Transition Reynolds Number Calculations	37
19	Local Reynolds Number Calculations for a Sharp Cone at Angle of Attack	42
20	Transition Movement with Angle of Attack for an 8-Degree Half Angle Cone At $M_\infty = 5.9$	43
21	Transition Movement with Angle of Attack for an 8-Degree Half Angle Cone with 30% Bluntness at $M_\infty = 5.9$	44
22	Transition Pattern At $\alpha = 2^\circ$, Sharp Tip	45

LIST OF ILLUSTRATIONS (CONCLUDED)

FIGURE	PAGE
23 Transition Pattern At $\alpha = 2^\circ$, 5% Bluntness	46
24 Transition Pattern At $\alpha = 2^\circ$, 10% Bluntness	47
25 Transition Pattern VS Angle of Attack, 10% Bluntness	48
26 Transition Pattern for Different Nosetips, $\alpha = 2^\circ$	49
27 Transition Asymmetry Due to Angle of Attack	50
28 Heat Transfer Coefficient Distribution (Recovery Factor of One) and Local Flow Calculations on a Biconic Configuration with a Sharp Tip At $M_\infty = 5.9$	53
29 Heat Transfer Coefficient Distribution (Recovery Factor of One) and Local Flow Calculations on a Biconic Configuration with a Blunt Tip At $M_\infty = 5.9$	54
30 Transition Movement with Angle of Attack for the Biconic Configuration At $M_\infty = 5.9$	55
31 Interferogram of the Sharp Biconic Configuration At $M_\infty = 5.9$	56
32 Interferogram of the Blunt Biconic Configuration At $M_\infty = 5.9$	57
33 Mach 1.8 Flared Nozzle Geometry	63
34 20-Inch Hypersonic Wind Tunnel with Mach 1.8 Flared Nozzle Installed	64
35 Pitot Pressure Distribution of Flared Nozzle	65
36 Axial Distribution of Pitot Pressure and Mach Number of Flared Nozzle	66
37 Model Geometry	67
38 Pressure Distribution, $P_{T_2} = 22$ psia, $T_0 = 1100^\circ\text{R}$	68
39a Heat Transfer Coefficient Distribution, $P_{T_2} = 22$ psia, $T_0 = 1100^\circ\text{R}$	69
39b Heat Transfer Coefficient Distribution, $P_{T_2} = 50$ psia, $T_0 = 1100^\circ\text{R}$	70
40 Side Profile Views of Ablated Camphor Models	71
41 Photographs of Camphor Ablation	72

NOMENCLATURE

ζ	Centerline of tunnel
d	Distance the model sting is off the tunnel centerline (in.)
D^*	Nozzle throat diameter (in.)
h, H	Local heat transfer coefficient (Btu/ft ² - sec°R)
L	Leeward side
M	Mach number
p	Surface pressure (used in nondimensional ratio, p/p_{st}) (or psia)
P_{T_2}	Pitot pressure (psia)
P_{0N}	Pressure upstream of flared nozzle (psia)
\dot{q}	Heat transfer rate (used in nondimensional ratio, \dot{q}/\dot{q}_{st})
R	Model nose or base radius (in.)
Re	Reynolds number
Re_{θ}	Reynolds number based upon conditions at the edge of the boundary layer and momentum thickness
Re_{x_T}	Transition Reynolds number based upon conditions at the edge of the boundary layer and surface distance from the sharp tip or stagnation point to the location of transition
t	Time (sec)
T	Temperature (°R)
T_{0N}	Total temperature in flared nozzle (°R)
W	Windward
X or S	Surface distance, distance downstream of nozzle exit (in.)
X_{sw}	Entropy layer swallowing distance (see Figure 8) (in.)
X_T	Distance from the sharp tip or stagnation point to the onset of transition (in.)
X_{TB} or $(X_T)_B$	Distance to onset of transition on blunt configurations (in.)
X_{TS} or $(X_t)_S$	Distance to onset of transition on sharp configurations (in.)

NOMENCLATURE (Concluded)

Y	Horizontal distance from tunnel centerline (in.)
Z	Vertical distance from tunnel centerline (in.)
α	Angle of attack (deg.)
θ_c	Cone half angle (deg.)
ϕ	Cone circumferential angle (deg.)
ψ	Angle of yaw (deg.)

SUBSCRIPTS

B	Base or blunt
N	Nose
O	Reservoir
S	Sharp
ST	Model Stagnation Point °
∞	Free stream

SECTION I
INTRODUCTION

Boundary layer transition is a problem that has plagued several generations of aerodynamicists. Although significant advances in stability theory and turbulence modeling have been made in recent years (Reference 1, 2), the technology in this area has lagged far behind most other aerodynamic areas. The development of the theory has been slow because of the extreme complexity of the problem and understanding through experimentation has been hampered by the difficulty of conducting a good experiment. The wind tunnel, which has been the major source of experimental aerodynamic data, has provided a vast amount of transition data; yet the majority of these data have produced empirical correlations without adding a great deal to the general understanding of transition phenomena. In recent years, it has been generally accepted that disturbances generated by the turbulent boundary layer on the nozzle wall of a supersonic or hypersonic wind tunnel can dominate wind tunnel transition results (Reference 3); hence, transition Reynolds numbers obtained in these wind tunnels cannot be related directly to flight. In spite of this short-coming of wind tunnel transition testing, valid transition trends can be obtained from "noisy" wind tunnel experiments. Also, a very important potential of transition experiments in wind tunnels and other ground test facilities is the ability to identify what Morkovin refers to as a transition bypass (Reference 4). A bypass is an occurrence of transition at a low Reynolds number which cannot be identified with concepts from linear stability theory; that is, transition occurring at very low Reynolds numbers in a region where linear stability theory would not predict Tollmien-Schlichting waves to be amplified. The now well known blunt body bypass found on highly cooled surfaces was identified in the laboratory in 1957⁽¹⁾ ($Re_{OT} \approx 250$) at a time when most boundary layer stability people were predicting the early copper heat sink Inter Continental Ballistic Missiles (ICBM's) would maintain a laminar boundary

(1) These results appeared in the unclassified literature in 1959 (Reference 5).

layer throughout reentry. The present wind tunnel experiments have shown that the nosetip bypass extends well beyond the nosetip and includes the forward portion of the cone frustum (reported also in Reference 6).

This transition investigation consisted of several phases. Initially, checks were made on the generality of the transition data obtained in the FDL Mach 6 wind tunnel to provide confidence that the transition trends obtained were not uniquely related to that facility. This involved a comparison of the new data with data obtained in other facilities. Transition data were obtained off the tunnel centerline to check the sensitivity of transition location to model position in the test rhombus.

The primary objective of this program was to investigate the effects of tip bluntness and angle of attack on boundary layer transition. The bluntness experiments extended previous work of Stetson and Rushton (Reference 7) on entropy layer swallowing effects and provided new, higher Mach number data to demonstrate the effects of free stream Mach number on transition of slender, blunted cones. Angle of attack effects were investigated in detail to explore transition location sensitivity to small angles of attack and the resulting asymmetric transition patterns obtained.

Exploratory experiments were conducted with a biconic configuration to investigate if a biconic configuration produced a delay in the onset of transition, when compared with a pure cone configuration.

An additional investigation, unrelated to the main program objectives, was conducted to assist in the study of hypersonic nosetip ablation; specifically the simulation capability of a low Mach number flared nozzle. The objective was to compare data obtained in a Mach 1.8 flared nozzle flow field with data obtained in a Mach 6 parallel flow field. Of particular interest was the ablation configurations obtained under conditions which produced boundary layer transition on the tip.

SECTION II

EXPERIMENTAL APPARATUS AND PROCEDURES

The experiments were conducted in the FDL Mach 6 and 20-inch wind tunnels and the Arnold Engineering Development Center (AEDC) Tunnel F. The location of boundary layer transition was obtained from heat transfer measurements.

The Mach 6 tunnel is a blow-down facility operating at a reservoir temperature of 1100°R and a reservoir pressure range of 700 to 2100 psia, corresponding to a Reynolds number per foot range of 9.7×10^6 to 30.3×10^6 . The test core of approximately 10 inches is produced by a contoured axisymmetric nozzle with a physical exit diameter of 12.3 inches. A sketch of the nozzle and diffuser collector is shown in Figure 1. Additional details of the tunnel can be found in Reference 8. The test model for the Mach 6 tunnel was a thin-skin (nominally 0.025 inches), 8-degree half angle cone containing two rays of thermocouples, located 180 degrees apart in the pitching plane. The base diameter of the model was 4 inches and the model had nosetips with the following bluntness ratios; $R_N/R_B = 0, 0.02, 0.05, 0.10, 0.15,$ and 0.30 . Nominal model surface finish was 15 microinches and the blunt nose tips were polished before each run. The model was cooled between runs so that the model surface temperature would always be the same at the start of each run (approximately 540°R). Heat transfer rates were calculated from the increase in the surface temperature of the model, during a time interval of one-half second, after the model arrived at the tunnel centerline. T_W/T_0 was generally in the range of 0.52 to 0.58.

The 20-inch wind tunnel was not utilized in its normal mode as a hypersonic wind tunnel but was modified to incorporate a supersonic flared nozzle. Details of the modification are given in Section VII.

The AEDC Tunnel F is an arc-driven wind tunnel of the hotshot type and capable of providing Mach numbers from about 7 to 13 over a Reynolds number per foot range from 0.2×10^6 to 50×10^6 . The test gas is nitrogen. This test was conducted with the 40-inch exit diameter contoured nozzle at a nominal free stream Mach number of 9. Because of the relatively short test times, the model wall temperature remained essentially invariant from the initial value of approximately 540°R , thus $T_w/T_o \approx 0.20$ to 0.38 . Since the tunnel operates with a constant volume reservoir, the reservoir conditions decay with time. Timewise variations in Reynolds number permit acquisition of data at different Reynolds numbers for the same run. The test model for Tunnel F was a 48-inch, 7-degree half angle cone with eight nose bluntness ratios, $R_N/R_B = 0, 0.01, 0.03, 0.05, 0.07, 0.10, 0.15,$ and 0.37 . The model contained 75 coaxial surface thermocouples and 10 surface pressure gages. Nominal model surface finish was 30 micro-inches and the blunt nosetips were polished before each run. Additional details of Tunnel F and the model instrumentation can be found in Reference 9.

1. CHECKS ON GENERALITY OF TRANSITION DATA

In order to utilize boundary layer transition trends obtained in a wind tunnel, one has to assume these trends are not uniquely related to the facility being used. The FDL Mach 6 wind tunnel had not previously been used for transition investigations and tunnel free stream disturbance measurements had not been made for this tunnel; therefore, the basic question of nonuniqueness of transition data had to be explored. Based upon the results of previous investigators (Reference 3), it was expected that aerodynamic noise, radiating from the turbulent boundary layers on the nozzle wall, would be the major tunnel factor influencing transition. That is, disturbances in the freestream of a wind tunnel have been identified as having three possible sources: (a) vorticity fluctuations (velocity fluctuations) (b) entropy fluctuations (temperature fluctuations) and (c) sound waves (pressure fluctuations). The vorticity and entropy fluctuations are essentially convected along streamlines and are traceable to conditions in the stilling chamber. Sound disturbances can travel across streamlines and can originate in the stilling chamber and from

the wall of the nozzle. For Mach numbers greater than 2.5 to 3, velocity and entropy fluctuations have been found to have a negligible effect on wind tunnel transition data. However, radiated sound generated by the turbulent boundary layer on the wall of the nozzle was found to be a major factor affecting transition in supersonic and hypersonic wind tunnels. Reference 3 contains an excellent review of these developments.

To compare the influence of aerodynamic noise on transition in the Mach 6 tunnel with other wind tunnels, sharp cone transition data were compared with the correlations of Pate (Reference 3). Pate made an extensive study of the relationship between wind tunnel freestream disturbances and boundary layer transition and developed a method to predict boundary layer transition in wind tunnels with Mach number, unit Reynolds number, and tunnel size as parameters. Figure 2 indicates Pate's predictions for the end of boundary layer transition on sharp cones in small size wind tunnels. The excellent agreement of these present transition data with the results of Pate indicated that boundary layer transition in the FDL tunnel is influenced by aerodynamic noise in a predictable manner, similar to the 17 wind tunnels considered by Pate. Furthermore, since the occurrence of transition on a wind tunnel model is the result of the combined effect of all disturbance parameters, such as tunnel free stream disturbances, model surface roughness, model vibration, flow angularity, etc.; the fact that transition Reynolds numbers were found to be the same in several wind tunnels would infer a similarity in the influence of the combined effect of disturbance parameters on boundary layer transition. Although the disturbance parameters have not been investigated in detail in the Mach 6 wind tunnel, the similarity of transition results with other wind tunnels was believed to be an indication that the reported transition trends were not unique to the FDL Mach 6 facility (the possibility still exists that all wind tunnels have some general uniqueness of transition data).

The AEDC Tunnel F was one of the tunnels considered in Pate's study and therefore has demonstrated a similarity with other tunnels.

A comparison of data from two other facilities provided a check on the trends of bluntness effects on transition. These results are shown in Figure 3. In addition to these present data, wind tunnel results of Muir and Trujillo (Reference 10) and shock tunnel results of Stetson and Rushton (Reference 7) are included. The data presented in this manner illustrate the rearward displacement of transition in terms of the entropy layer swallowing. Additional discussions of this manner of presenting blunting data and related blunting characteristics will be included later. The central message to be obtained from this figure is the good agreement of data obtained from different facilities. All three facilities produced the same blunting features and trends, indicating the results were not unique to the facility being used.

Figure 4 compares transition location on the windward ray of a sharp cone with data from a shock tunnel (Reference 7), a Ludwig tube (Reference 11), and another wind tunnel (Reference 12). Both theory (Reference 13) and experiment (References 7, 11, 12) consistently indicated a rearward movement of transition location on the windward ray with angle of attack. The expected magnitude of this rearward displacement is uncertain. All of the facilities shown in Figure 4 indicate a trend of rearward displacement with angle of attack, with variations in magnitude. These variations in magnitude do not necessarily indicate trends which are facility-peculiar. Angle of attack data from a single facility are often presented in this nondimensionalized format with the implication that they represent a universal curve; however, it is believed that this point requires further substantiation before being accepted. That is, the influence of parameters such as Mach number, cone angle, surface roughness, and wall temperature cannot be identified; and these effects may account for some of the observed variations.

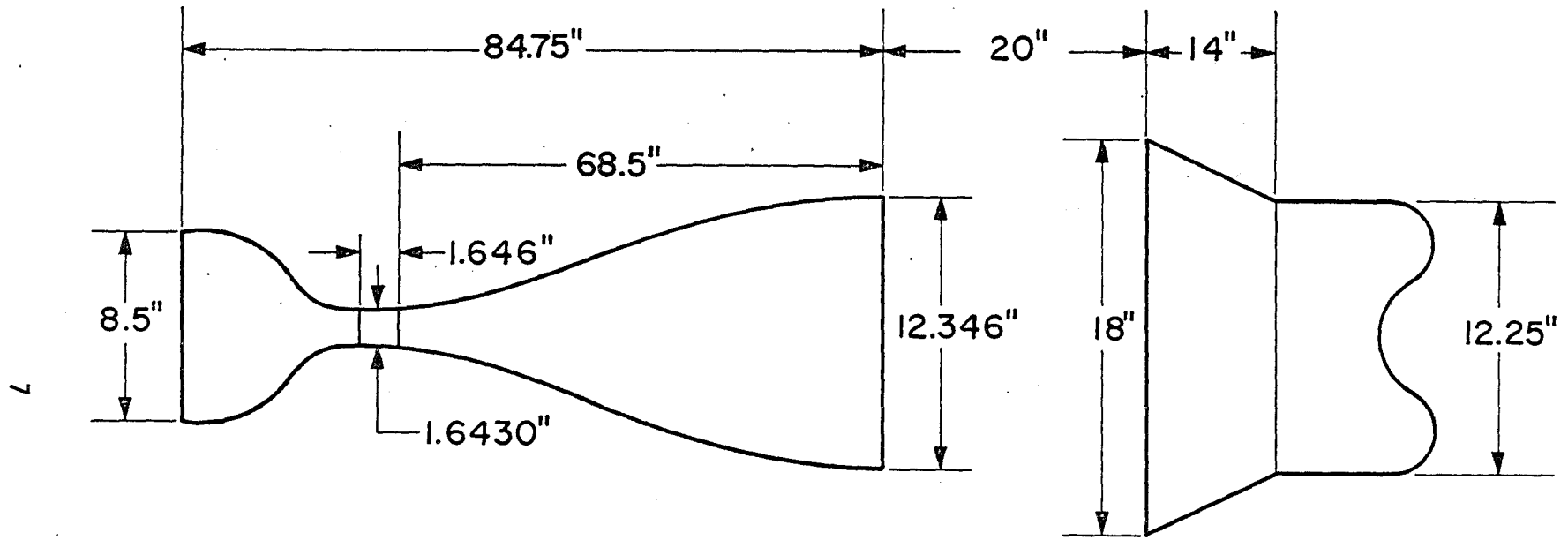


Figure 1. M=6 Wind Tunnel Nozzle, Jet and Collector Configuration

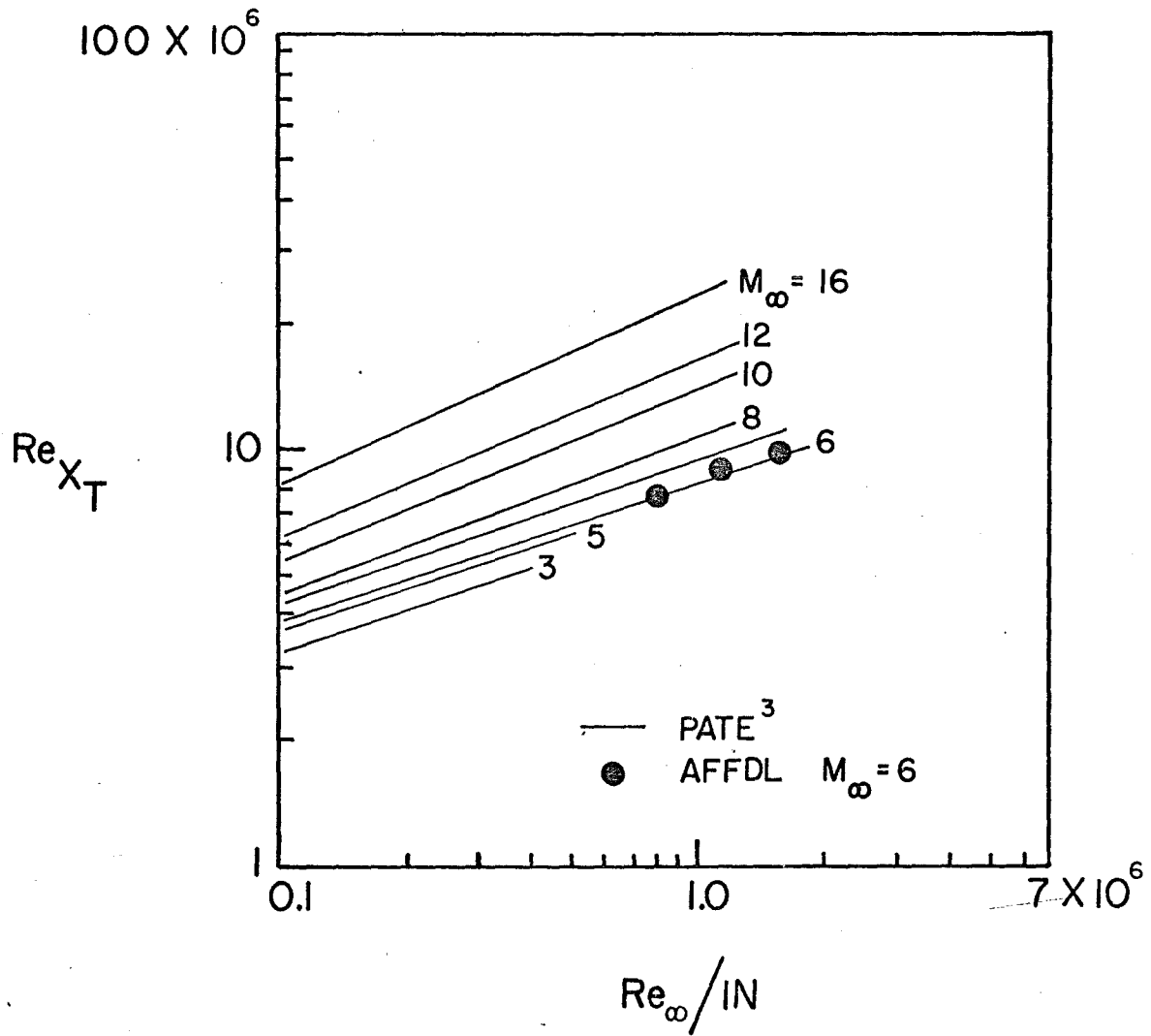


Figure 2. Effect of Mach Number and Unit Reynolds Number on Sharp Cone Transition for Small Size Wind Tunnels (Re_x is the End of Transition)

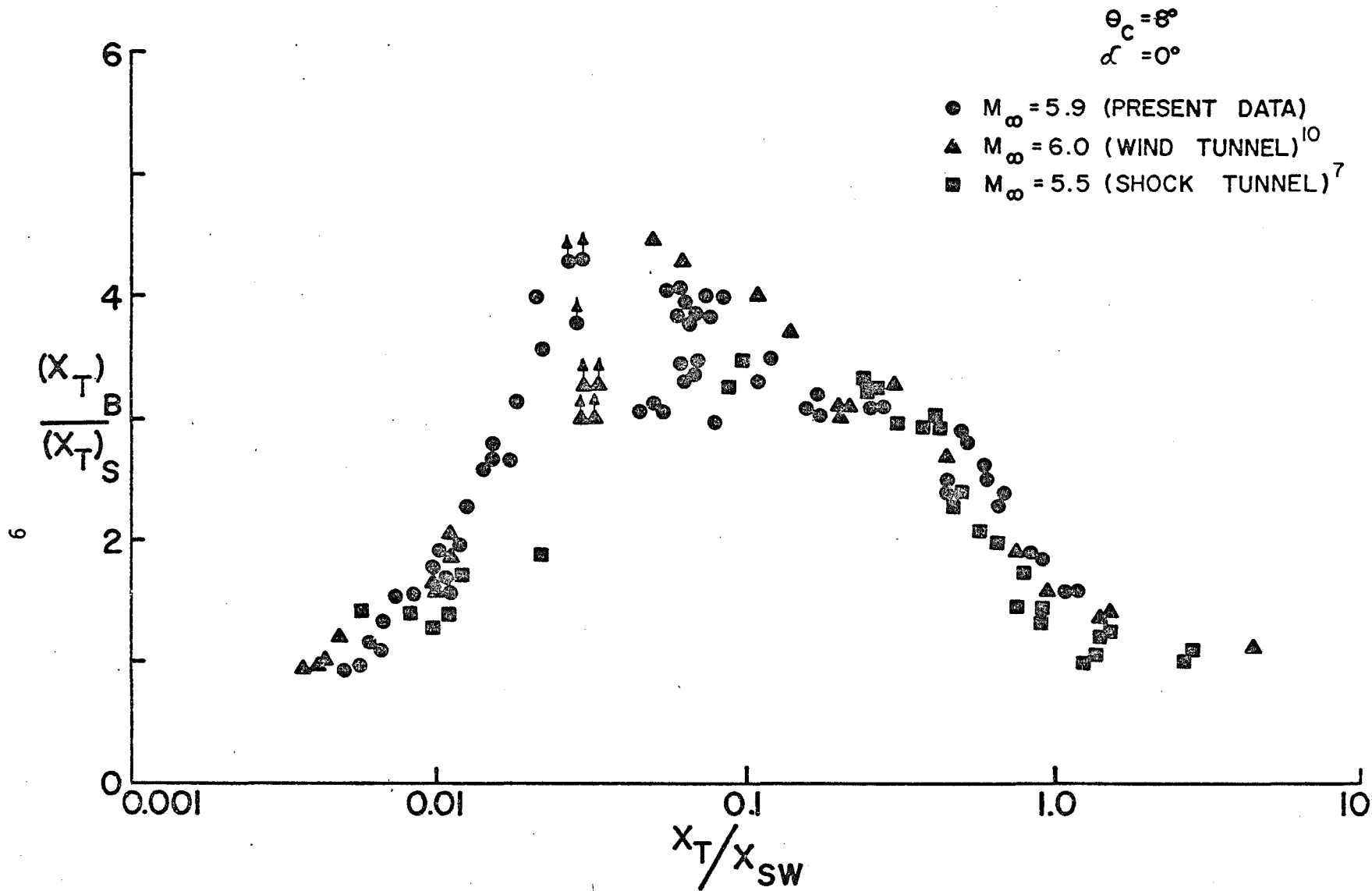


Figure 3. A Comparison of Bluntness Effects in Three Facilities

10

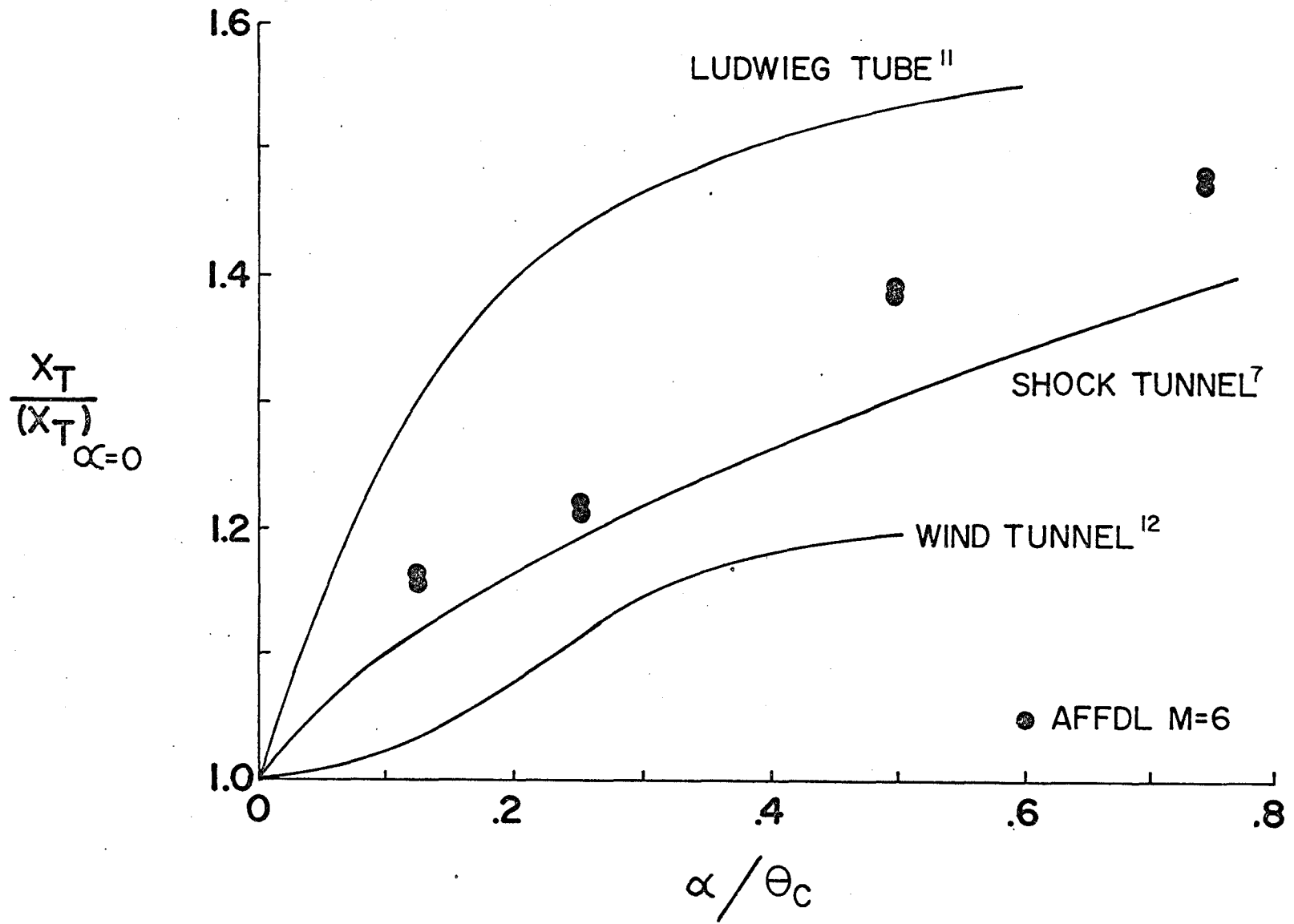


Figure 4. A Comparison of the Movement of Transition on the Windward Ray of a Sharp Cone

SECTION III

BOUNDARY LAYER TRANSITION EXPERIMENTS OFF TUNNEL CENTERLINE

In regard to the study of transition trends in wind tunnels, this author believes that angle of attack transition results may not have received enough scrutiny. Experimenters usually overlook or neglect the possibility that the results may be influenced by variations of parameters across the test section. When a model is pitched to angle of attack, the nosetip is displaced from the tunnel centerline and may be located in a different environment than zero angle of attack. Several effects may influence the location of transition. For axisymmetric nozzles (particularly in small wind tunnels where nozzle coordinate tolerances may be significant compared to the boundary layer thickness (Reference 14), there may be some focusing of aerodynamic noise at the tunnel centerline, with some variations radially away from the centerline. Also, variations in pressure and flow angularity away from the centerline may influence the location of transition. Flow angularity was checked at several locations within the test rhombus of Mach 6 wind tunnel and the maximum angularity found was ± 0.05 degrees (Reference 8). Some variations in flow properties across the test section are typical in open-jet axisymmetric nozzles and Mach 6 tunnel calibrations found Mach number variations up to about 1.5% within the test rhombus. Figure 5 is a sample of the Mach number distribution obtained for the Mach 6 tunnel at a station 2.5 inches from the nozzle exit. Variations in aerodynamic noise within the test rhombus of the Mach 6 wind tunnel have not been determined. It was not possible to assess the individual contributions of the above parameters regarding transition movement. However, the accumulative effect of all variations is the information needed to evaluate angle of attack transition trends obtained in this tunnel, and these details could be obtained by conducting boundary layer transition experiments off the tunnel centerline. A brief series of experiments were performed to assess this problem.

Data were obtained at two off-centerline stations; at 0.7 and 1.83 inches below the tunnel centerline. This was accomplished by inserting a collar on the injection strut to limit the travel of the model support system. The model could not be pitched in the off-centerline position. Data were obtained at $\alpha = 4^\circ$ by utilizing a bent sting configuration.

Figure 6 shows the location of the model in the centerline and off-centerline positions. The tip of the sharp cone was one inch downstream of the nozzle exit.

1. RESULTS

Figure 7 shows the heat transfer coefficient plotted versus the surface distance along the model from the tip for the sharp cone at $\alpha = 0^\circ$ for the two positions off the tunnel centerline. Transition on the tunnel centerline is shown for comparison as a solid curve. Transition occurred earlier on the bottom ray for both positions. For the top ray, transition occurred at different locations for each position. At 1.83 inches from the centerline, transition was at essentially the same location as found on the centerline, whereas at 0.7 inches transition was delayed.

The off-centerline results obtained with the sharp cone pitched to $\alpha = 4^\circ$ are shown in Figure 8. The trend of early transition on the bottom ray (windward) persisted at $\alpha = 4^\circ$. Unfortunately, details of transition on the leeward side are not clear because of its forward location. However, the end of transition appeared to be unchanged at all three locations. Note from Figure 6 that when the model was in the 0.7 inch off-centerline location, the model tip was nearly on the centerline.

When the sharp tip was replaced with a spherically blunt tip whose radius was 10% of the base radius, different transition trends were observed. These results are shown in Figure 9 with the model at $\alpha = 4^\circ$. The onset of transition for both positions off the centerline, although delayed slightly, were not significantly different from the centerline locations. These data suggest that not only is the location of the model relative to the tunnel centerline and model attitude important, but also the model bluntness. Repeat runs were made for all of the data and the excellent repeatability demonstrated that the trends shown existed consistently.

Information regarding the changes in transition off the tunnel centerline could be obtained by observing the trends in the temperature versus time plots of the thermocouples while the model was being injected. Since the heat transfer rate is proportional to the slope of the T vs t curve, a change in slope (in addition to the normal change resulting from increase in the surface temperature of the model) relates to a change in the heat transfer coefficient. Figure 10 illustrates this point for the sharp cone at $\alpha = 0^\circ$. The model enters the region of uniform flow at approximately two seconds and reaches the tunnel centerline at 3.45 seconds. Zero time relates to the start of the data acquisition system and not the start of model injection. The time of arrival at the tunnel centerline is recorded information. The thermocouples at $S = 4.0$ and 4.5 inches (Figure 10a) indicated a constant heat transfer coefficient throughout the injection phase and equal to that obtained at the tunnel centerline. Reference to Figure 7 confirms that at these stations the heat transfer coefficients did not vary with model position and were at a laminar level. The temperature history at 5.5 and 6.0 inches illustrates the case of a changing heat transfer coefficient. The slopes become smaller as the centerline is approached, with an increase in slope at the centerline. By looking at Figure 7 (for the top ray) it can be seen that the heat transfer coefficients at these model locations decreased at the position nearest the centerline and then increased at the centerline. This sequence of events indicated for this region on the model the onset of transition when the model was well away from the centerline, a change to a laminar boundary layer as the model approached the centerline, and transition again when the model was on the tunnel centerline.

Figure 10b illustrates the case of a reduction in the heat transfer coefficient when the model reached the tunnel centerline. Again these results may be correlated with the data of Figure 7.

2. CONCLUSIONS

This brief investigation of boundary layer transition with the model off the tunnel centerline has demonstrated that transition location on a wind tunnel model can be influenced by its location within the test rhombus. Transition locations were found to vary approximately 10% for the sharp cone configurations. These variations were the accumulative effect of all nonuniform distributions present. The movement of transition location appeared to be dependent upon model position relative to the tunnel centerline, model attitude, and nosetip bluntness. These effects, although significant, are not believed to be a dominant influence in regard to the angle of attack conclusions derived from this investigation.

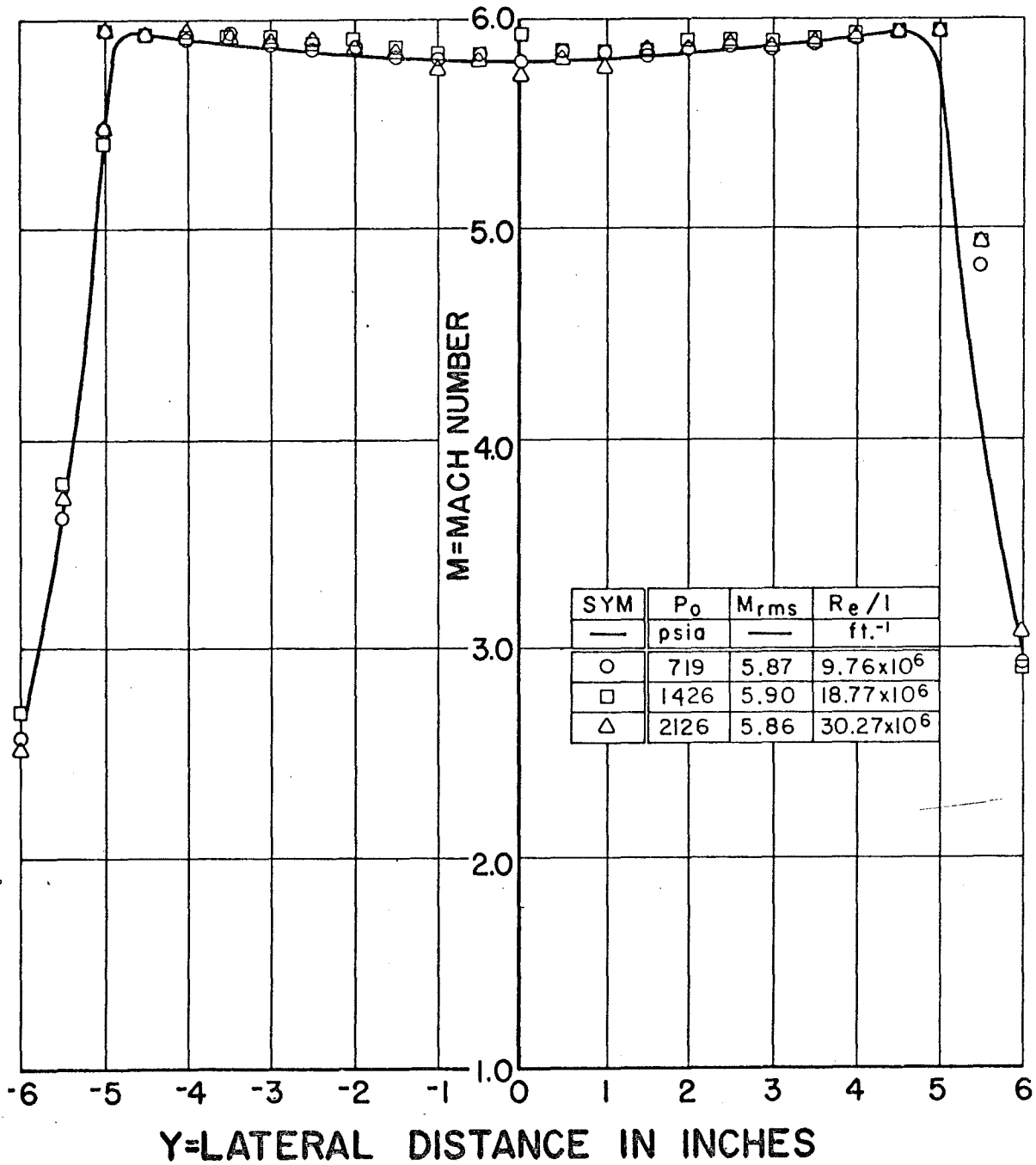


Figure 5. Lateral Mach Number Distribution at X = 2.5 Inches

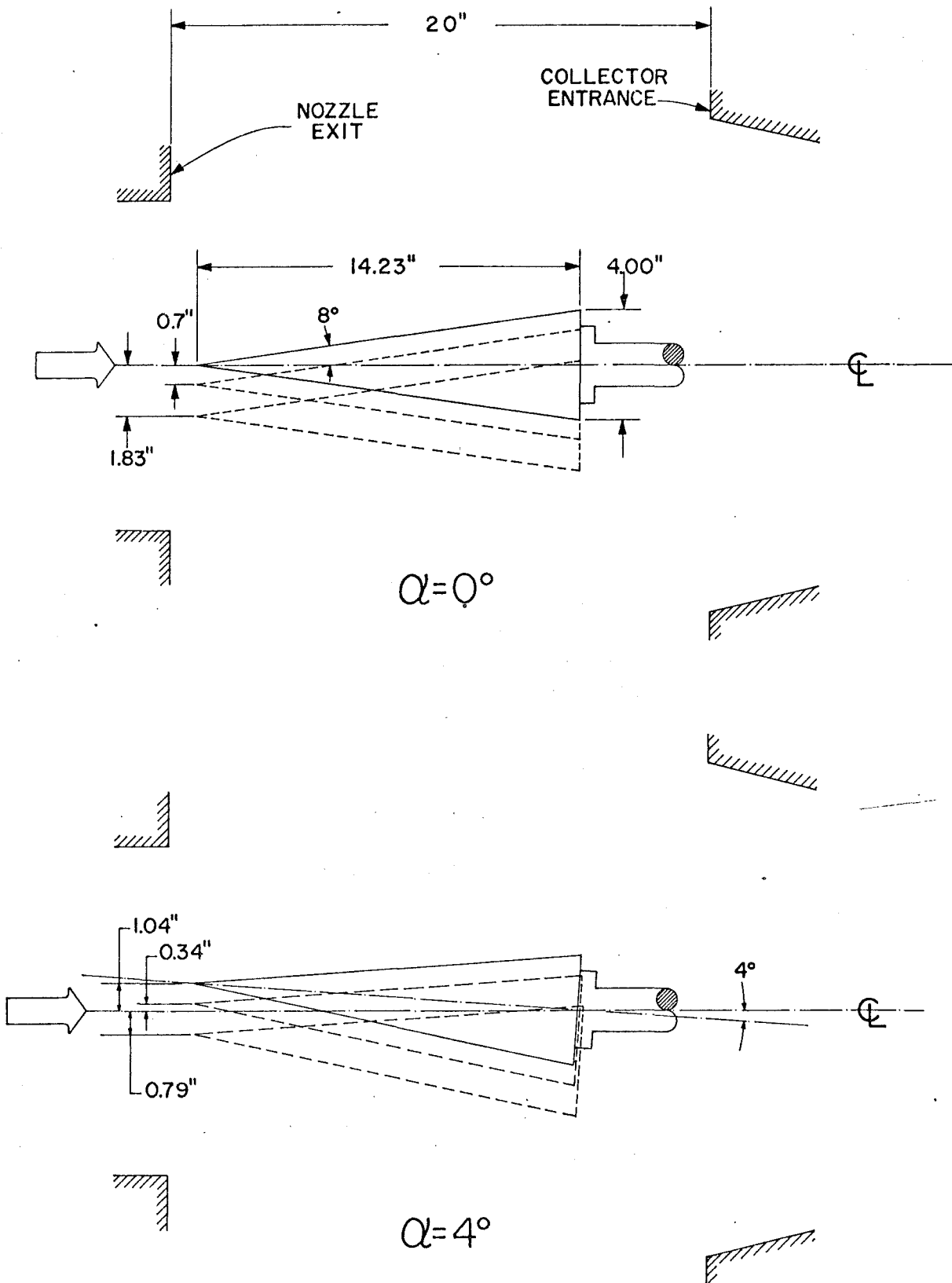


Figure 6. Sharp Cone Positions for $\alpha = 0^\circ$ and $\alpha = 4^\circ$

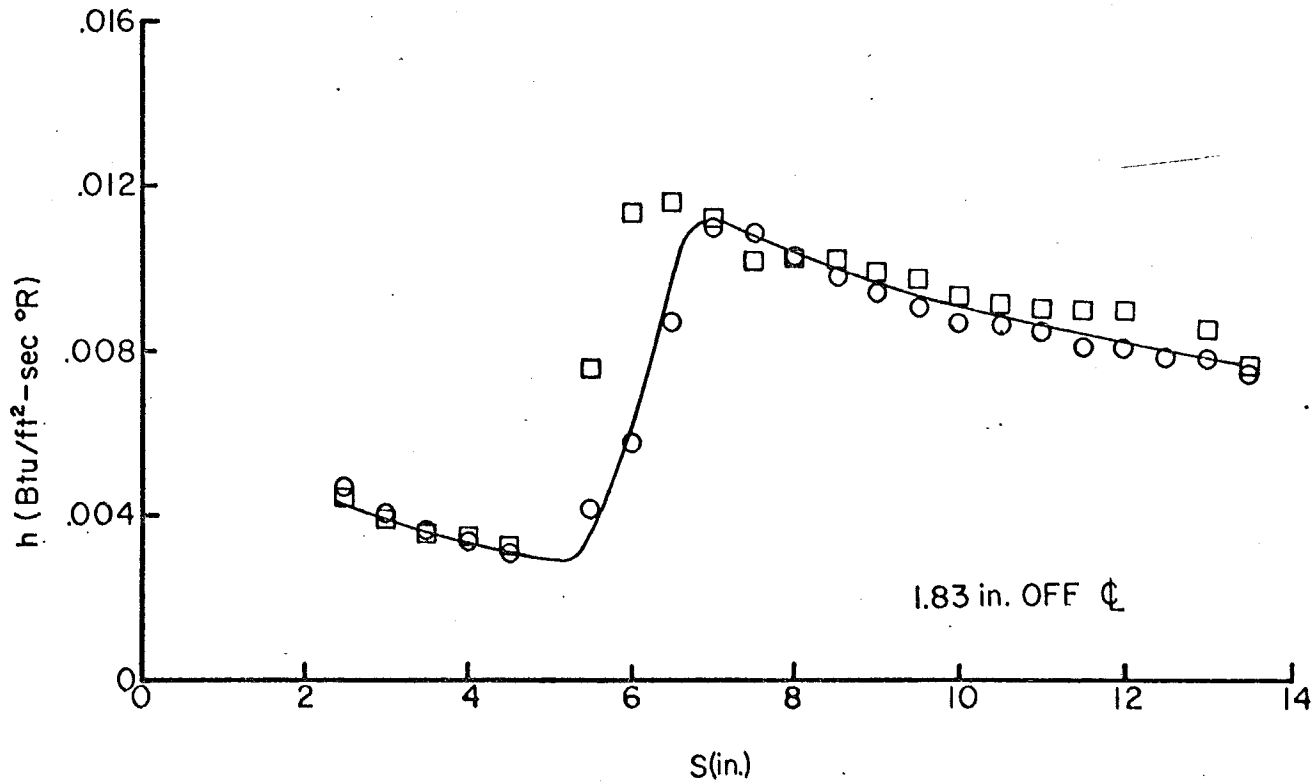
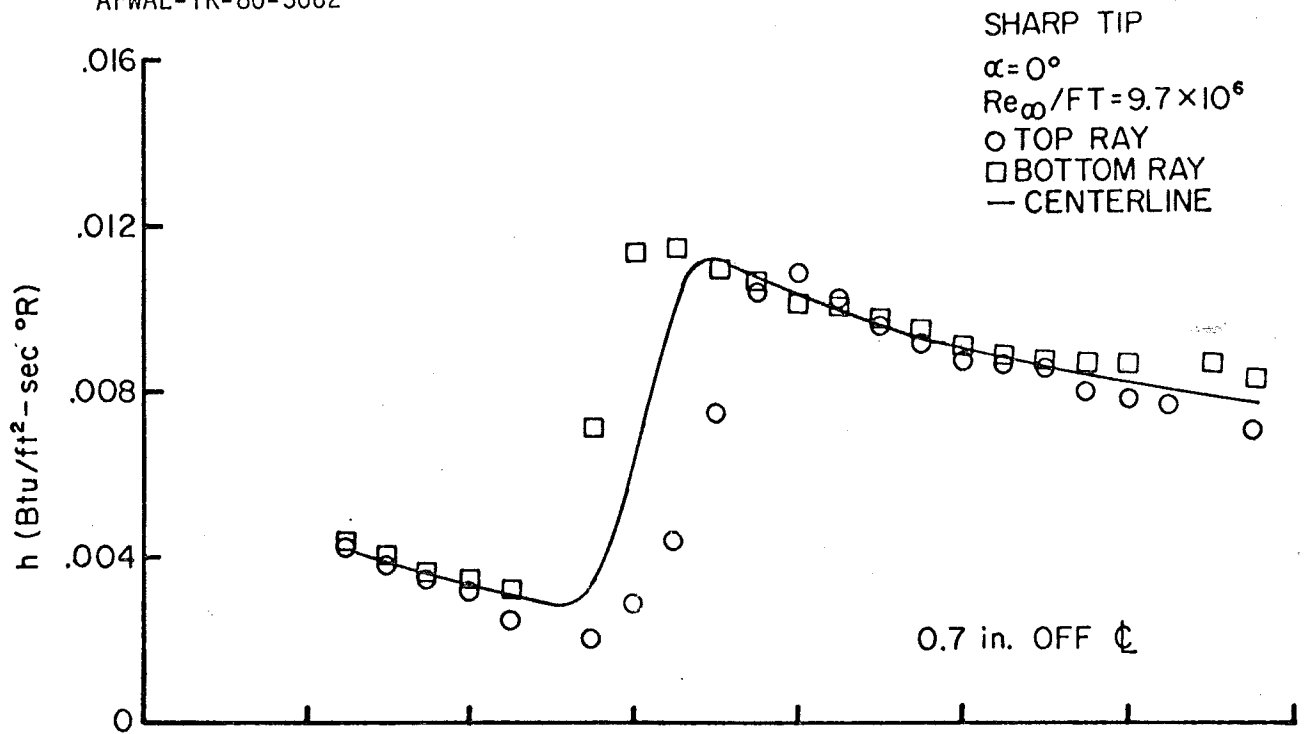


Figure 7. Transition Location for Different Model Positions, Sharp Tip, $\alpha = 0^\circ$ (Recovery Factor of One)

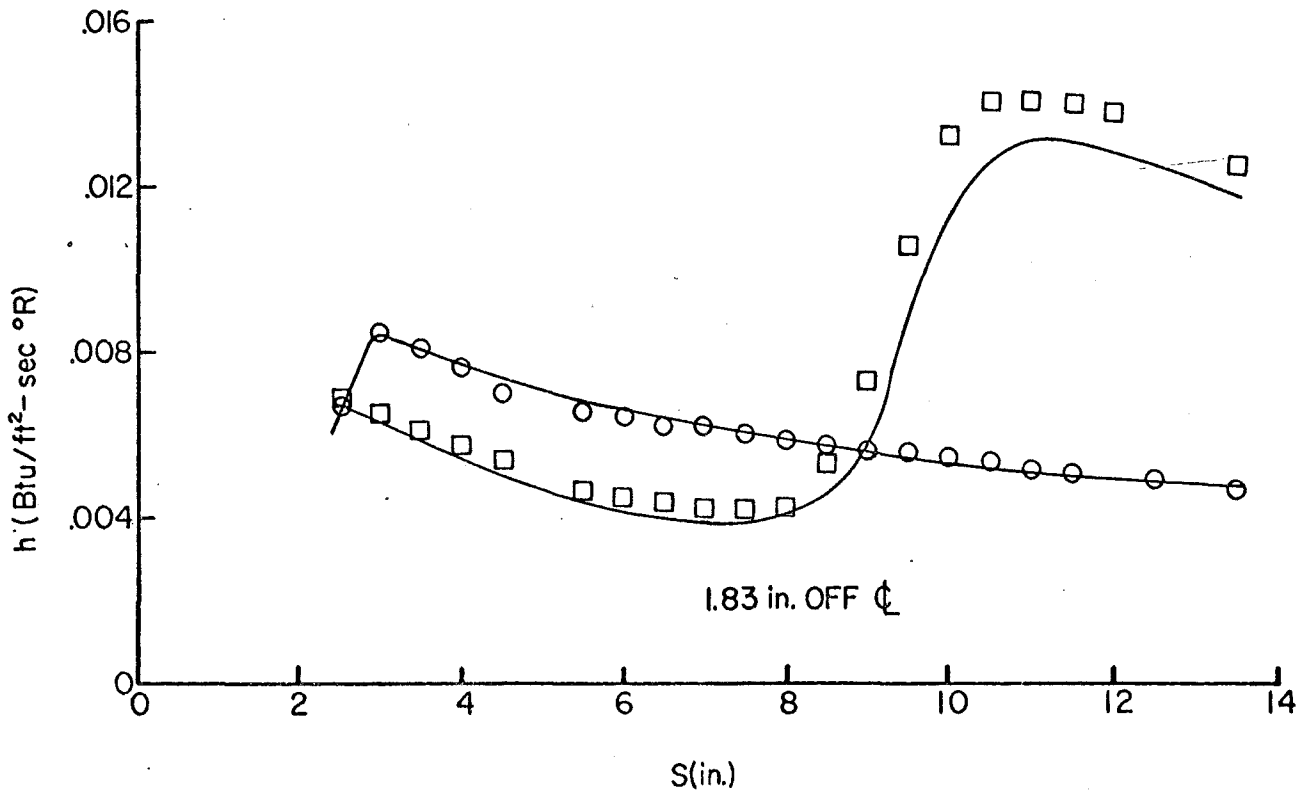
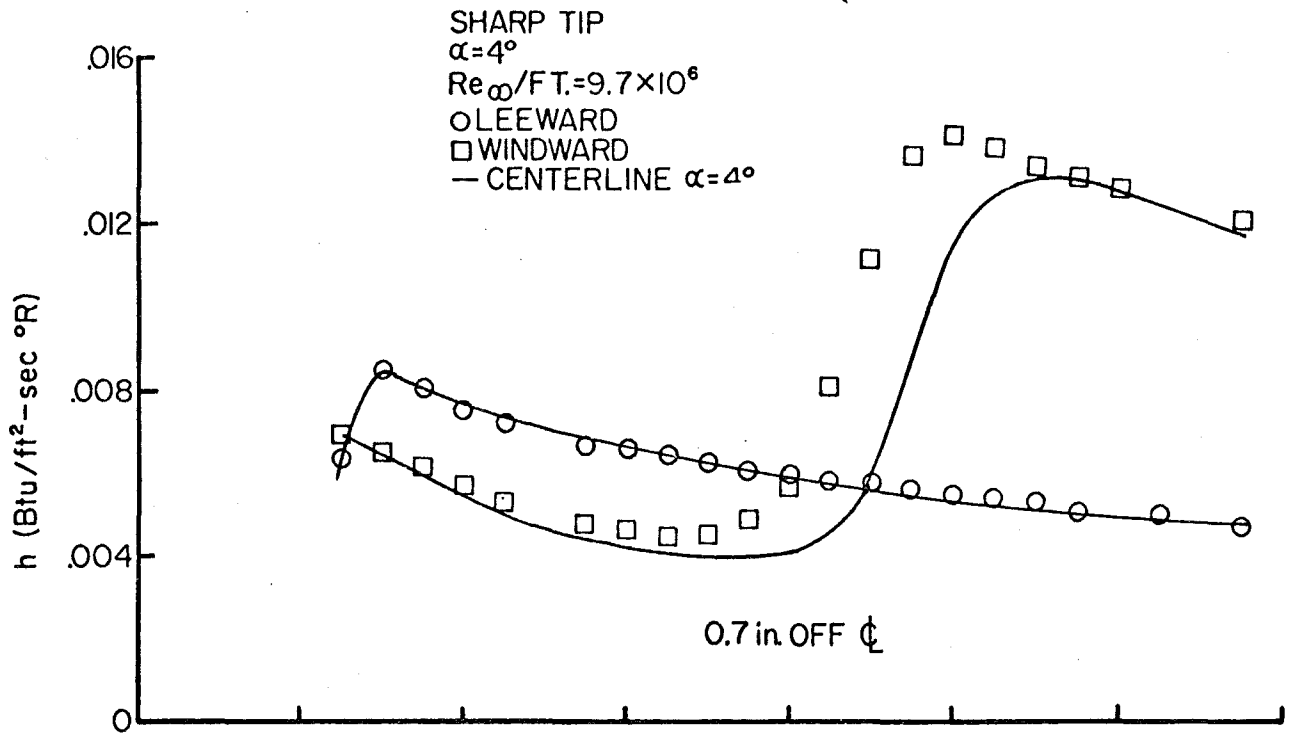


Figure 8. Transition Location for Different Model Positions, Sharp Tip, $\alpha = 4^\circ$ (Recovery Factor of One)

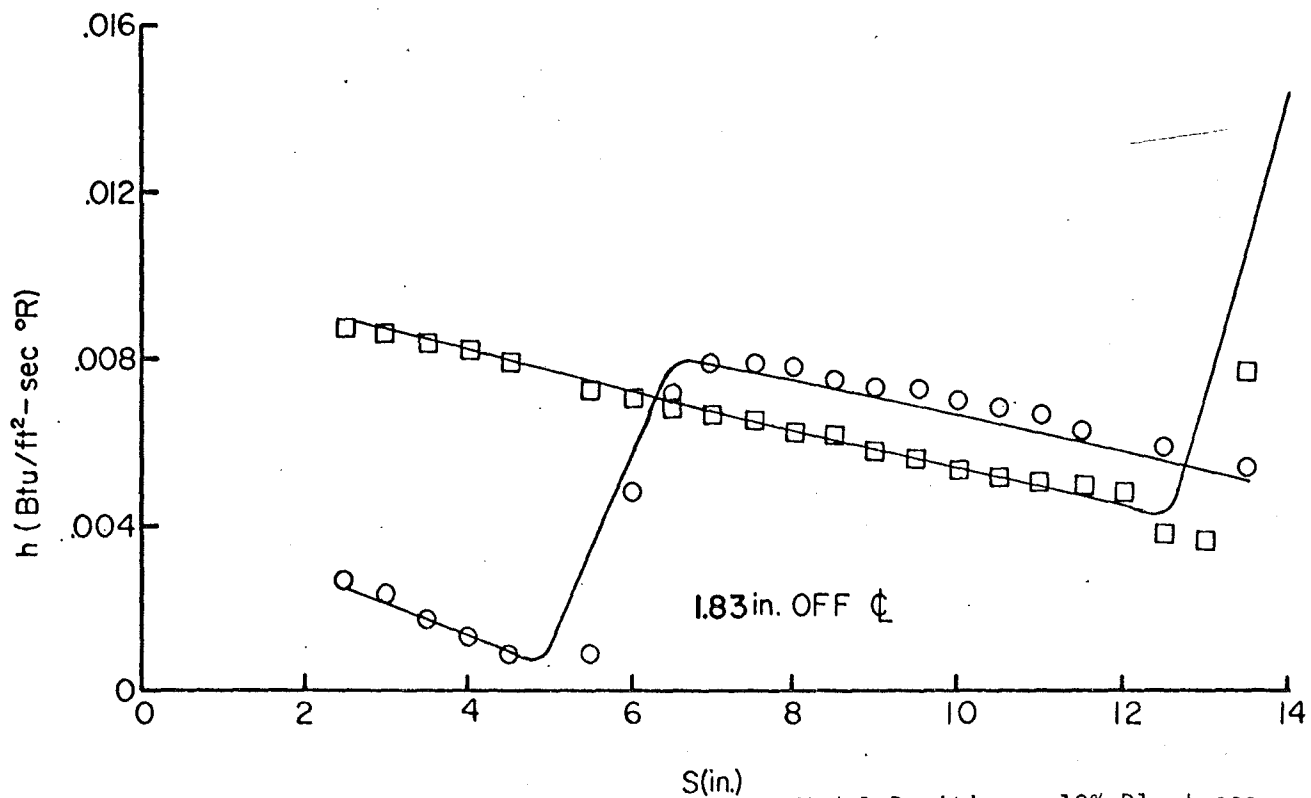
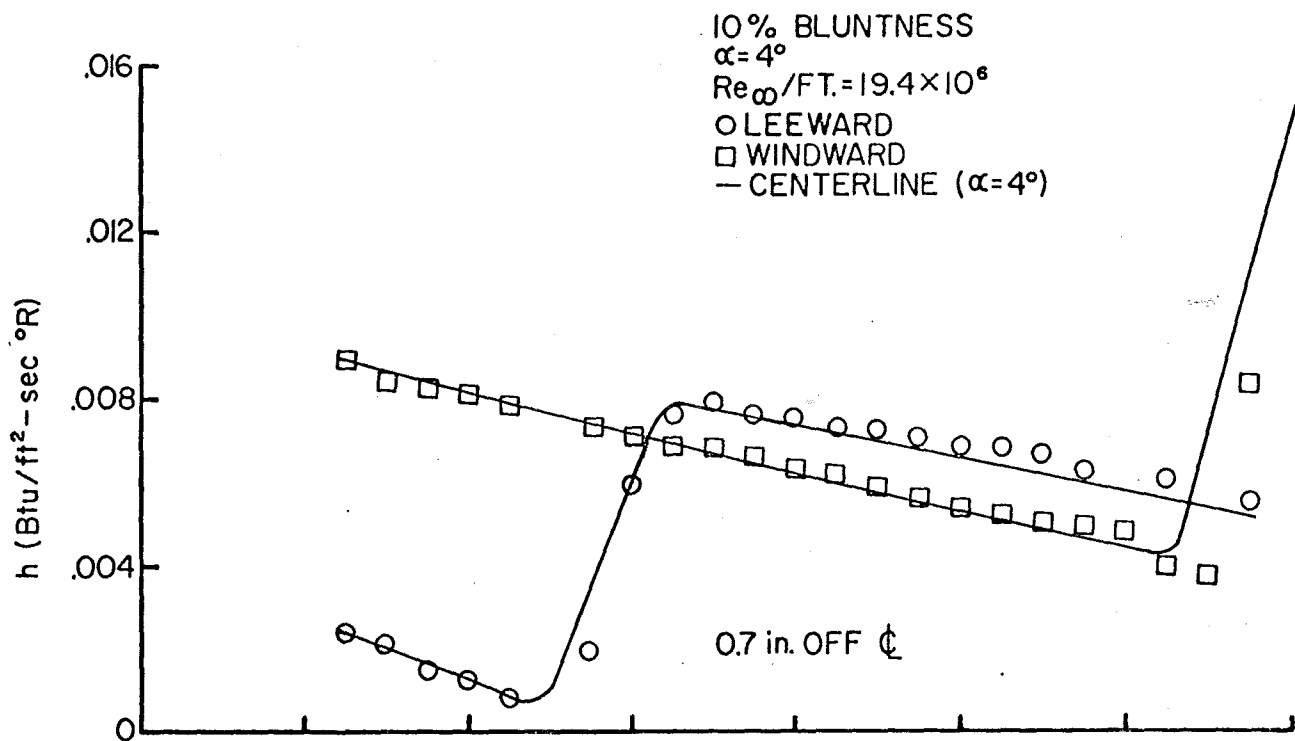


Figure 9. Transition Location for Different Model Positions, 10% Bluntness, $\alpha = 4^\circ$ (Recovery Factor of One)

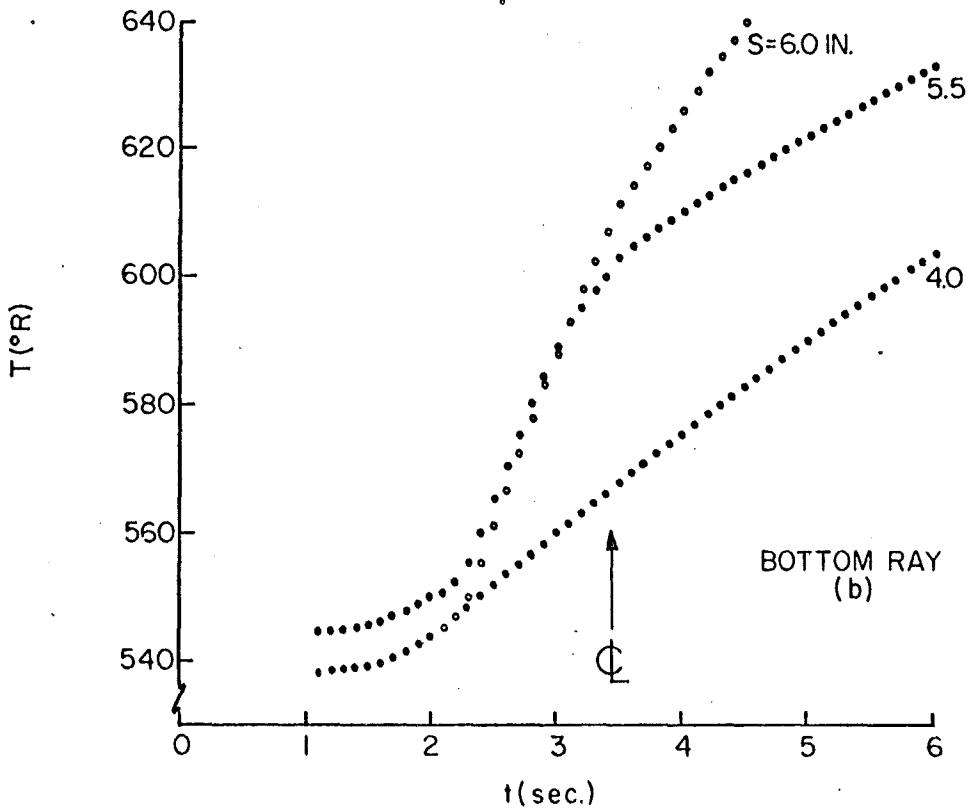
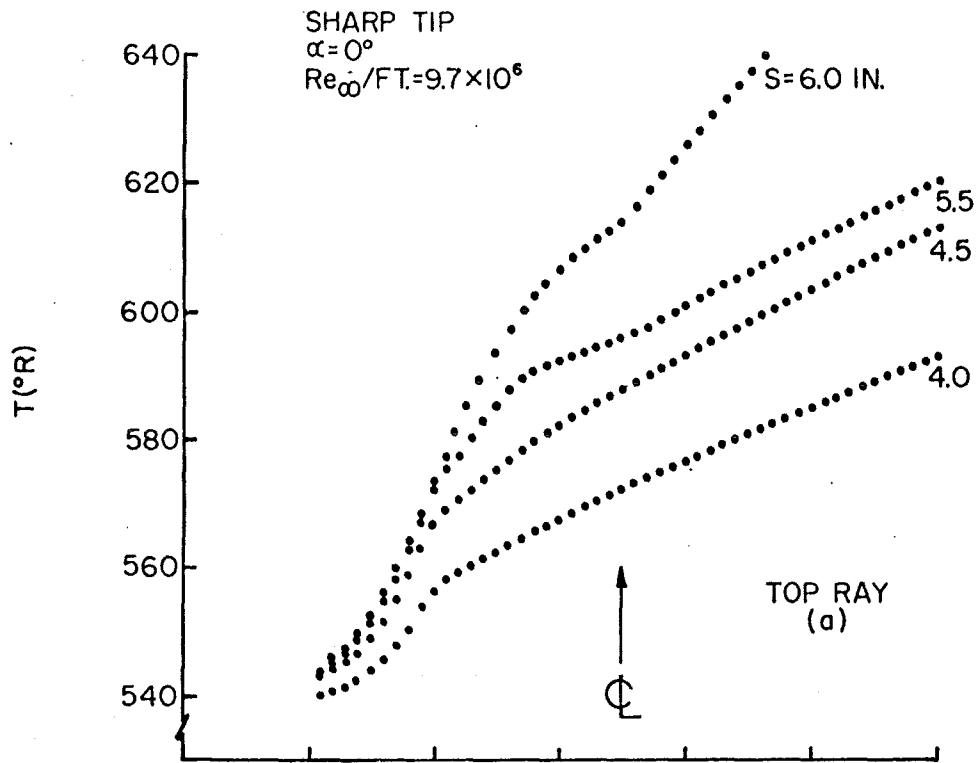


Figure 10. Surface Temperature History for the Sharp Cone At $\alpha = 0^\circ$

SECTION IV
BLUNTNESSE EFFECTS ($\alpha = 0^\circ$)

Although the state of the boundary layer on a slender, blunted cone has been under study as an engineering problem for many years, the influence of nosetip bluntness on cone frustum transition remains an area which is poorly understood. The question of why nosetip blunting displaces the onset of transition rearward and how much rearward displacement should be expected has never been adequately resolved. From the results of early blunting investigations (References 15, 16) it was concluded that the rearward displacement of transition was probably due to a reduction in local Reynolds number related to the pressure losses across the bow shock. Stetson and Rushton (Reference 7) also concluded that Reynolds number reduction due to blunting was the dominant effect. However, Softley's results (Reference 17) which included a re-interpretation of the data of Stetson and Rushton, obtained local transition Reynolds number twice the sharp cone values. Such a conclusion would suggest that the rearward displacement of transition also involved significant changes in the growth of disturbances in a laminar boundary layer. It appears that both Reynolds number reduction and changes in the stability mechanisms of the laminar boundary layer are important for transition on a slender, blunted cone; each influencing transition in varying degrees, depending upon geometric and flow factors. On the basis of available information, it is speculated that Reynolds number reduction is the dominant effect for the rearward displacement of transition and changes in boundary layer stability are the dominant effect in the reversal of this trend and the resulting forward movement of transition. Details of the stability of the laminar boundary layer on a slender, blunted cone cannot be answered from transition experiments such as these and must await the results of microscopic experiments.

Intuitively, it could be predicted that the experimentally observed rearward displacement of transition on the frustum of a slender cone with increasing bluntness (at a given flow condition) must reach a maximum displacement and then be followed by a forward movement. This results from the fact that transition Reynolds numbers have been found to vary

more than two orders of magnitude between the nosetip and the frustum. For example, transition experiments on blunt bodies such as spherical configurations have consistently found low transition Reynolds numbers; often less than 500,000 (based on surface distance) and 300 (based on momentum thickness) (References 18, 19, 20). Based upon the Mach number independence principle, it would be expected that transition in such flows would be essentially independent of free stream Mach number. However, on the frustum of a slender cone, where the entropy layer produced by the blunt tip has been essentially swallowed by the boundary layer, significantly larger transition Reynolds number have been observed, with the magnitude being Mach number dependent, (References 21, 22, 23). Local Reynolds numbers, based on surface distance, exceeding 50×10^6 have been obtained. To understand and predict transition location on a slender blunted cone, knowledge of the local flow properties is required. One of the problems that currently exists is the inability to assess the uncertainty in local flow calculations and to sort out the variations found by using different boundary layer codes. The results of Softley (Reference 17) illustrate this problem. Using the data of Reference 7, he arrived at conclusions different from those of the original investigation. These differences can be attributed directly to the different techniques used for obtaining local flow properties. Since it may be some time in the future before this problem is adequately resolved, caution should be exercised in drawing conclusions regarding slender, blunted cone transition which are based upon local Reynolds number calculations.

In the transition literature, reference is often made to such expressions as small bluntness and large bluntness when discussing tip bluntness effects on boundary layer transition on the frustum of a cone. This can be misleading since these expressions should not be related only to the physical dimensions of the tip. A given tip size can be either small or large, depending upon where transition occurs relative to the tip. An example is the case of a vehicle entering the earth's atmosphere. In order to relate frustum transition location with tip bluntness phenomena, some reference to a quality describing the bluntness effect, rather than a physical dimension such as nosetip radius, would seem a

better choice. To provide such a relationship, Stetson and Rushton (Reference 7) introduced the entropy swallowing length as a transition parameter. The swallowing distance is defined as the location on the cone frustum where the fluid which has gone through the strong portion of the bow shock has been swallowed by the boundary layer. The local Mach number and flow properties at the edge of the boundary layer at this location are nearly the same as would be obtained on the same cone with a sharp tip (Figure 11). For this investigation, the method of Rotta (Reference 24) was used to obtain swallowing distances. Rotta developed a method of obtaining certain boundary layer parameters as a function of a similarity parameter based upon swallowing distance, free stream Reynolds number, and nose radius. The curves of Figure 12 are based upon Rotta's results. This method provided a simple and easy hand calculation technique which is convenient for handling a large amount of experimental data and maintaining a common reference base for comparing results.

1. RESULTS

Figure 13 presents local properties on a 8-degree half angle cone with a spherical nosetip radius of 0.04 inches in a $M_\infty = 5.9$ flow. The cone frustum distance is X , with $X = 0$ corresponding to the point of tangency between the tip and cone. These results were obtained with a recently developed boundary layer code (Reference 25) based upon integral solutions of the boundary layer equations. Also shown is the entropy layer swallowing length obtained for this situation by the method of Rotta. The calculated value of X_{sw} corresponds to a location on the cone where the boundary layer code indicated the local Mach number to be $0.97 M_{sharp}$. Thus, the hand calculated value of X_{sw} is considered to be compatible with these boundary layer code results. For a given cone half angle and free stream Mach number, the swallowing distance varies as $(Re_\infty/FT.)^{1/3}$ and $(R_N)^{4/3}$. Therefore, as the nose radius of the cone is systematically increased, the swallowing distance also increases. For moderate-to-large nosetip bluntness, the entire model is then engulfed with low Mach number, and low unit Reynolds number flow. The region of local flow properties where the maximum rearward displacement of

transition location occurred is indicated on Figure 13. Thus, maximum displacement of transition location on the slender sphere-cone was found to be associated with essentially blunt-body flow. Even with allowances for possible variations of local properties by utilizing different boundary layer codes, it is believed that this blunt body conclusion should remain valid. This point will be discussed in more detail later. Figure 14 shows blunting results for four different Mach numbers. The $M_\infty = 3.1$ data were obtained by Rogers (Reference 26) in a conventional wind tunnel; the $M_\infty = 5.5$ data are shock tunnel results of Stetson and Rushton (Reference 7); the $M_\infty = 5.9$ results are new data from the FDL wind tunnel; and the $M_\infty = 9.3$ data are new data from AEDC's arc driven Tunnel F facility. The transition lengths for the blunt cones $(X_T)_B$ were normalized by the transition length for the sharp cone $(X_T)_S$ [$(X_T)_S$ was different for each facility]. This provides a measure of the rearward displacement of transition on a cone when the sharp tip is replaced with a blunt tip. The abscissa is the transition distance normalized by the swallowing distance (X_{SW}) . The swallowing distance for all of these data was based on the results of Rotta (Figure 12). The right side of the figure ($X_T/X_{SW} > 1$) corresponds to situations where transition occurs on a location on the cone where the entropy layer has been essentially swallowed and the conditions at the outer edge of the boundary layer are nearly the same as would be obtained if the cone had as sharp tip. The left side of the figure (X_T/X_{SW} small) corresponds to locations on the cone just downstream of the tip. The conclusions given below from this type of presentation are not very sensitive to X_{SW} . That is, if a different method of calculating X_{SW} were used which gave different values, the effect would be to shift the data to the right or left and not alter the basic conclusions. Data points shown with an arrow indicate conditions where the entire model had a laminar boundary layer. Transition would then occur at some unknown higher value. The main points to observe in Figure 14 are as follows:

a. The effect of tip blunting on cone frustum transition is very sensitive to free stream Mach number, with large Mach numbers producing large rearward displacement of transition. The reason for this sensitivity with free stream Mach number is believed to be primarily

related to the Reynolds number reduction associated with pressure losses across the bow shock.

b. Small bluntness systematically moved the transition location rearward until the maximum displacement was obtained.

c. A blunting transition reversal occurred. That is, additional increases in nosetip radius, or free stream Reynolds number reduced the value of X_T/X_{SW} and produced a forward movement of transition. This forward movement was very sensitive to both nose radius and Reynolds number. For example, for a given nose radius, a small increase in free stream unit Reynolds number could produce large forward movements of transition. In this situation, it was often observed that portions of the cone frustum could be completely laminar while other areas of the model had early transition (this situation may have special significance for persons concerned with the effect of frustum transition on vehicle motion).

d. Maximum rearward displacement of transition occurred in situations where X_T/X_{SW} was small, indicating that the local Mach number was low and the flow was essentially of the blunt-body type (Figure 13).

Figure 15 illustrates the forward movement of transition on a 7-degree half angle cone at a Mach number of about 9.1. At a free stream Reynolds number per foot of 5.4×10^6 , the cone had a completely laminar boundary layer. A small increase in free stream Reynolds number caused transition to appear near the cone mid-point at a local Reynolds number of about 550,000. Further increases in free stream Reynolds number steadily moved the transition location to the sphere-cone tangency point where the local transition Reynolds number was slightly over 300,000. This forward movement slowed as it progressed through the increasing favorable pressure gradient. These events occurred in a situation where the pressure gradient became increasingly more favorable, yet the transition Reynolds number decreased from 550,000 to nearly 300,000. Further increases in the free stream Reynolds number produced transition in the subsonic region of the tip, with a local transition Reynolds number of about 250,000. The local Reynolds number mentioned above was

calculated by the finite difference boundary layer code developed by Adams (Reference 27) and co-workers. With the exception of the two largest Reynolds number conditions, all of the data of Figure 15 were obtained during a single run in Tunnel F. These variations in Reynolds number occurred during a 59 millisecond time period while the Mach number varied between 9.1 and 9.0 and the wall temperature remained essentially constant. All of the data shown were obtained along the same ray of the model. This situation, as in most boundary layer transition problems, reflects the results of several competing effects and any explanation of this cone frustum transition behavior at this time would be mostly speculative. The rapid movement of transition from the sphere-cone tangency point to the subsonic region of the tip is not a new observation. This transition pattern was first observed by Stetson (Reference 5) over 20 years ago and has been observed by several investigators since that time.

The recent analyses of Merkle (Reference 20) based upon linearized stability theory combined with nosetip roughness effects, provide an interesting comparison with this experimentally observed forward movement of transition. Merkle postulates two unstable regions on a sphere-cone; one associated with the tip, and the other with the cone frustum. He anticipated that transition on the frustum, due to the second unstable region, would occur at classical transition Reynolds numbers for cones in the appropriate Mach number regime. Merkle suggested that, with increasing free stream unit Reynolds number (such as a reentry vehicle descending), the transition location would move gradually forward on the frustum and would be generated by the second unstable region. During this time, the growth of disturbances on the nosetip would reach larger and larger amplitudes, but would not get sufficiently large to trigger transition. These disturbances in the boundary layer on the nosetip would grow for a time as they proceeded along the tip and then emerge from the unstable region associated with the tip and decay rapidly, thus being of no consequence in triggering transition. At some critical free stream unit Reynolds number, the peak amplitude of disturbances in the unstable region on the nosetip would

surpass the level at which significant non-linear interactions begin, and transition would jump discontinuously from the frustum to the subsonic region of the nosetip.

Thus the rapid forward movement of transition on the cone frustum at a free stream unit Reynolds number of 5.7×10^6 and the resulting low local Reynolds number for transition at this condition does not seem to be compatible with the predictions of Merkle. It appears from these present results that the unstable region associated with the nosetip extends well beyond the tip and includes the forward portion of the cone frustum.

Figure 16 was prepared to illustrate the sensitivity of transition location to free stream Mach number. The local Mach number and Reynolds number on an 8-degree half angle cone with a 0.60 inch nose radius was calculated with the boundary layer code of Reference 27. The cone frustum distance is X , starting at the point of tangency of the tip and cone. Note that the local Mach number was low for both cases and relatively insensitive to free stream Mach number. As far as local Mach number is concerned, the two flows were quite similar. The surface pressure distributions (not shown) differ somewhat, due to the fact that the region of overexpansion and subsequent recompression are Mach number dependent. Significant differences were found in the local Reynolds number. These differences are related to the fact that the total pressure losses across the bow shock increased with Mach number. The experimentally observed transition location for these two free stream Mach number situations are indicated and it can be seen that even though the transition locations differ considerably, the local Reynolds number for transition was essentially the same for both cases. These results indicated that the difference in transition location for the two cases shown can be accounted for by the Reynolds number reduction associated with the total pressure losses across the bow shock.

Figure 17 provides additional information to demonstrate the relationship between transition location and Reynolds number reduction. The trend of maximum transition displacement with free stream Mach number clearly follows the trend of Reynolds number reduction. These

results, as well as those of previous figures, provide convincing evidence that the maximum rearward displacement of transition is strongly related to the Reynolds number reduction.

Figure 18 is shown partly to demonstrate the problem of calculating local Reynolds number and partly to illustrate the different flow situations found on a blunted, slender cone. The local Reynolds number for these present $M_\infty = 5.9$ data was obtained by using the unit Reynolds number profile shown in Figure 13 and assuming that the relationship between Rotta's swallowing distance and this profile was the same for all of the data (for example, at 50% X_{sw} , $(Re/ft)_{local} = 40\% (Re/ft)_{sharp\ cone}$). The results of Softley (Reference 17), with local transition Reynolds numbers of twice the sharp cone value, are shown for comparison. Since Softley's results had the entropy layer being swallowed much more rapidly than these present calculations, the local Reynolds numbers he calculated for transition were significantly larger in the small to medium bluntness regime. Since it is not possible to adequately assess at this time the accuracy of flow field calculations of this type, the correct trend for a local Reynolds number plot such as this is not known. The fact that the maximum Reynolds number shown for Softley's results coincides with the large increase in Re_{XT} for these present data is believed to be fortuitous since the swallowing distances for the two sets of data are not compatible. The data on the left side of the figure which should be relatively insensitive to the particular method used for calculating local Reynolds number since entropy layer swallowing plays a minor role, indicate frustum transition Reynolds numbers become small; of the same order as those found on nosetips when transition occurs early on the cone frustum. It appears that for cases of small bluntness, local transition Reynolds numbers greater than those obtained on a sharp cone are possible; however, attaching a specific number seems to have little significance at this time. Martellucci (Reference 29) also calculated local Reynolds numbers for the data of Reference 7, using a finite-difference boundary layer code, and obtained local transition Reynolds numbers, for the case of small bluntness, somewhat larger than the sharp cone values.

2. CONCLUSIONS

a. The rearward displacement of transition on the cone frustum due to tip bluntness was found to be quite sensitive to free stream Mach number as well as to bluntness. At $M_\infty = 9.3$, transition could be displaced rearward as much as nine times the transition length for a sharp cone.

b. Small bluntness systematically moved the transition location rearward until the maximum displacement was obtained.

c. A blunting transition reversal occurred. That is, additional increases in nosetip radius, or free stream Reynolds number, produces a forward movement of transition.

d. The forward movement of transition took place rapidly, with small changes in Reynolds number or nose radius. Asymmetric transition fronts at $\alpha = 0^\circ$ were common for this situation.

e. The maximum rearward displacement of transition occurred under situations of low local Mach number flow.

f. The trend of maximum transition displacement with free stream Mach number followed the trend of Reynolds number reduction. Reynolds number reduction is believed to be the dominant effect associated with the rearward displacement of transition.

g. Low transition Reynolds numbers, of the order found on the nose-tip, extended onto the front portion of the cone frustum. It appears that the transition by-pass, associated with blunt bodies, includes the forward portion of the cone frustum on a sphere-cone configuration.

h. Transition correlations based on local Reynolds number should be used cautiously, since it is not possible at this time to assess the accuracy of the Reynolds number calculations.

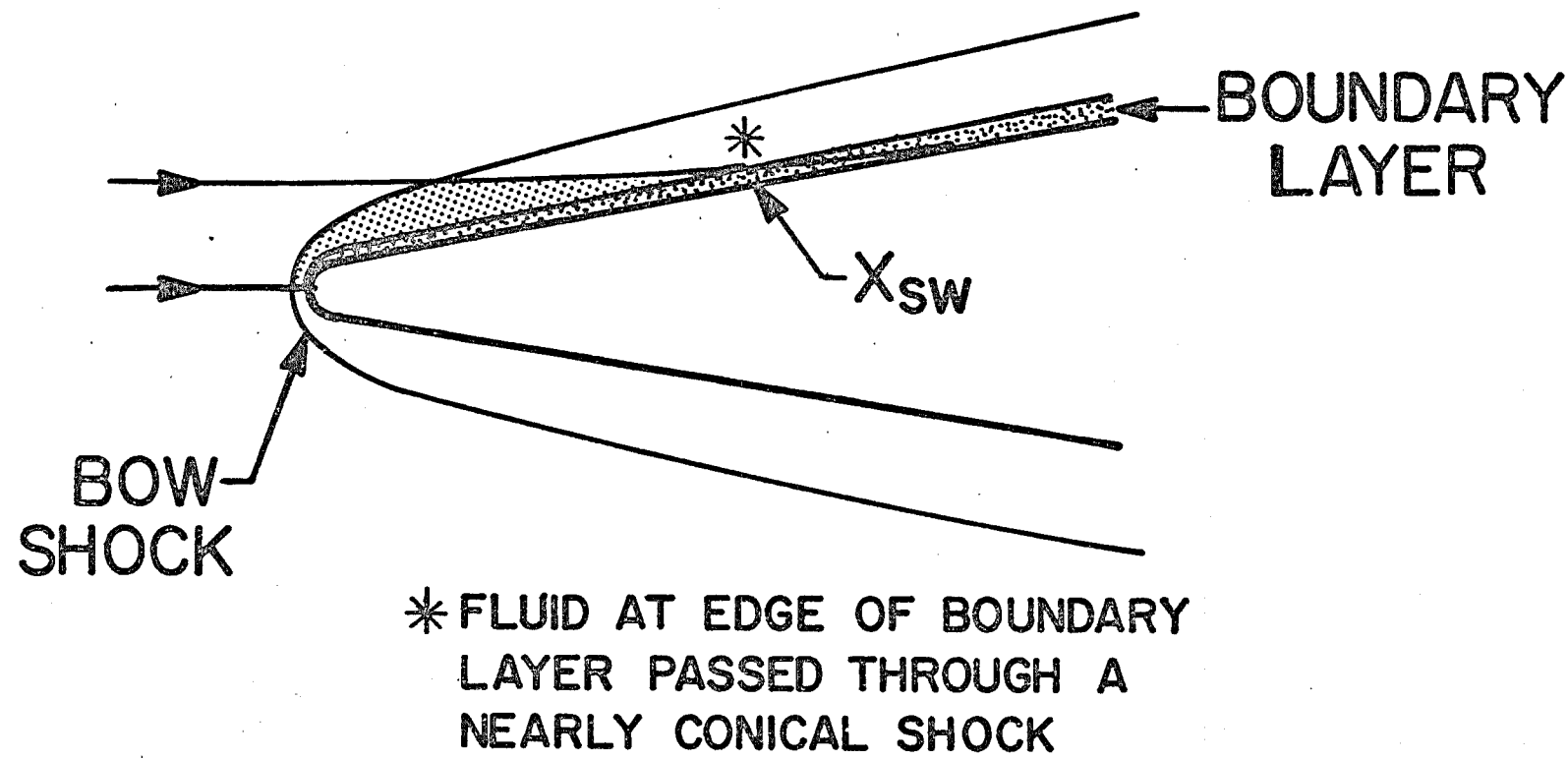


Figure 11. A Schematic Illustration of Flow Over a Slender, Blunt Cone

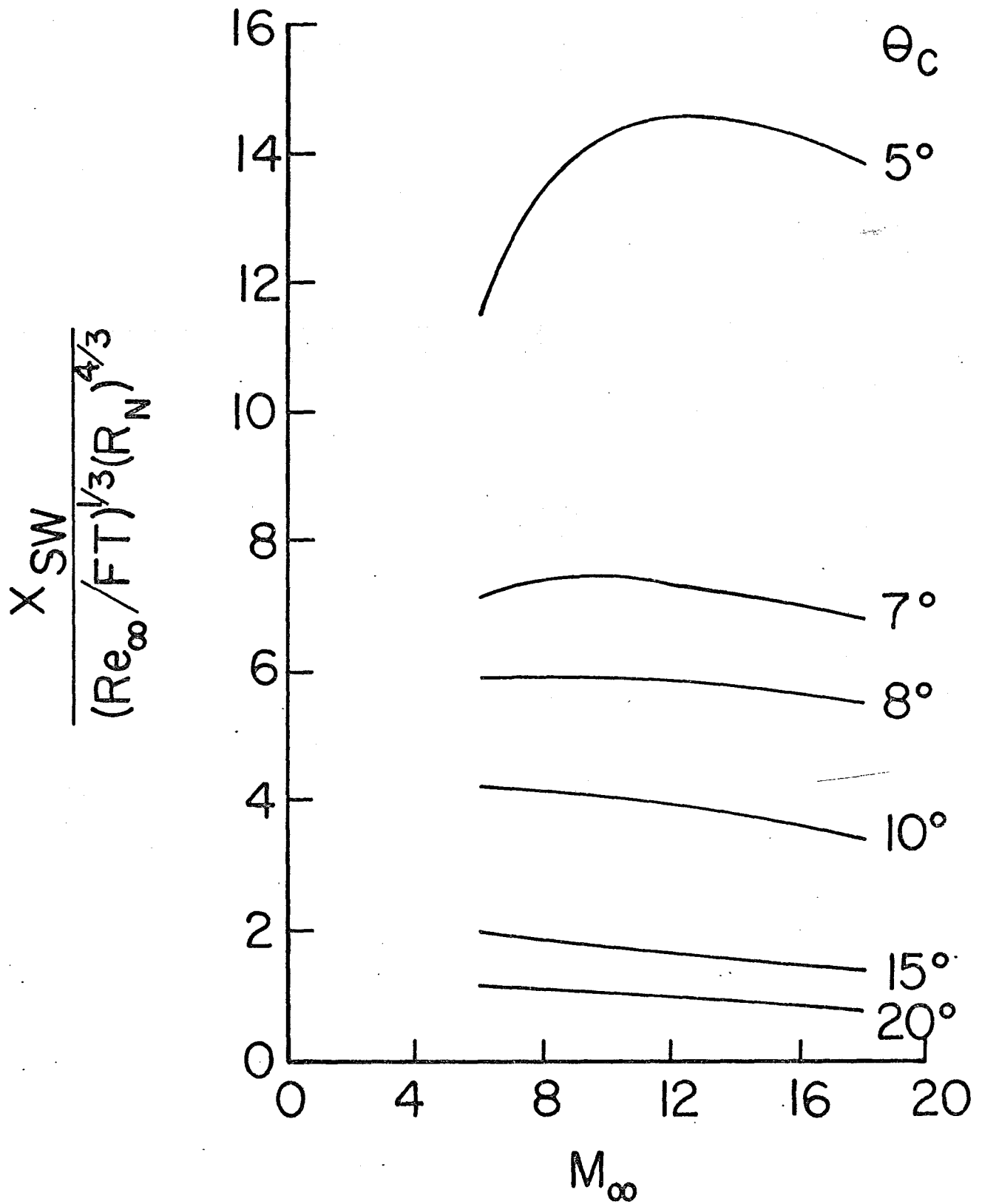


Figure 12. Entropy Layer Swallowing Distance Parameter

32

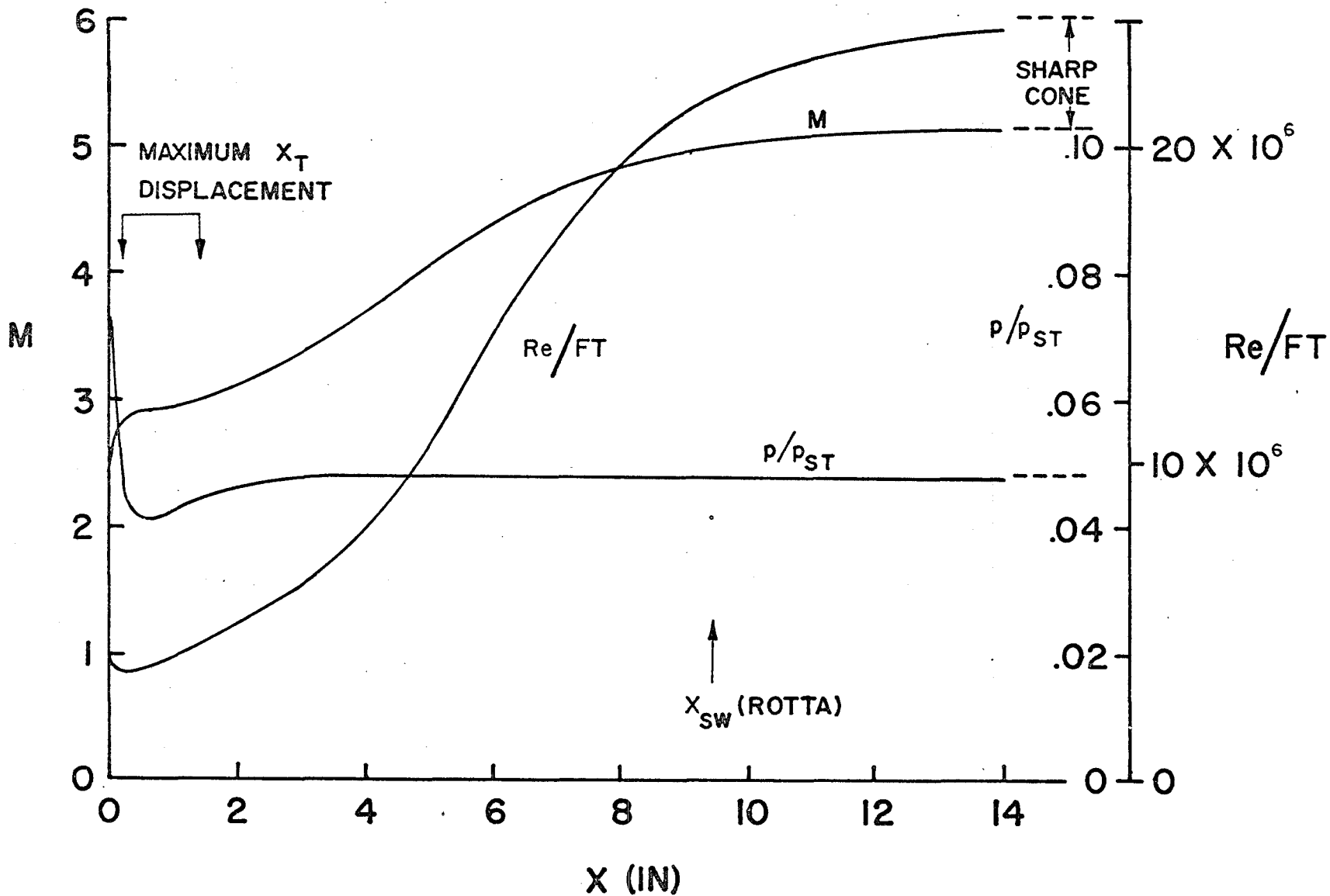


Figure 13. Calculations of Local Flow Properties on an 8-Degree Half Angle Cone with 2% Bluntness At $M_\infty = 5.9$

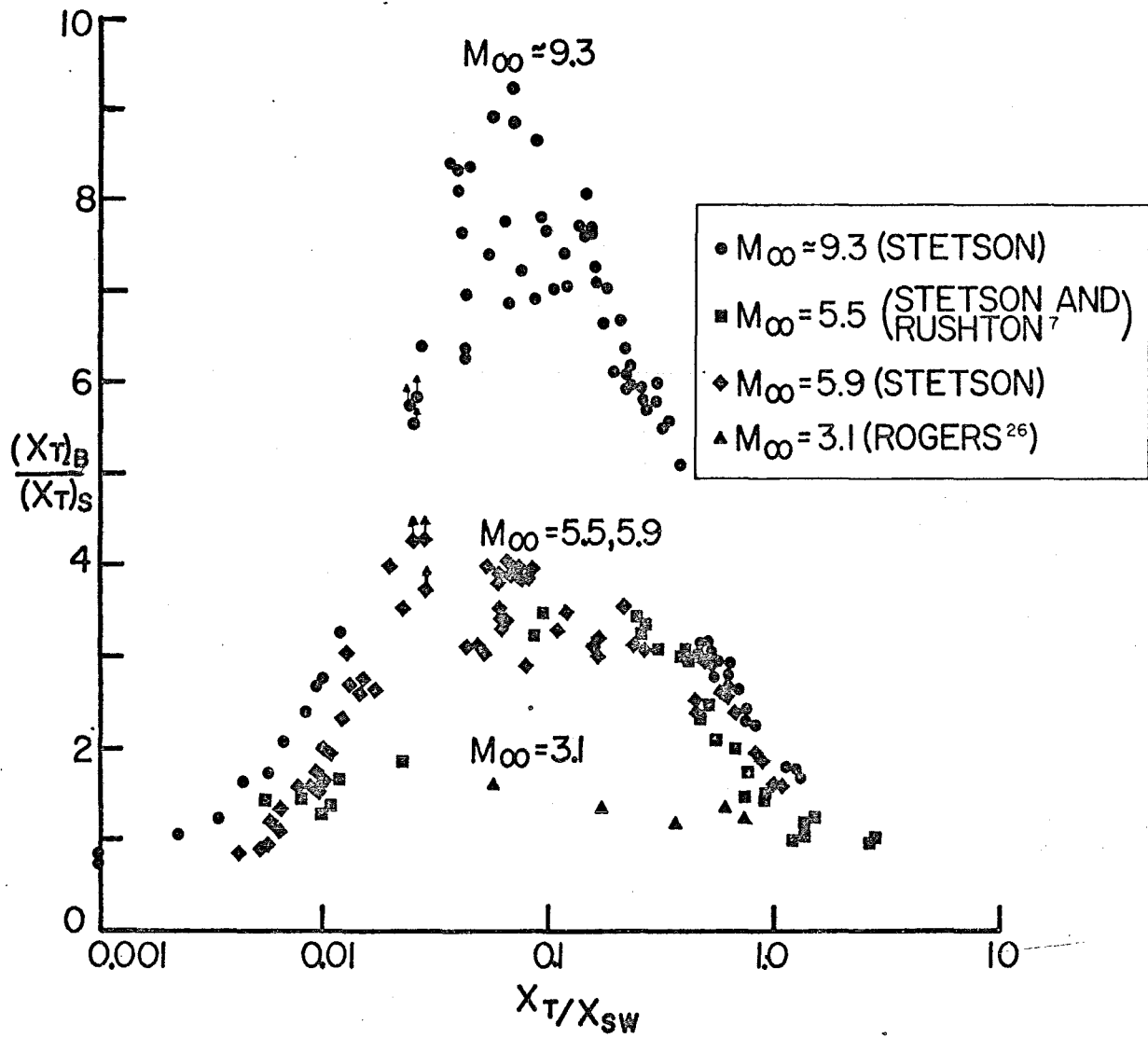


Figure 14. Effect of Nose Bluntness on Transition Location

TRANSITION PROGRESSION TO NOSE TIP

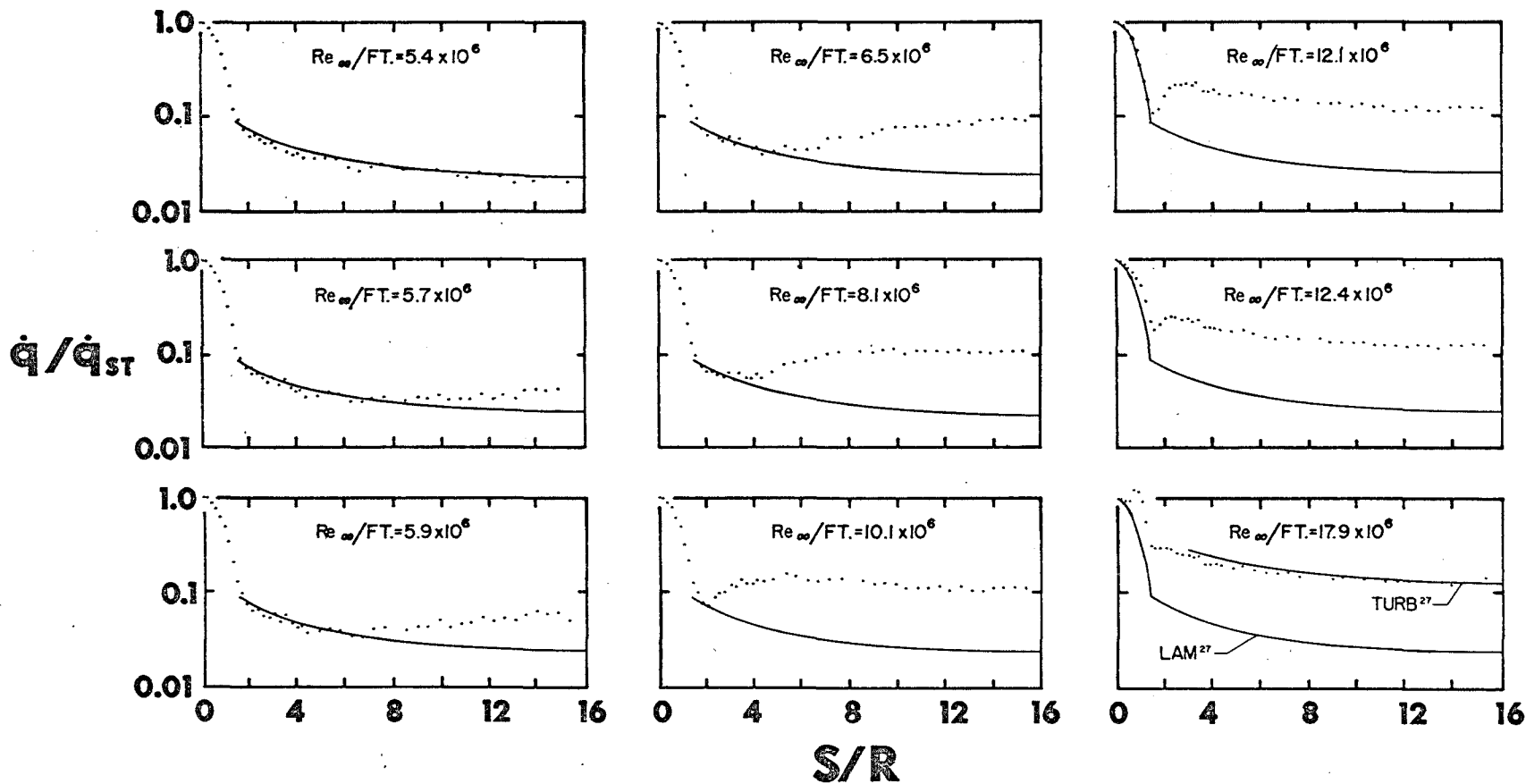


Figure 15. Transition Movement from Cone Frustum to Nostip on a 7-Degree Half Angle Cone At $M_{\infty} \approx 9.1$

35

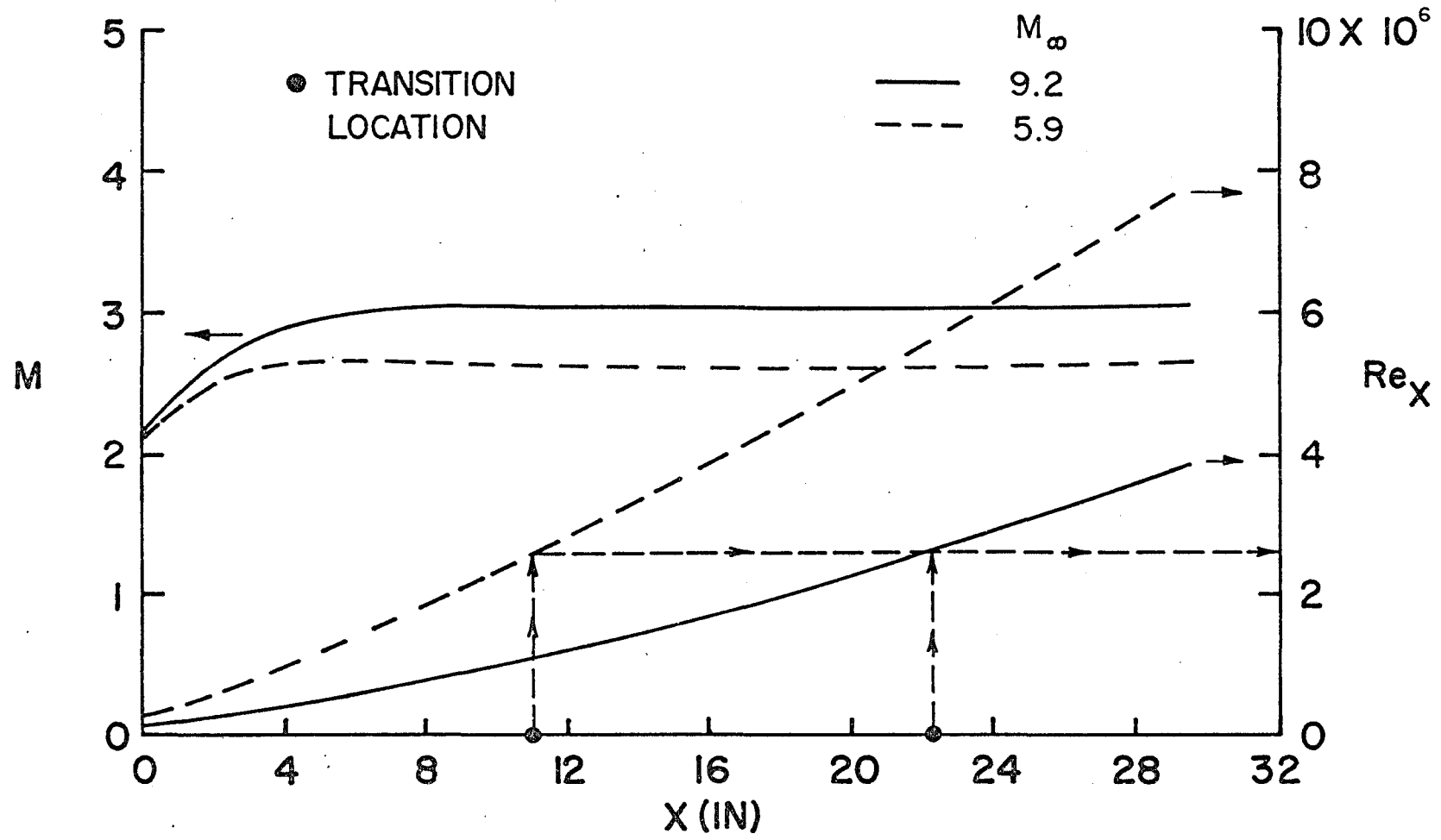


Figure 16. Transition Location and Local Mach Number and Reynolds Number on an 8-Degree Half Angle Cone with a 0.60 Inch Nose Radius at M_∞ = 5.9 and 9.2; Re_∞/Ft = 18.5 x 10⁶ in Both Cases

36

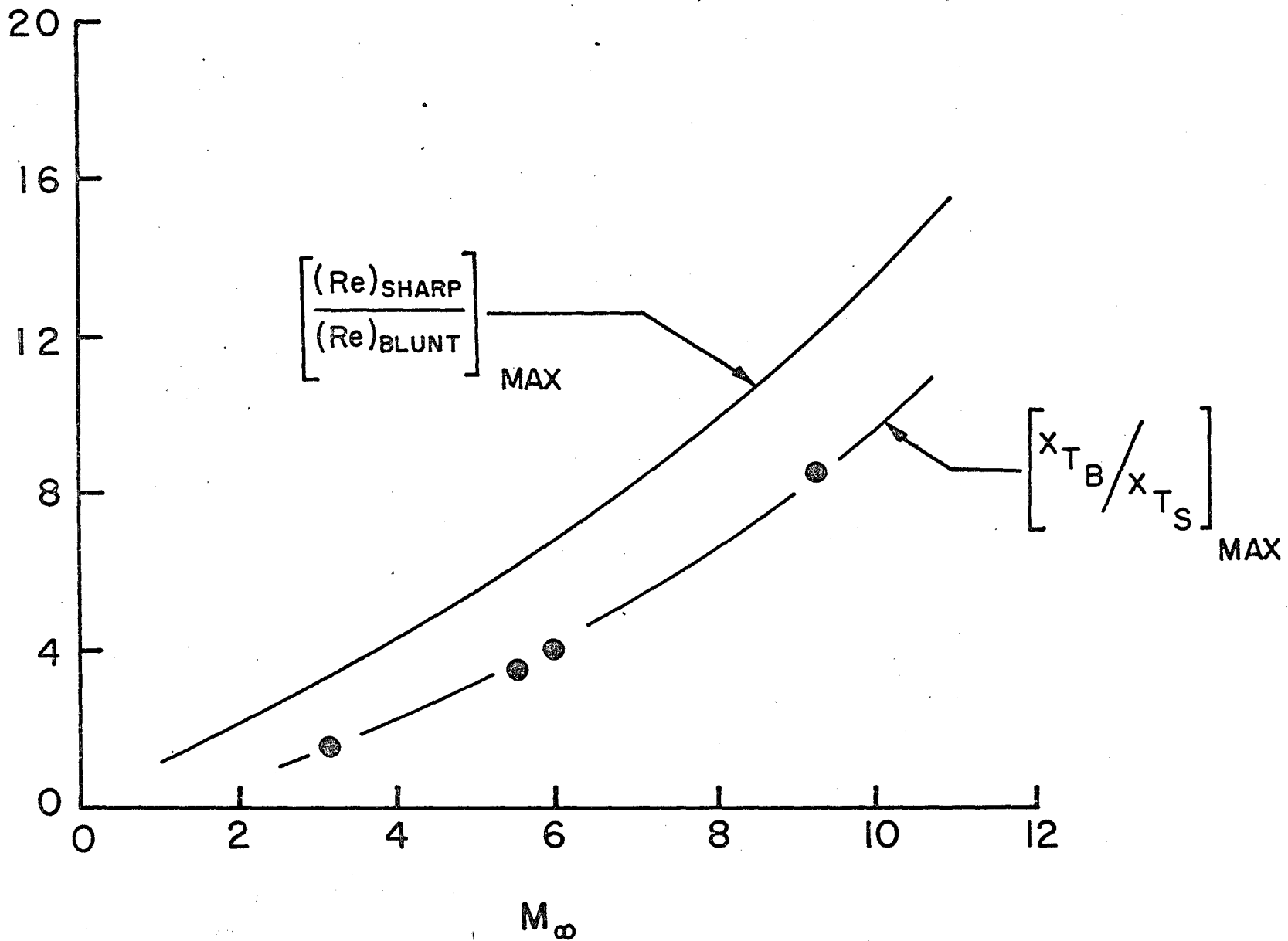


Figure 17. Transition Displacement Trend with Mach Number (Data Points from Figure 14)

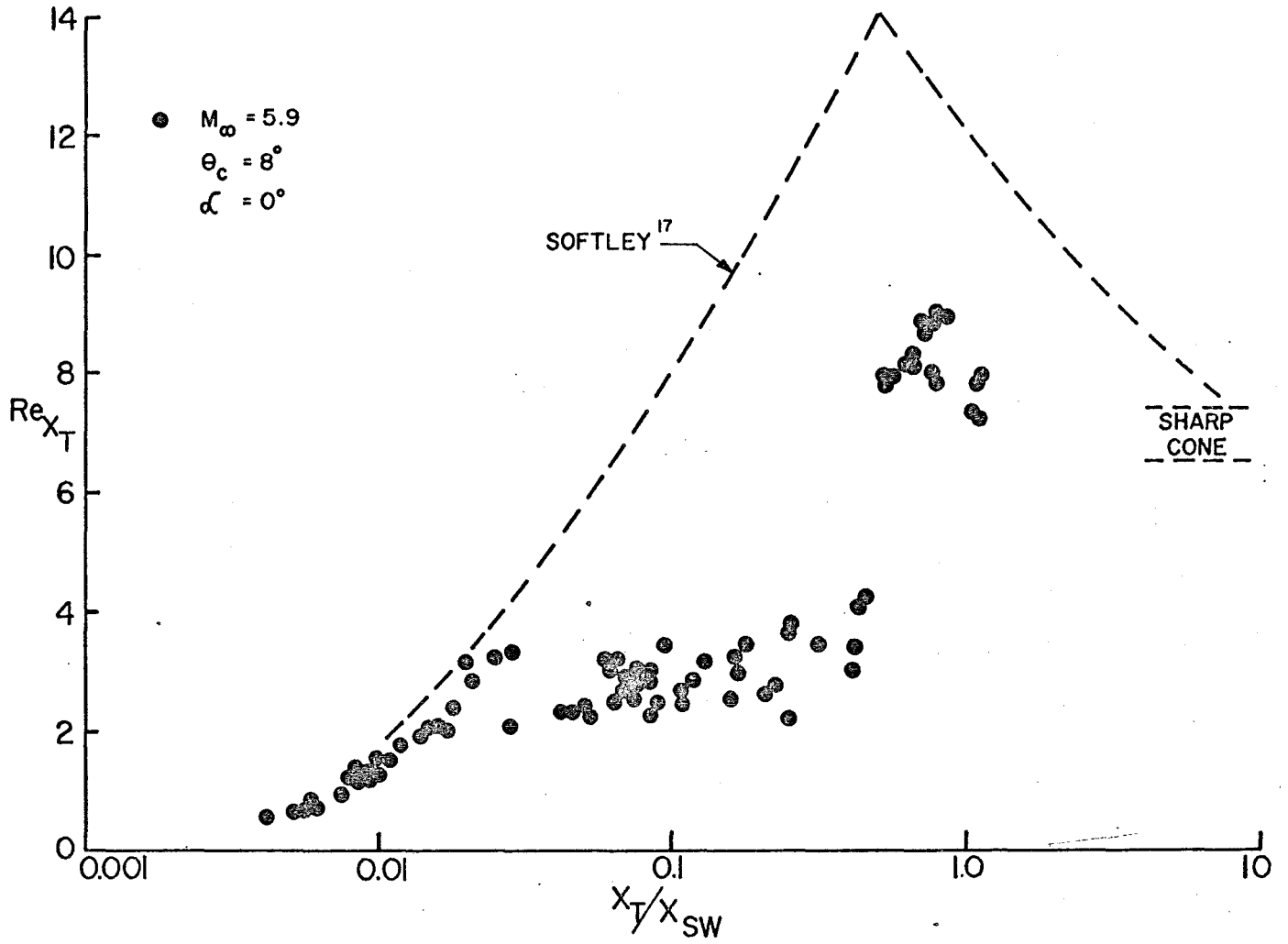


Figure 18. Local Transition Reynolds Number Calculations

SECTION V

ANGLE OF ATTACK EFFECTS

Although transition trends on a sharp cone at angle of attack may defy one's intuition, there seems to be general agreement regarding the expected movement of transition. Theory and experiment both indicate a rearward movement of transition on the windward ray and a forward movement on the leeward ray. Moore's results (Reference 13) show that the boundary layer profiles assume a more stable shape on the windward side and a more unstable shape on the leeward side. Hot wire experiments of Kendall at $M_\infty = 4.5$ (Reference 30) which measured the boundary layer fluctuation spectra on the windward and leeward rays of a 4-degree half angle sharp cone, qualitatively confirm these theoretical predictions. References 7, 11, and 12 provide additional examples of confirmation of these trends.

1. RESULTS

Figure 19 presents results of local Reynolds number calculations for a sharp, 8-degree half angle cone at angle of attack. Also shown are the locations of transition obtained from these experiments. Comparison of the experimental transition locations with the calculated Reynolds numbers provides local transition Reynolds numbers. The local transition Reynolds number increased on the windward ray and decreased on the leeward ray as the angle of attack was increased.

Figure 20 illustrates the transition movement on the windward and leeward rays of an 8-degree half angle cone at $M_\infty = 5.9$. The transition distance (X_T) is normalized by the transition distance on the sharp cone at $\alpha = 0^\circ$ [$(X_T)_S$ at $\alpha = 0$ varies with unit Reynolds number]. It was planned to test all of the blunt configurations at the same free stream unit Reynolds number; however, for the 15% blunt tip, transition moved off the end of the model at $\alpha = 2^\circ$. Therefore this configuration was tested at a slightly larger Reynolds number. The sharp cone transition trends were consistent with expected results as noted earlier. The blunt configurations, however, have trends which are somewhat different from those of Reference 7. These differences relate to the windward ray at small angles of attack.

Reference 7 had the maximum rearward displacement at $\alpha = 0^\circ$ and a forward movement with angle of attack. The present data consistently had a rearward movement initially, as for the sharp cone, and then a forward movement at larger angles of attack. The reason for these differences is not known. Intuitively it would seem reasonable that the blunt cone boundary layer profiles might assume a more stable shape with angle of attack, analogous to the sharp cone, and therefore cause transition to move rearward on the windward ray. Transition would not continue to move rearward, as for the sharp cone, since the effect of bluntness diminishes with angle of attack. It would be expected that the curve would turn and approach the sharp cone curve. At some large angle of attack all of the curves should merge into a single curve. Variations of tunnel environment, as discussed earlier, may have a small influence on these data; however, it is not believed to be an effect capable of altering the major trends shown in Figure 20.

The data obtained with the 30% blunt nosetip are presented separately (Figure 21) due to the nature of the results. Initial experiments were conducted at $Re_\infty/Ft. = 19.4 \times 10^6$, as were the other blunt configurations of Figure 20. The windward ray was completely laminar at all angles tested (the all laminar condition is indicated with an arrow on the data point). Increasing the free stream unit Reynolds number produced a condition where the laminar boundary layer previously had been observed to be in a rather delicate balance; one in which transition could be easily initiated (in Figure 14 this corresponds to situations where X_T/X_{SW} is in the range of 0.02 to 0.03 and is also illustrated in Figure 15 for the Tunnel F data). The $\alpha = 0^\circ$ data shown in Figure 21 are the same data shown in Figure 14. A small change in Reynolds number (open circles) produced a wide range in transition locations. A unit Reynolds number of 28 million was selected for the angle of attack tests in order to keep transition from moving off the model on the windward ray. The results are shown with the solid circles. The transition locations seemed to have two preferred locations - a large displacement and a short displacement. It can be seen from this figure that several transition trends are possible at this condition; that is, either a forward or rearward movement with angle of attack, and it was not possible to predict where transition would occur.

Ideally, to observe transition shape patterns, one would like to have a model completely saturated with heat transfer gages. Usually such a practice is not possible and compromises are necessary. For this series of experiments, the model had two rays of thermocouples and circumferential patterns were obtained by rolling the model and making repeat runs. Test conditions could be duplicated very closely and the transition location for a given situation could be closely reproduced. Transition patterns were obtained by making a composite picture from the results of several runs. It is believed the results of this procedure provided a good representation of the pattern occurring during a single test. Figures 22 through 24 are samples of the transition asymmetries found at two degrees angle of attack and $M_\infty = 5.9$. The windward meridian is $\phi = 0^\circ$ and $\phi = 180^\circ$ is the leeward meridian. The shaded area represents the transition region with "B" indicating the beginning of transition and "E" the end of transition. The beginning and end of transition at $\alpha = 0$ is shown for reference along with calculated values of local Re_θ at $\alpha = 2^\circ$.

Figure 25 illustrates how the transition front moves with angle of attack. The data shown are for the 8 degree half angle cone with a 10% blunt tip. All data were obtained at $M_\infty = 5.9$ and a free stream Reynolds number of 19.4×10^6 per foot. Small angles of attack were found to produce large transition asymmetries.

Figure 26 illustrates how the transition front moves as a function of noisetip bluntness. Model and test conditions are the same as indicated in Figure 25. Large transition asymmetries were associated with all three noisetips and the transition front moved rearward with increased bluntness.

For utilization of experimental results and comparison with other data, data are often presented in a nondimensionalized format. Potter, for example (Reference 31), prepared a data base of wind tunnel angle of attack transition data in nondimensionalized form in order to correct ballistic range transition data for angle of attack effects. A problem he encountered was a scarcity of angle of attack transition data. These

present data add to the angle of attack data base; however, it is still not possible to evaluate the generality of the results. The present results have the advantage of coming from one data source, whereas Potter's results represent a composite picture made up from several sources. Figure 27 presents the results found for the 8-degree half angle cone with a sharp tip, tested at $M_\infty = 5.9$ and $Re_\infty/Ft = 9.7 \times 10^6$. Potter's results are shown for comparison. Differences were found between the present results and those of Potter. The present results displayed a larger variation in transition location on the windward side of the model ($\phi = 0^\circ$ to 90°) and less variation on the leeward side ($\phi = 90^\circ$ to 180°). Also, the forward movement of transition on the leeward side ceased at $\alpha/\theta_c = 0.25$. The general trend of a rearward movement on the windward ray and a forward movement on the leeward ray with angle of attack was consistent with all data.

2. CONCLUSIONS

a. Transition locations were sensitive to small changes in angle of attack. Both the sharp and blunt tips produced a rearward movement of transition on the windward ray at small angles of attack.

b. The 30% blunt cone produced several transition trends and it was not possible to predict where transition would occur.

c. Large transition asymmetries were obtained at small angles of attack for both sharp and blunt tip configurations.

d. Some differences in angle of attack transition trends were observed when comparing the present data with other data.

42

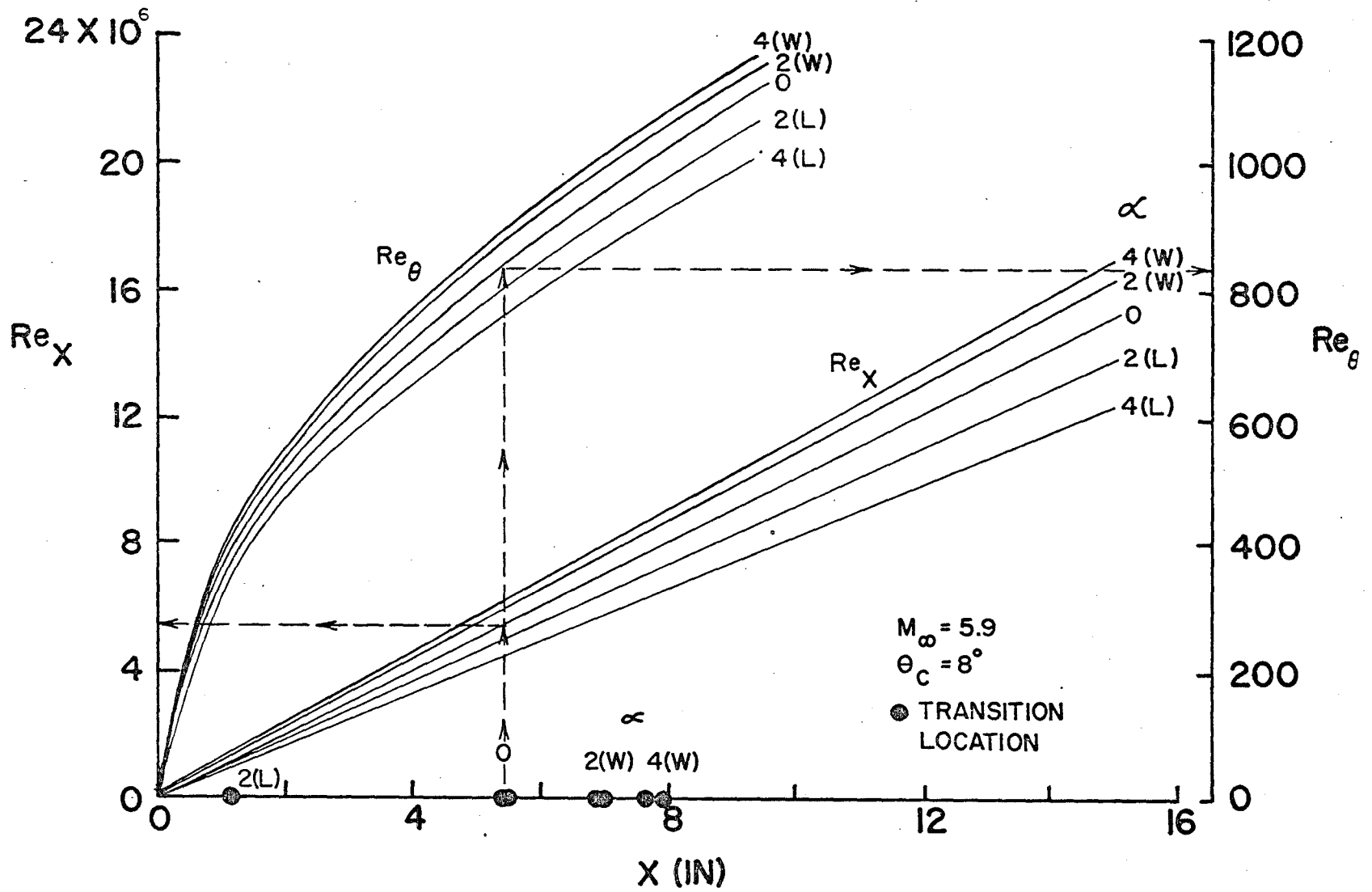


Figure 19. Local Reynolds Number Calculations for a Sharp Cone at Angle of Attack

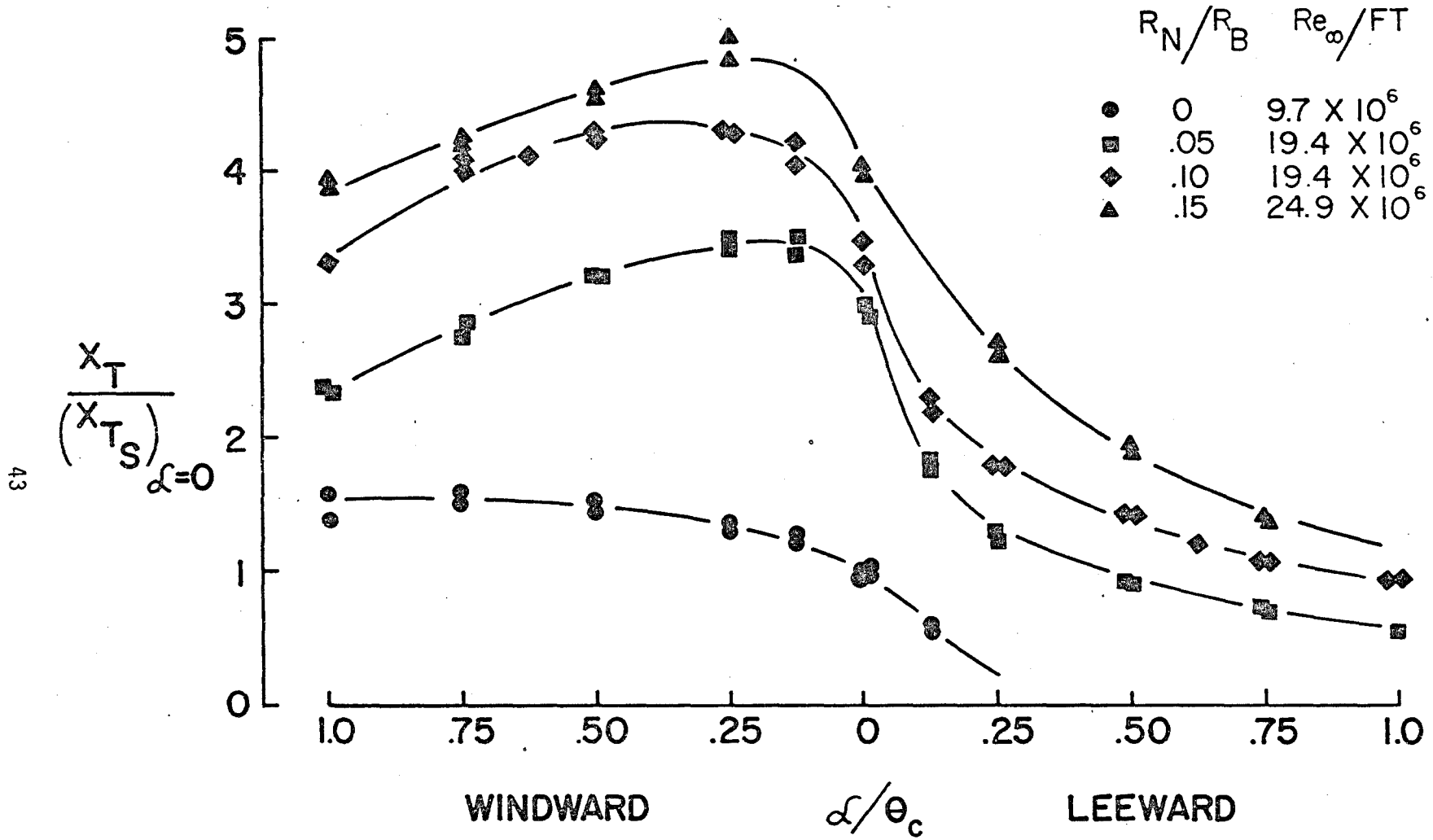


Figure 20. Transition Movement with Angle of Attack for an 8-Degree Half Angle Cone At $M_\infty = 5.9$

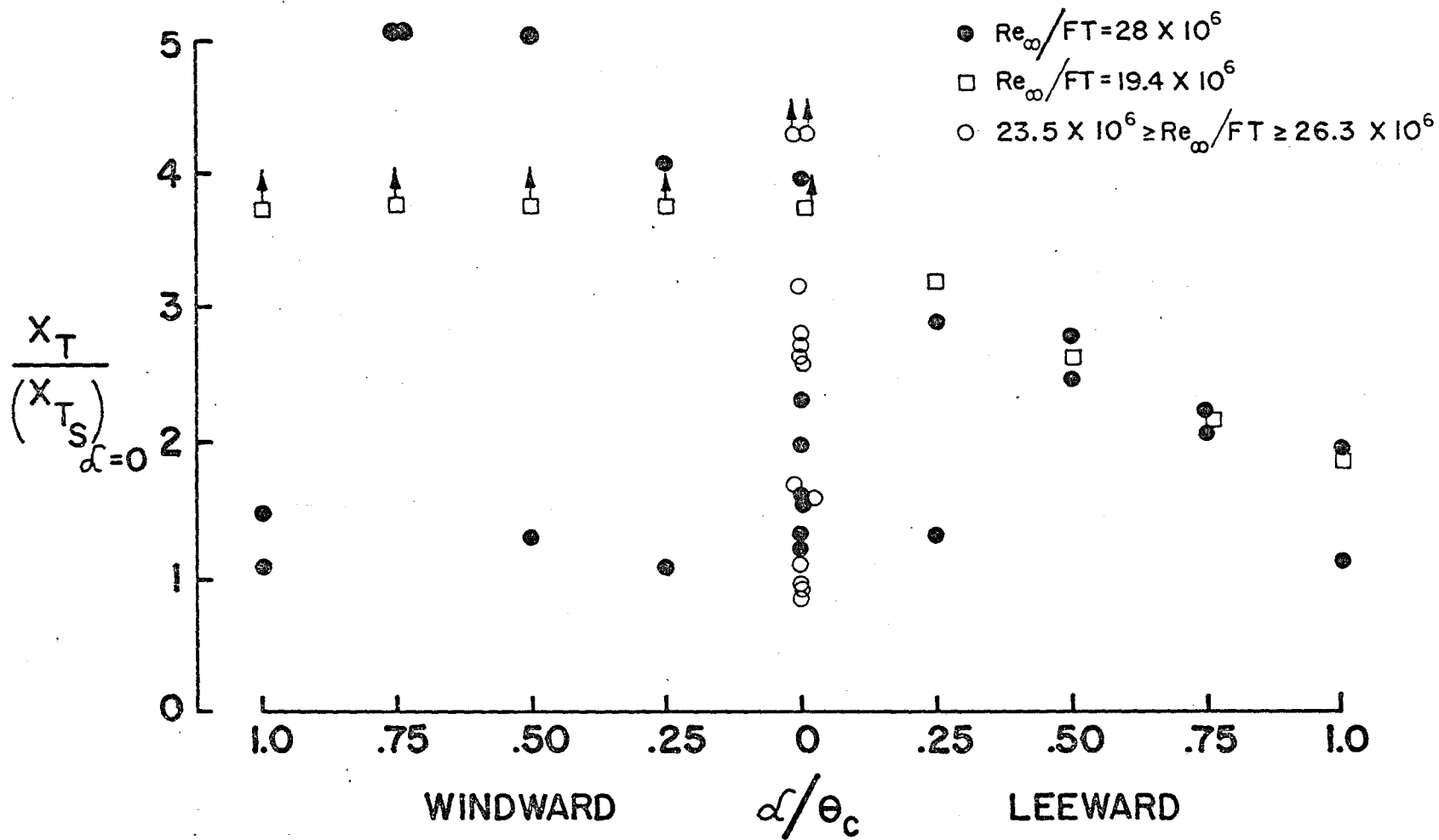


Figure 21. Transition Movement with Angle of Attack for an 8-Degree Half Angle Cone with 30% Bluntness At $M_{\infty} = 5.9$

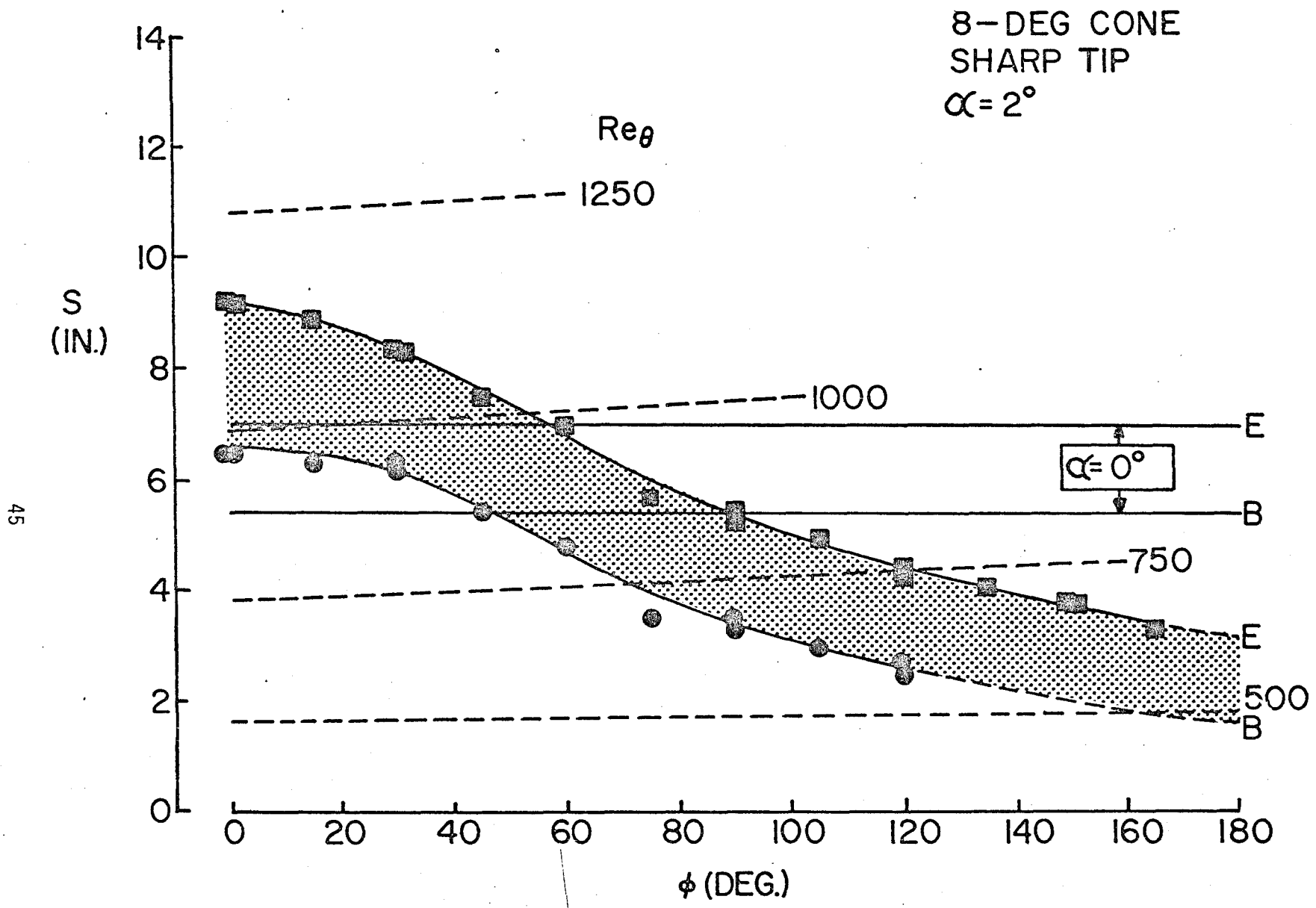
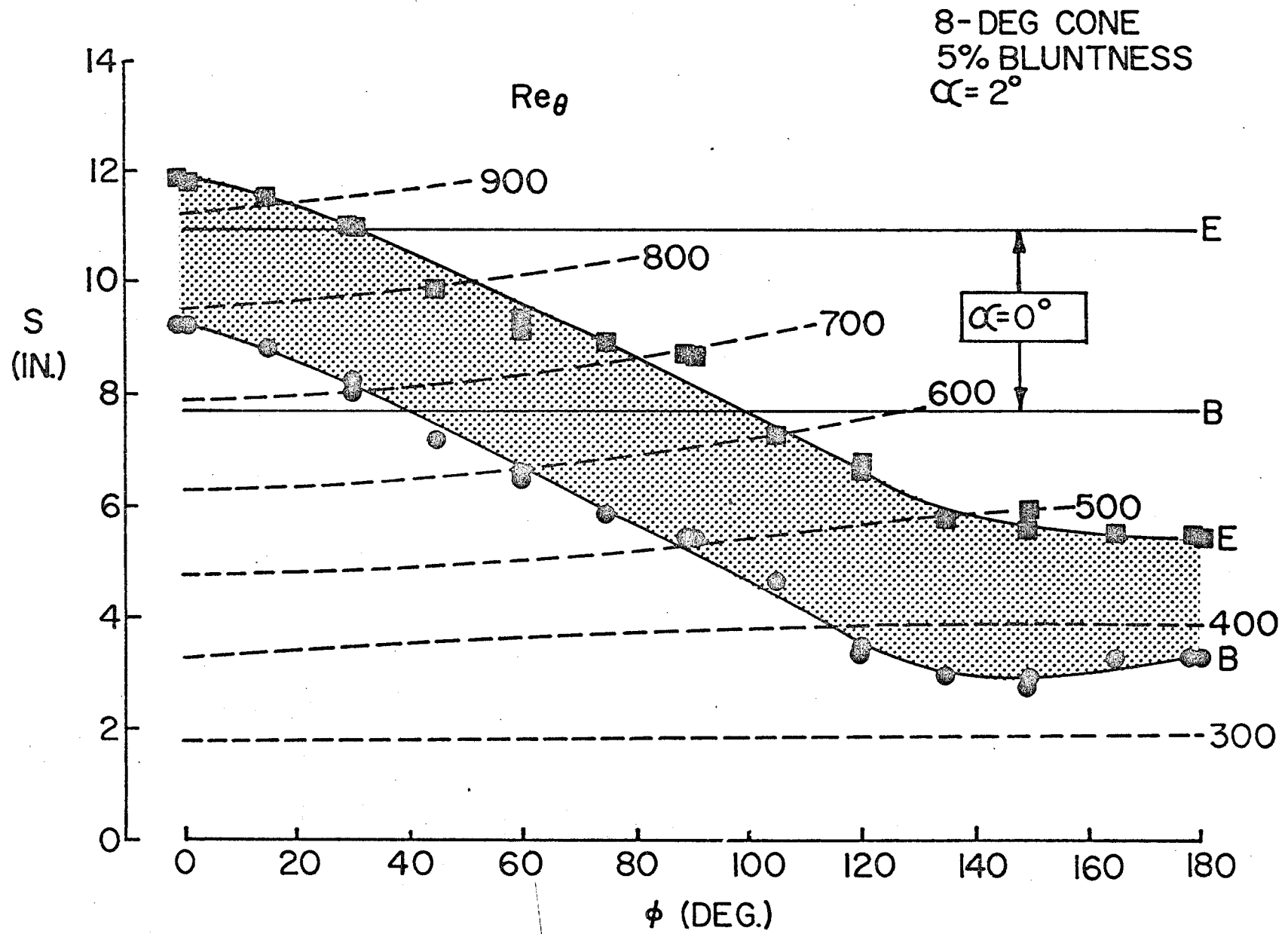
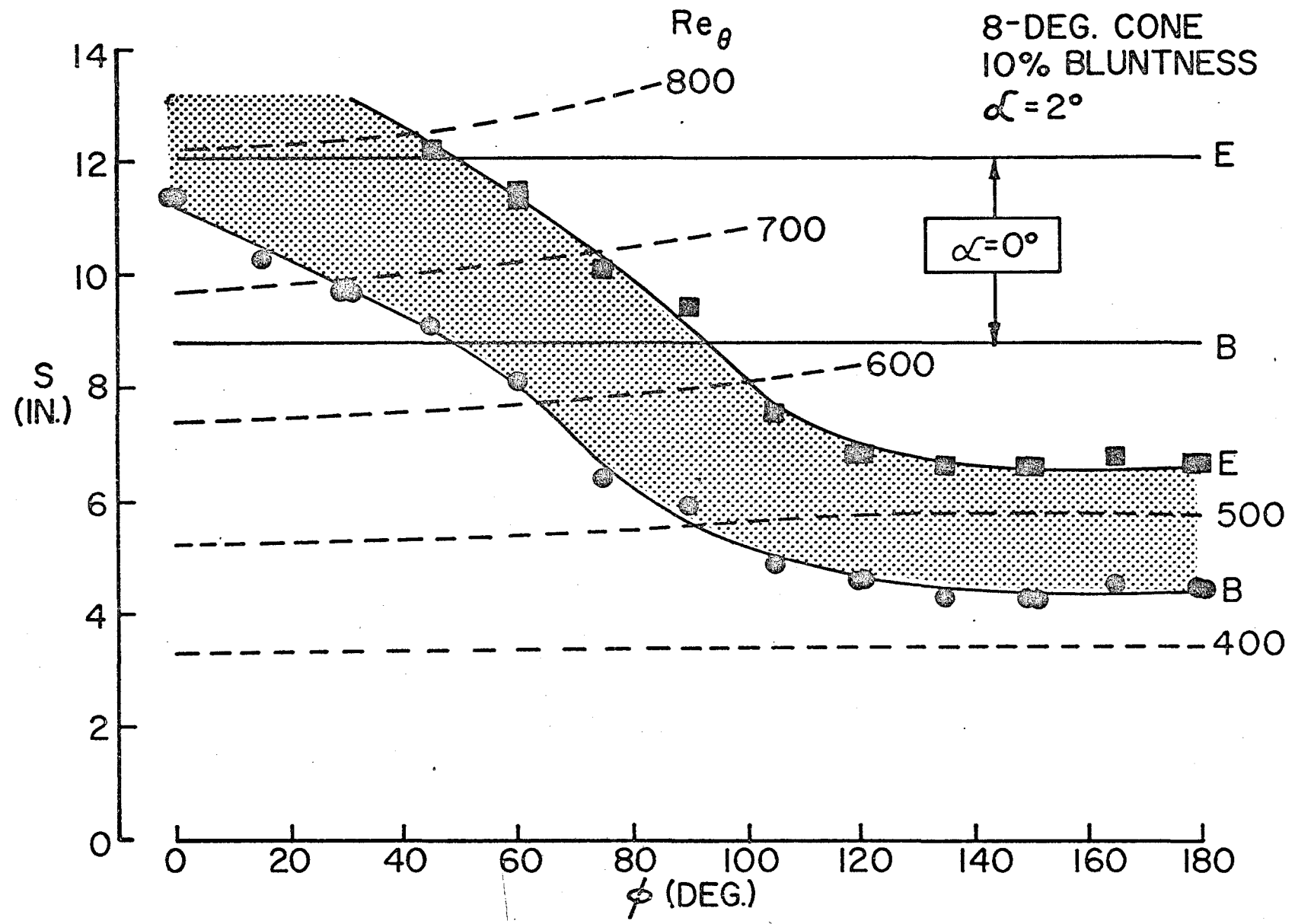


Figure 22. Transition Pattern At $\alpha = 2^\circ$, Sharp Tip



46

Figure 23. Transition Pattern At $\alpha = 2^\circ$, 5% Bluntness



47

Figure 24. Transition Pattern At $\alpha = 2^\circ$, 10% Bluntness

10% BLUNTNESS
SIDE VIEW

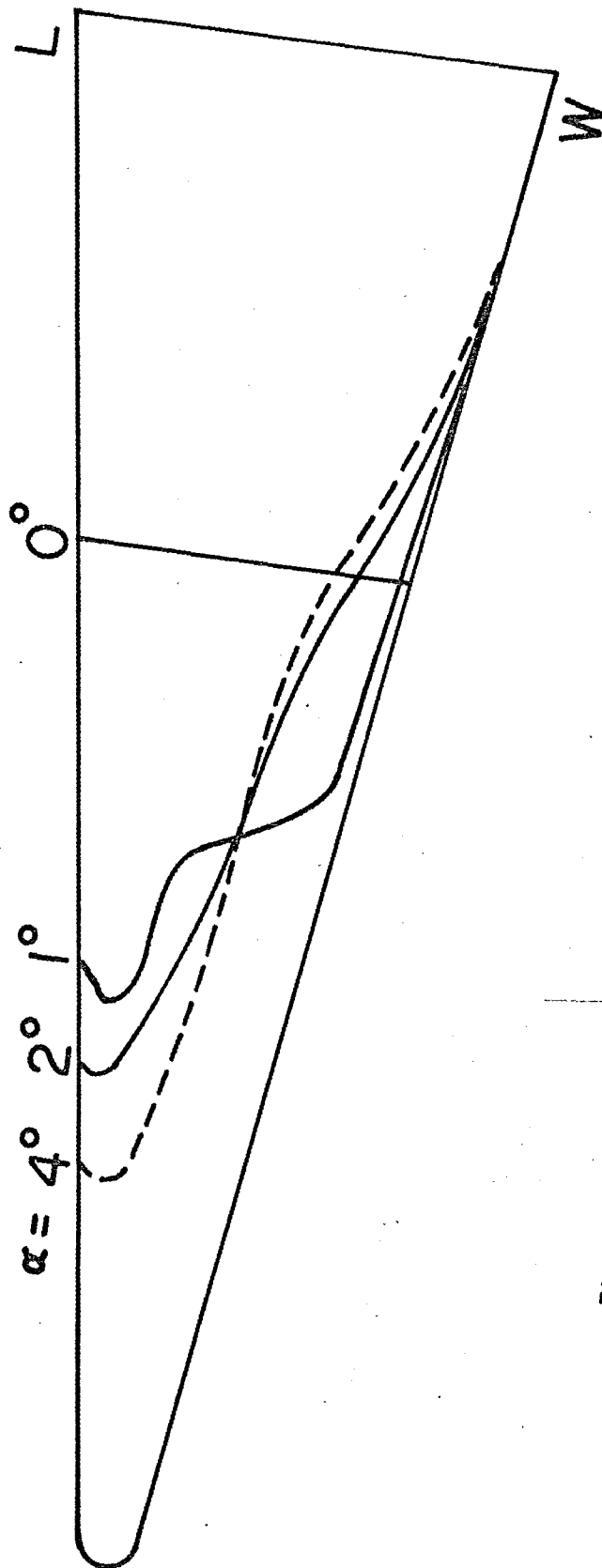
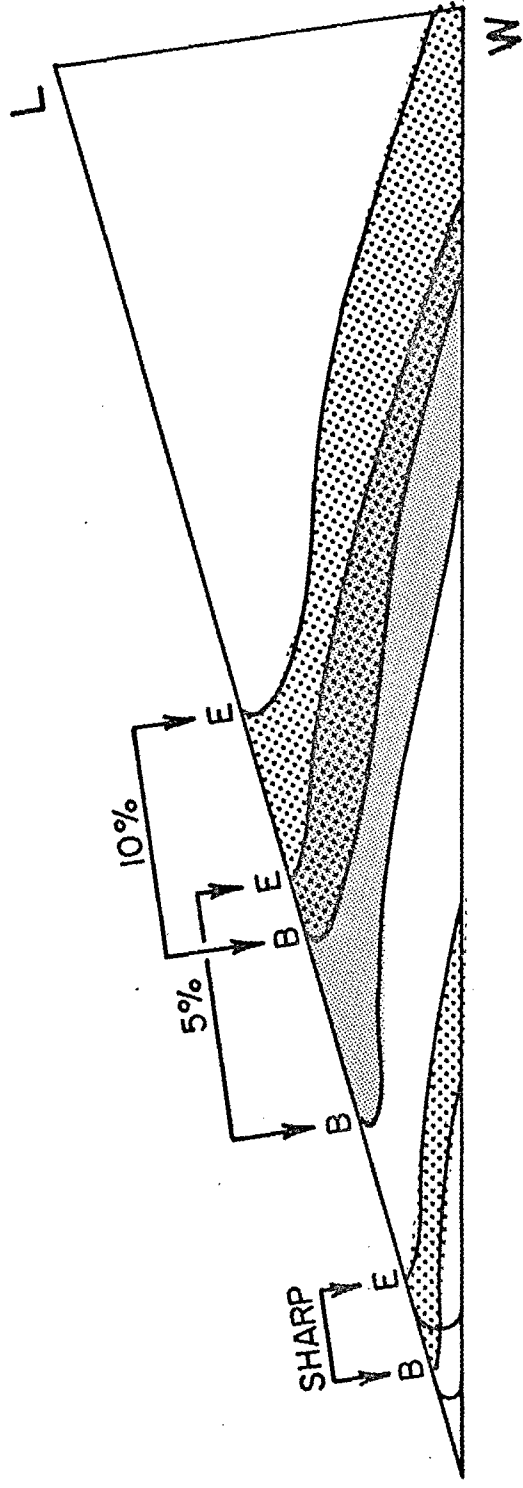


Figure 25. Transition Pattern VS Angle of Attack, 10% Bluntness

$\alpha = 2^\circ$
SIDE VIEW



Transition Pattern for Different Nosetips, $\alpha = 2^\circ$

Figure 26.

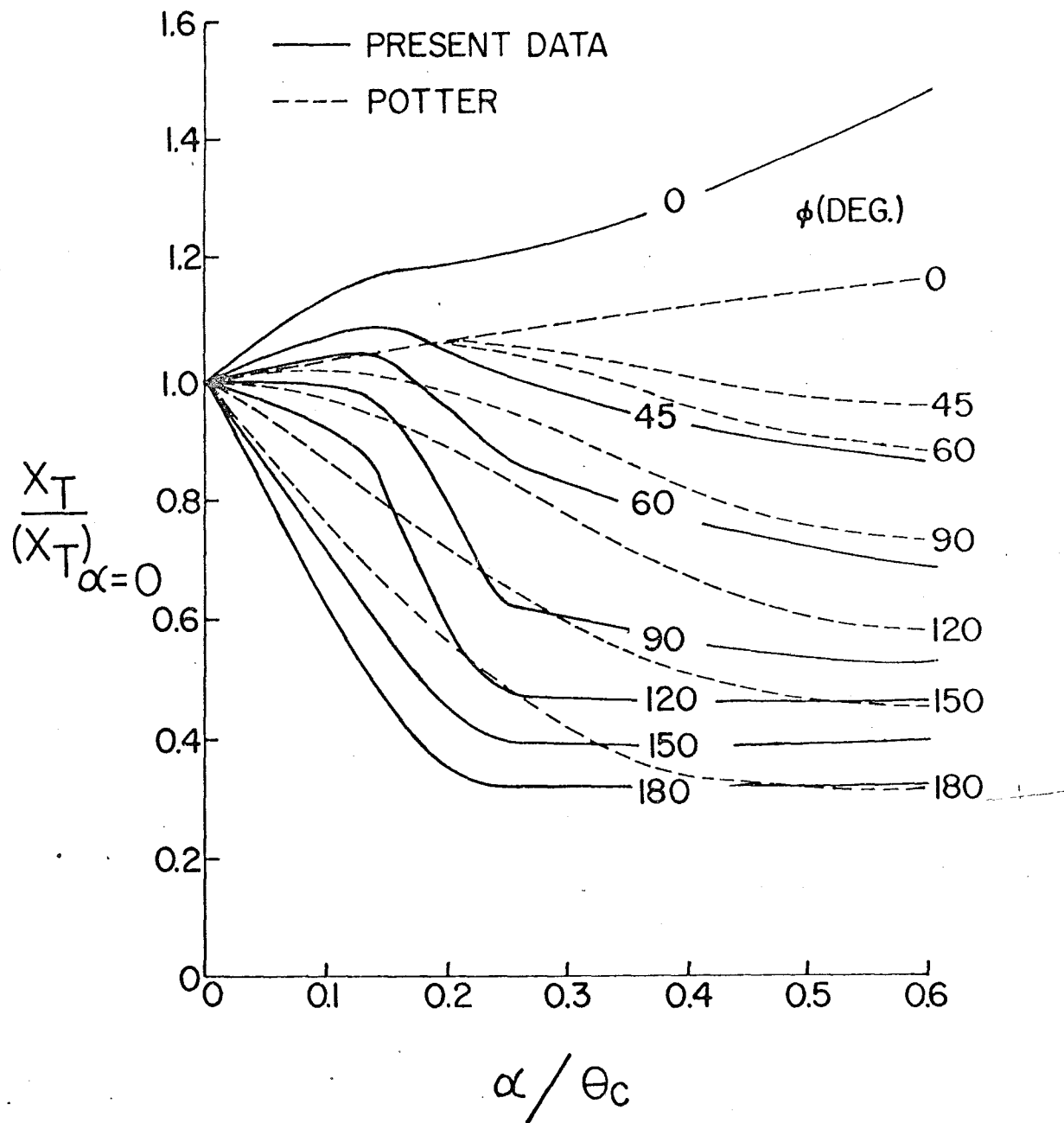


Figure 27. Transition Asymmetry Due to Angle of Attack

SECTION VI
TRANSITION ON A BICONIC CONFIGURATION

A 14-degree half angle cone section was added to the front portion of the 8-degree cone to obtain data on a biconic configuration. The junction of the two cones was at a station 35% of the sharp 8-degree cone length. Two tip configurations were tested; sharp and 7.4% of the base radius (21% of the base of the 14-degree cone). The tests were conducted in the Mach 6 wind tunnel.

1. RESULTS

A sample of the transition data on the biconic configuration with a sharp tip is shown in Figure 28. The local values of Mach number, Reynolds number and heat transfer coefficient (for a recovery factor of one) predictions were obtained from the boundary layer code of Reference 25. The local Reynolds number at the transition location was about 6 million. Similarly, transition Reynolds number on the sharp, 8-degree cone were nearly 6 million for this freestream condition. Figure 29 presents similar results for the blunt biconic configuration. The local transition Reynolds number for this situation was about 3 million, which was comparable to local transition Reynolds numbers on the 8-degree cone with moderate blunting (Figure 18).

Figure 30 indicates the transition locations on the windward and leeward rays of the sharp and blunt biconic configurations. The data are normalized with the transition location on the sharp biconic at $\alpha = 0^\circ$, in a manner similar to that used for the 8-degree cone data. It was found that the junction between the two cones often acted as a boundary layer trip in an unpredictable manner. In respect to this apparent tripping of the boundary layer, it should be noted that special care was taken in the construction of the model to avoid surface irregularities at this junction. The 14-degree nose piece was constructed with a slight rearward facing step at the junction; then after the model was assembled it was polished to provide a smooth connection. The upper windward curve for the blunt biconic corresponds to transition on the aft cone. The lower windward data correspond to transition near the

junction of the two cones. For the sharp biconic, the upper curve also relates to transition on the aft cone. At $\alpha = 4^\circ$, transition occurred on the windward ray at the junction of the cones for both tests. At $\alpha = 8^\circ$, one test produced transition on the aft cone and a duplicate run had transition on the fore cone.

Figures 31 and 32 are interferograms obtained for the sharp and blunt biconic configurations with a dual plate holographic interferometry system.

2. CONCLUSIONS

a. The answer to the question of whether or not boundary layer transition was delayed on the biconic configuration depends upon the manner in which the data are interpreted. In terms of local Reynolds number there was no significant delay since the local transition Reynolds numbers were essentially the same for the biconic and cone configurations. However, when considering the location of transition and the length of laminar run before transition, transition moves rearward on the biconic configuration ($X_T \approx 5.4$ inches for the sharp cone and $X_T \approx 6.6$ inches for the sharp biconic configuration; when both configurations were tested at $M_\infty = 5.9$ and $Re_\infty/Ft = 9.7 \times 10^6$).

b. The junction of the two cones often promoted an early transition.

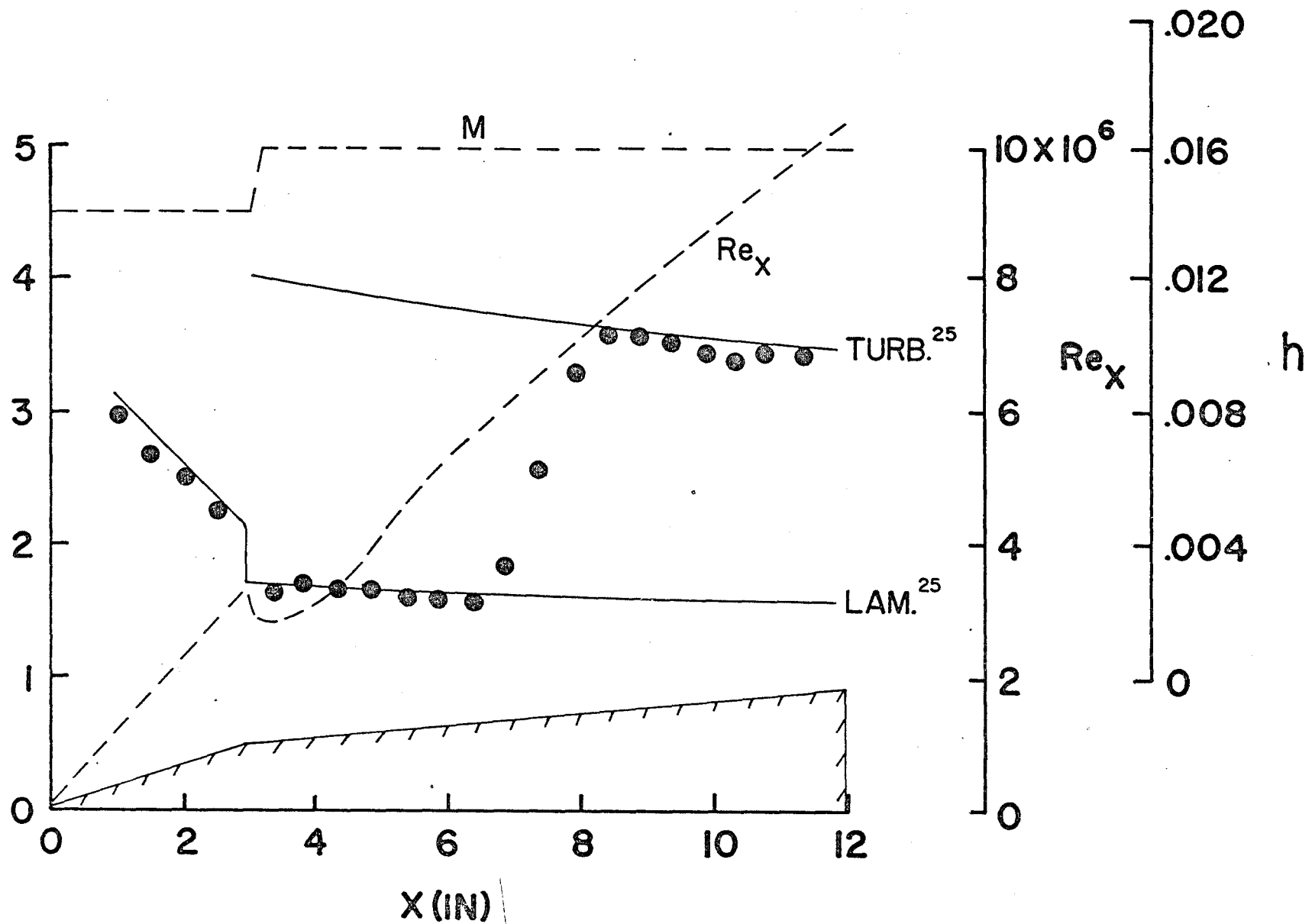


Figure 28. Heat Transfer Coefficient Distribution (Recovery Factor of One) and Local Flow Calculations on a Biconic Configuration with a Sharp Tip At $M_\infty = 5.9$

54

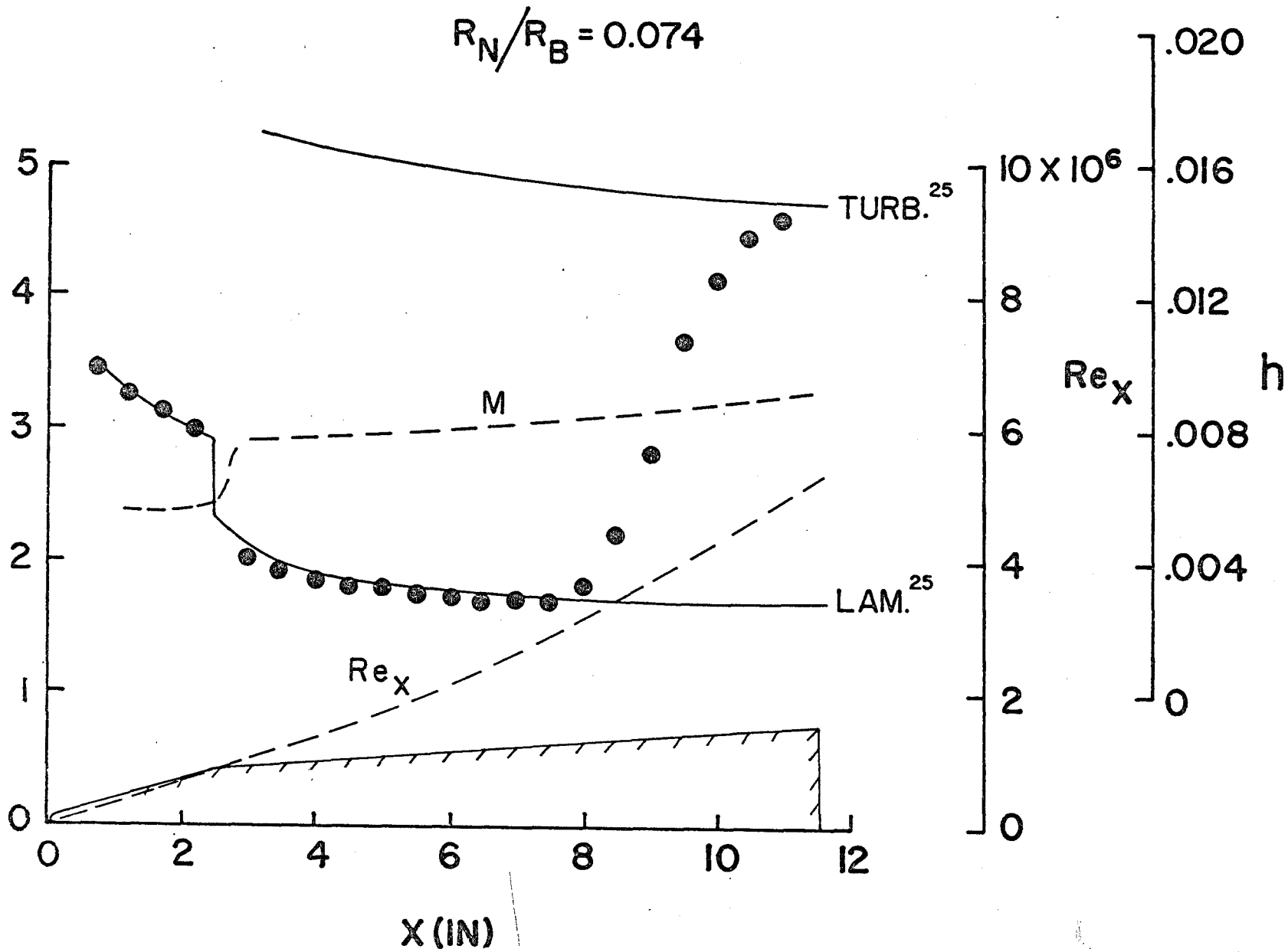


Figure 29. Heat Transfer Coefficient Distribution (Recovery Factor of One) and Local Flow Calculations on a Biconic Configuration with a Blunt Tip At $M_\infty = 5.9$

55

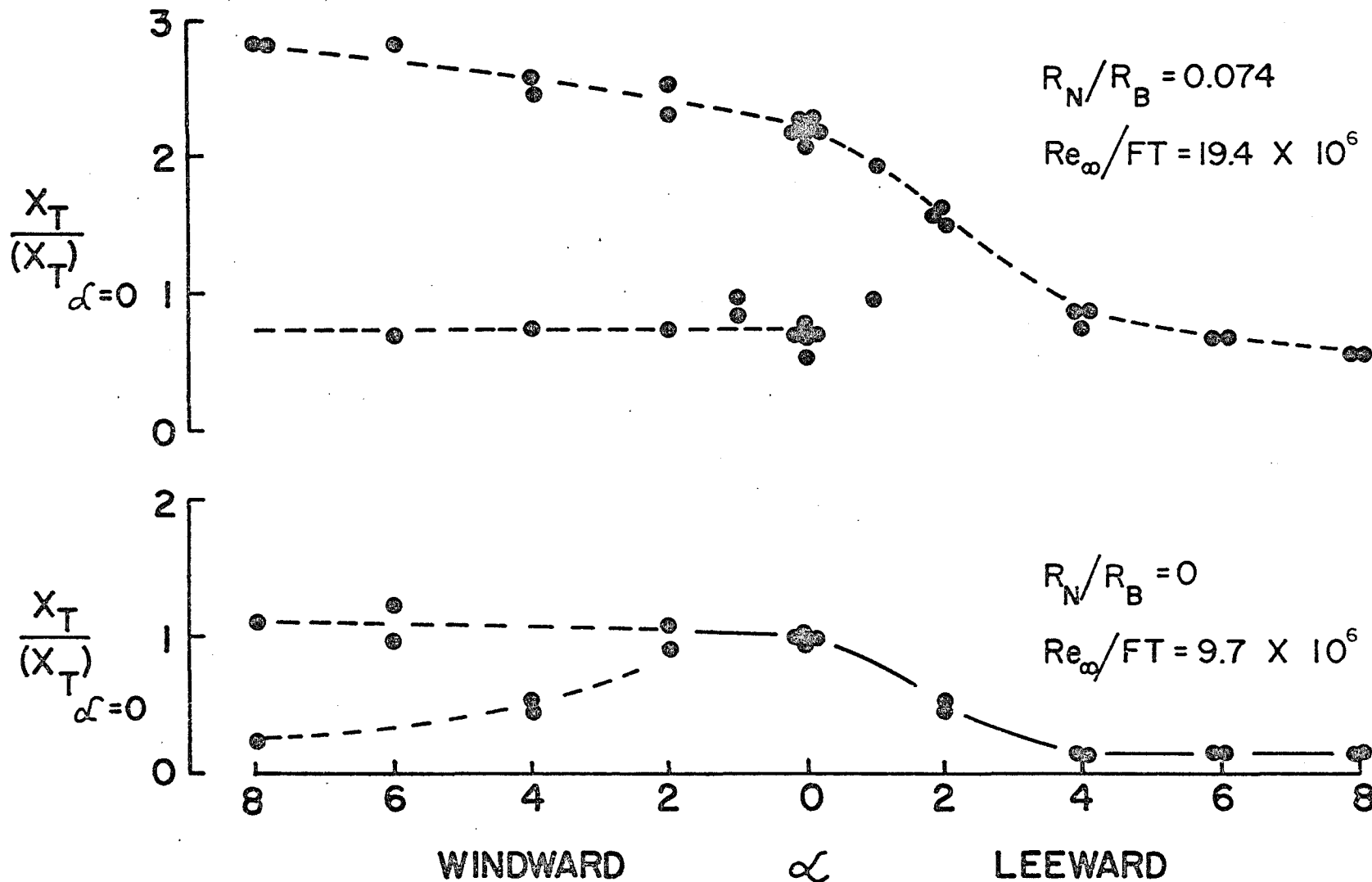


Figure 30. Transition Movement with Angle of Attack for the Biconic Configuration At $M_\infty = 5.9$

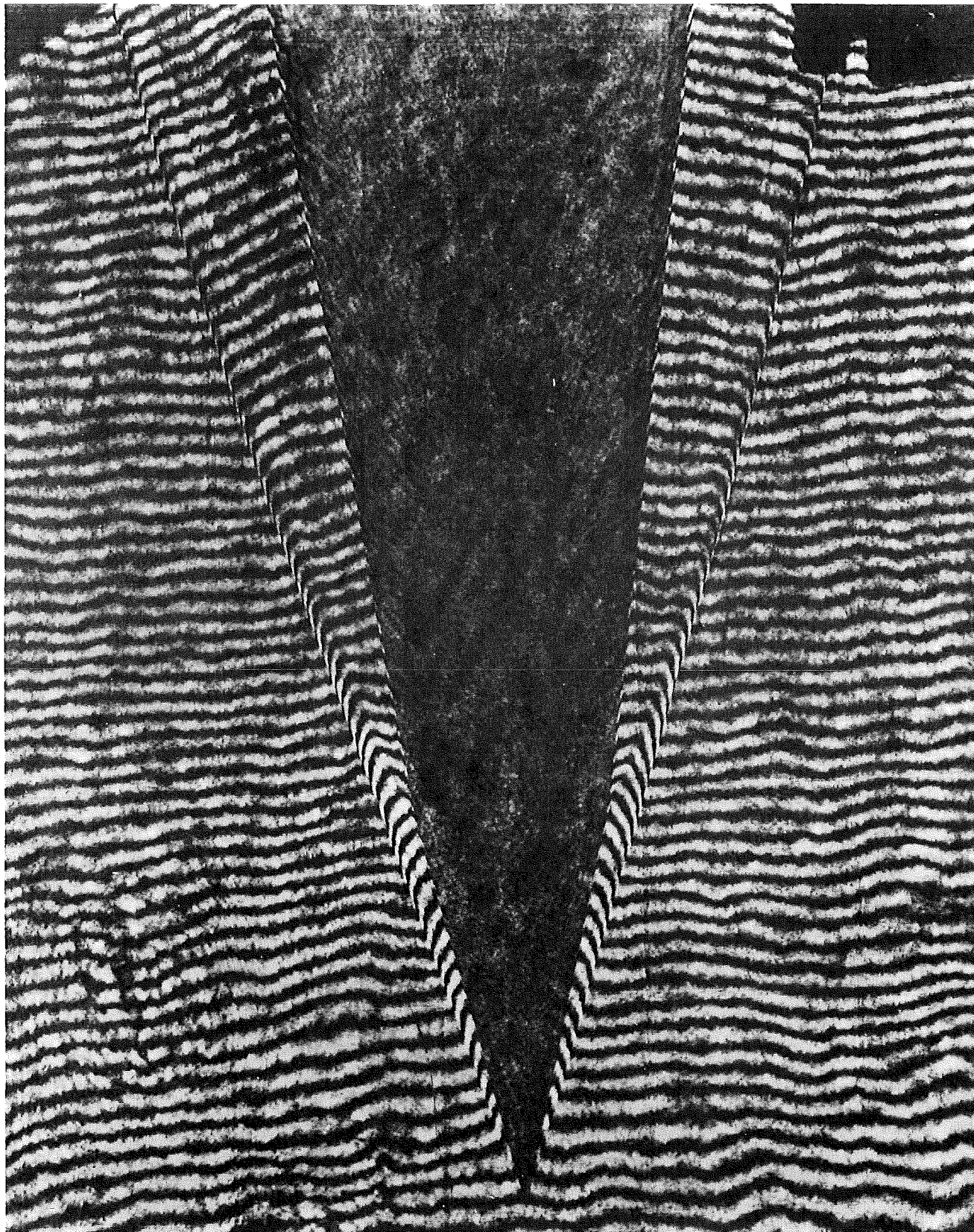


Figure 31. Interferogram of the Sharp Biconic Configuration At $M_\infty = 5.9$

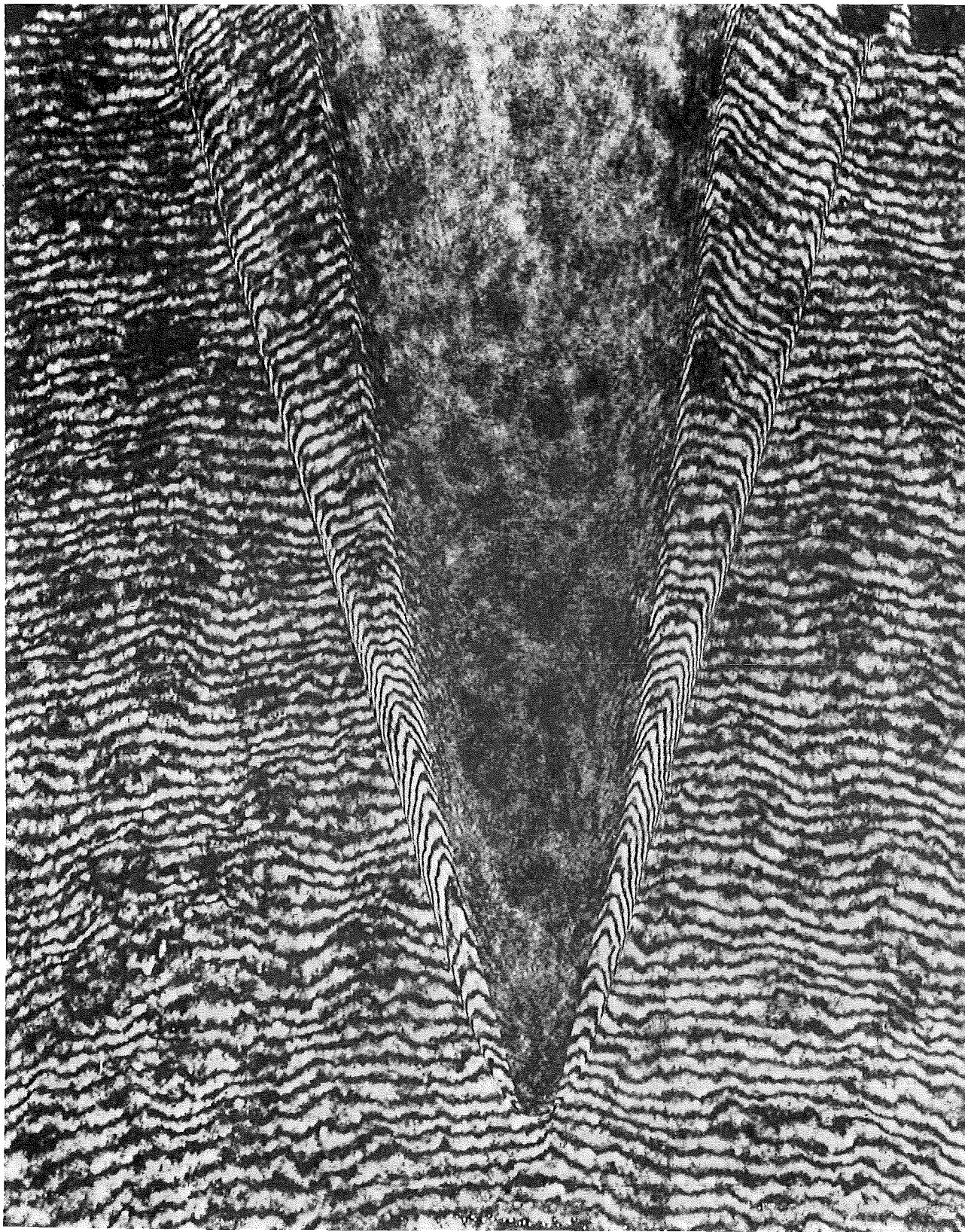


Figure 32. Interferogram of the Blunt Biconic Configuration At $M_\infty = 5.9$

SECTION VII

EXPERIMENTAL STUDIES OF THE FDL FLARED-NOZZLE
ABLATION SIMULATION TECHNIQUE

The arc-jet facility, such as the FDL Re-Entry Nosetip (RENT) Facility, provides the major source of ground test experimentation for reentry nosetip ablation studies. The large power requirements of such facilities and technology limitations of arc-jets have imposed constraints upon the simulation capability of these facilities. The flow region usable for testing is small and the flow Mach number is low supersonic in order to achieve desired stagnation conditions. The RENT facility was modified to compensate for its low Mach number (1.8) by installing a flared nozzle (Reference 32) in place of the usual contoured nozzle designed to produce parallel flow. This nozzle has a flared expansion section producing a diverging flow in order to closely duplicate the hypersonic pressure and heat flux distributions around the nosetip of a model.

The primary motivation for this test program was to assist in the study of the hypersonic nosetip simulation capability of a low Mach number flared nozzle by comparing data obtained in a Mach 1.8 flared nozzle flow field with that in a Mach 6 parallel flow field. Of particular interest was the ablation configurations obtained under test conditions which produced boundary layer transition on the tip.

1. EXPERIMENTAL APPARATUS

The experiments were conducted in two of FDL's wind tunnel facilities, the 20 Inch Hypersonic Wind Tunnel and the Mach 6 High Reynolds Number Facility. The 20 Inch HWT (References 33, 34) was equipped with a flared nozzle that was geometrically scaled by a factor of two from the flared nozzle (Reference 32) used in the RENT leg of the FDL 50MW Facility. This flared nozzle (Figure 33) was installed at the outlet of the hypersonic nozzle of the 20 Inch HWT. Flow straighteners were installed upstream of the flared nozzle and this portion of the hypersonic nozzle served as a reservoir for the flared nozzle. A sketch of the modified facility is shown in Figure 34. The Mach 6 High Reynolds

Number Facility (Reference 8) was operated in the normal configuration. Both of these facilities are essentially perfect gas wind tunnels because of their moderate flow temperature.

Before the tests were conducted in the 20 Inch HWT, a series of calibration runs was made to determine the flow field characteristics of the flared nozzle configuration. Pitot pressure surveys were made at six different stations downstream of the nozzle exit at one inch intervals and the distribution along the tunnel axis was measured at 0.2 inch intervals. An example of the transverse surveys is shown in Figure 35. These data are for a flared nozzle reservoir pressure of 60 psia, but all of the data exhibited similar results. The flow field has the characteristics of the jet of an under-expanded nozzle. The axial distributions of both pitot pressure and Mach number are shown in Figure 36. Data for three different reservoir pressures are included in Figure 36 and all show the same distributions. Included in Figure 36 are some data (Reference 32) from the flared nozzle installed in the FDL RENT Facility. The characteristics are similar but the pitot pressure decays faster in the FDL RENT flared nozzle than in the 20 Inch HWT configuration. This difference may be due, in part, to the differences in the state of the gas in the two facilities. The RENT Facility has a bulk flow enthalpy of approximately 3000 Btu/lb. compared to the moderate flow enthalpy of approximately 270 Btu/lb. for these tests. In general, it was concluded that the flow field existing in the 20 Inch HWT with the scaled up flared nozzle was quite similar to the flow field that exists in the 50 MW RENT leg.

The RENT standard 10 degree half angle sphere-cone model configuration was utilized for all of the tests. The geometry of the model is shown in Figure 37. The model nose diameter was made equal to the flared nozzle throat diameter in order to maintain geometric scaling with the RENT facility. A pressure model, a thin-skin heat transfer model, and a number of camphor models were all fabricated of the same sphere-cone configuration. The camphor models were machined from billets formed by vacuum compression molding of granular material stock, following the technique used extensively by Acurex Corporation/Aerotherm for the Passive Noretip Technology (PANT) program.

The pressure and heat transfer data were recorded by an analog to digital computer. The ablation characteristics were filmed by two 70mm movie cameras at approximately 5 frames/second. The cameras were positioned so that both a side view and a top view of the ablation model were filmed during each test.

2. RESULTS

Data were obtained with both the flared nozzle and the parallel flow Mach 6 nozzle under identical model stagnation pressures and total temperatures.

Figure 38 shows the sphere-cone pressure distributions obtained in the two different flow fields. Numerical calculations (Reference 35) for Mach 20 flow over the tested sphere-cone configuration are also shown. The pressure distribution on this sphere-cone configuration is only weakly dependent on Mach number for hypersonic flow conditions and the Mach 6 data were, as expected, just slightly higher than the Mach 20 calculated results. The flared nozzle data indicated that the flow overexpanded around the nosetip and cone such that the pressures were lower than those of a hypersonic distribution.

Samples of the heat transfer rate distributions obtained are shown in Figure 39. The Mach 20 laminar heat transfer rate distribution predicted by Lees (Reference 36) is shown for comparison. Figure 39a shows the heat transfer rate distributions obtained for a model stagnation pressure of 22 psia and a total temperature of 1100°R. The free stream Reynolds number in the Mach 6 tunnel is $9.7 \times 10^6/\text{ft}$. for this condition and the local momentum thickness Reynolds number at the end of the model was approximately 400. At these stagnation conditions, a laminar boundary layer was obtained in both nozzle flows. As would be expected, the laminar heat transfer rate distributions followed the same trends as the pressure distributions with the Mach 6 data being slightly above the Mach 20 prediction and the flared nozzle data being slightly below. Figure 39b shows data obtained with a model stagnation pressure of 50 psia. Two sets of data obtained with the flared nozzle are shown. One set indicated a boundary layer which was still laminar

and the other shows an increase in heating which is possibly the onset of transition on the spherical tip, with the conical portion of the model remaining laminar. The Mach 6 distributions indicated transition on the nosetip and a turbulent boundary layer on the cone. These Mach 6 data were obtained after repeated use of the model and some increase in surface roughness of the nosetip resulted from particle (tunnel dust) impact. Therefore, only an approximate comparison of nosetip transition from the two nozzle flows can be made. The momentum thickness Reynolds number at the sonic point of the model in the Mach 6 flow was approximately 180 at this test condition.

Camphor models were ablated in both nozzles under identical model stagnation point conditions. The ablation history was recorded by 70mm cameras showing side and top views. Molds were made of the final ablated shape. Figure 40 contains side view profiles of the ablated shapes for three different tunnel conditions. Figure 40a ($P_{T_2} = 22$ psia) shows laminar nosetip ablation for both nozzle flows, with the maximum recession rate occurring at the stagnation point. Figure 40b ($P_{T_2} = 33$ psia) presents examples of transitional shapes. Although tests with the steel heat transfer model indicated a completely laminar boundary layer on the spherical tip for this condition, the camphor models produced configurations which have been identified with transitional flow. That is, a laminar plateau exists in the stagnation region, followed by regions of increased ablation. These data indicate that transition occurred closer to the stagnation point on the ablating models than on the non-ablating heat transfer models (although not necessarily at a smaller momentum thickness Reynolds number). This is consistent with the findings of other investigators (Reference 37). There was a general similarity of configuration obtained from both nozzles. Figure 40c ($P_{T_2} = 44$ psia) shows the results of a further increase in tunnel pressure. The laminar plateau soon disappeared and a conical-type configuration developed. The higher heating rates on the conical portion of the model in the Mach 6 nozzle flow produced greater ablation in this area. Figure 41 shows several photographs made from the 70mm movie film. The test conditions are the same as for the data of Figure 40c.

3. CONCLUSIONS

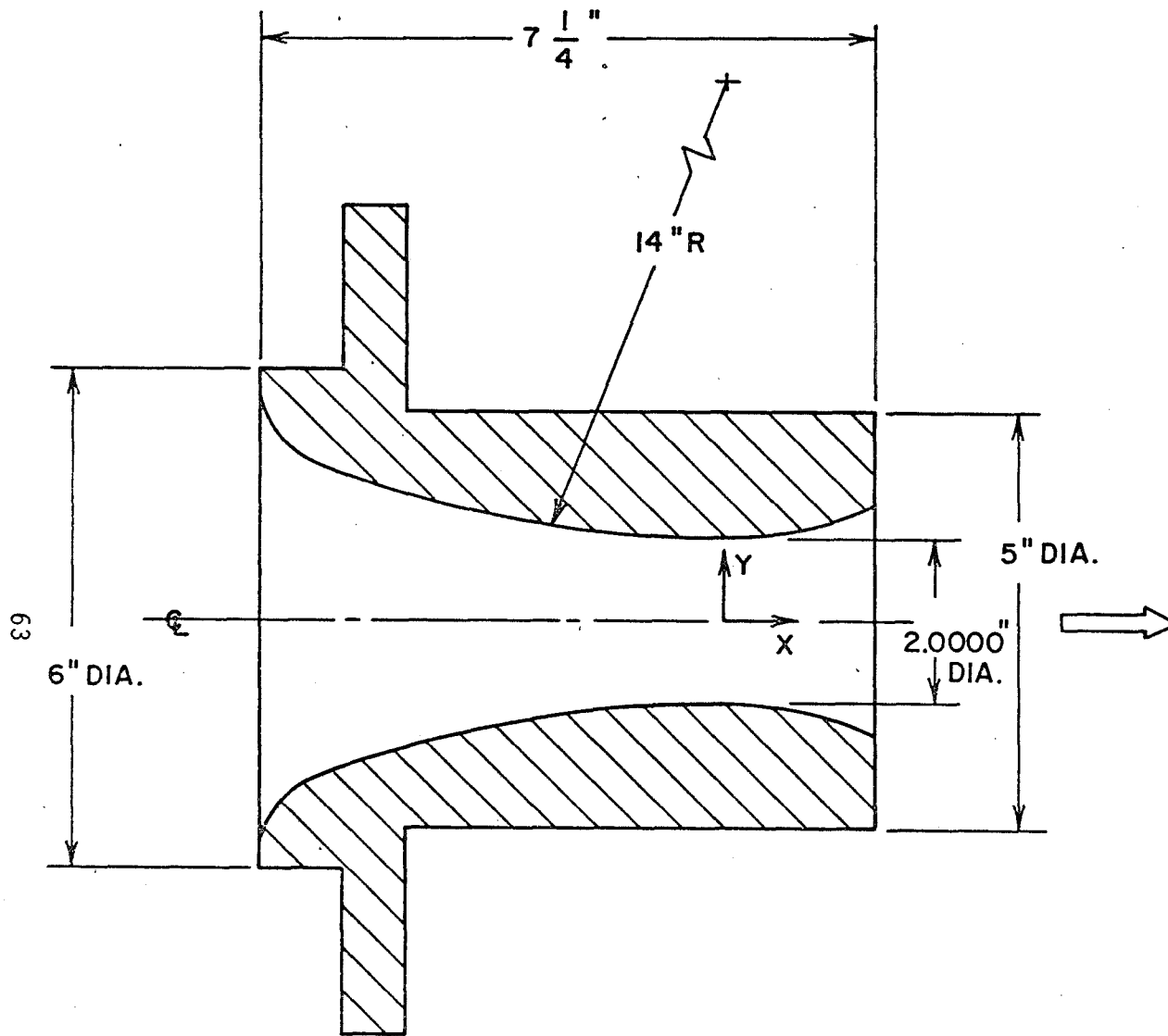
A sphere-cone configuration was tested in a Mach 6 parallel flow field and in a Mach 1.8 flared nozzle flow field. A comparison was made between the pressure distributions, heat transfer rate distributions, and ablated shapes measured in these two flow fields for identical model stagnation point conditions. The major conclusions were as follows:

a. The hypersonic pressure distribution on a sphere-cone configuration can be closely duplicated with a low supersonic flared nozzle flow. However, the diverging flow of the flared nozzle tested did produce a pressure distribution that was lower than numerical calculations for Mach 20 parallel flow.

b. At the lowest model stagnation conditions, both nozzle flows produced heat transfer distributions that closely followed the trends of the measured pressure distributions and agreed closely with the Mach 20 laminar predictions. At higher stagnation conditions, the heat transfer data obtained from the two nozzle flow fields indicated differences in the onset of the boundary layer transition both in the subsonic region of the model nosetip and on the cone portion of the model. Since the pressure distributions in the subsonic region did not differ greatly, variations in transition in this region are believed to be largely due to increased surface roughness caused by the impact of tunnel-generated particles during repeated use of the model. On the cone portion of the model, the larger differences in pressure are believed to be the major source of transition differences in this region.

c. For identical stagnation conditions, a general similarity of ablated camphor shapes was observed for both nozzle flows. The only distinct difference was associated with the higher ablation rates on the cone portion of the model in the Mach 6 parallel nozzle flow.

d. The results of the two series of tests substantiate that a low supersonic flared nozzle flow provides a practical and realistic extension to ground test facilities for nosetip ablation studies.



X (IN)	Y (IN)
0.00	1.0000
0.10	1.0012
0.20	1.0048
0.30	1.0106
0.40	1.0188
0.50	1.0294
0.60	1.0432
0.70	1.0576
0.80	1.0752
0.90	1.0952
1.00	1.1176
1.10	1.1422
1.20	1.1692
1.30	1.1982
1.40	1.2306
1.50	1.2644
1.60	1.3008
1.70	1.3396
1.80	1.3808

NOZZLE
COORDINATES

Figure 33. Mach 1.8 Flared Nozzle Geometry

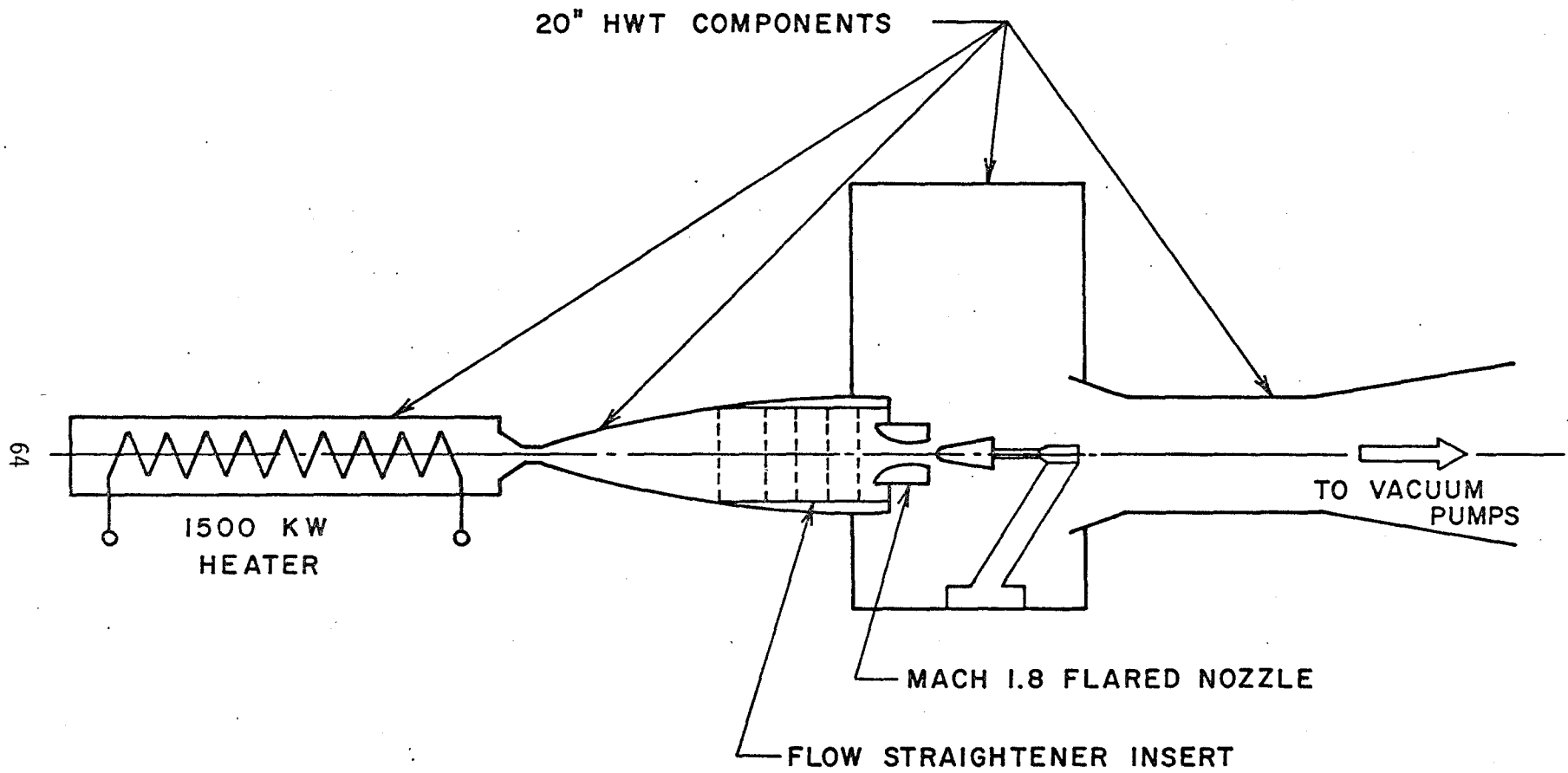


Figure 34. 20-Inch Hypersonic Wind Tunnel with Mach 1.8 Flared Nozzle Installed

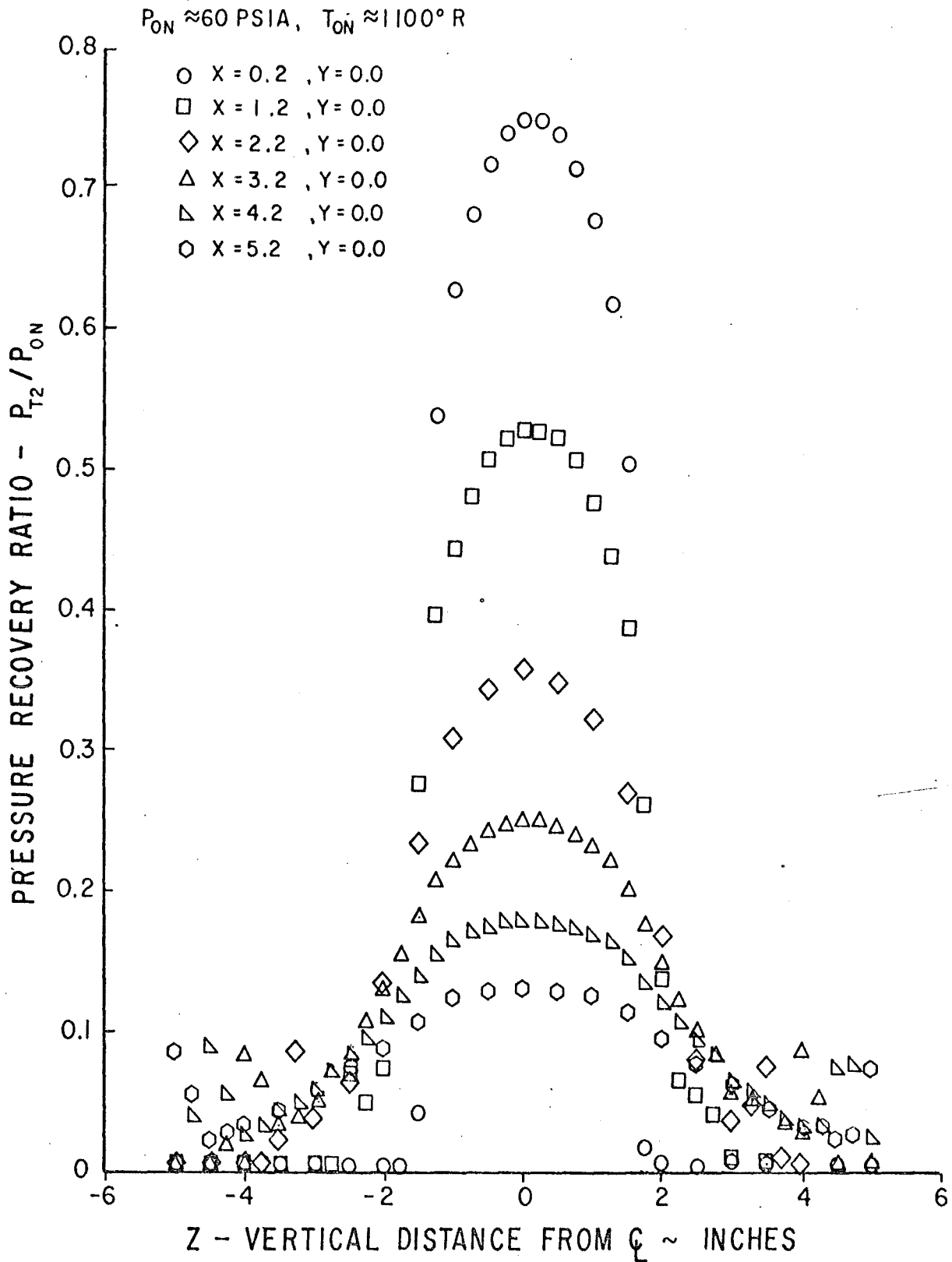


Figure 35. Pitot Pressure Distribution of Flared Nozzle

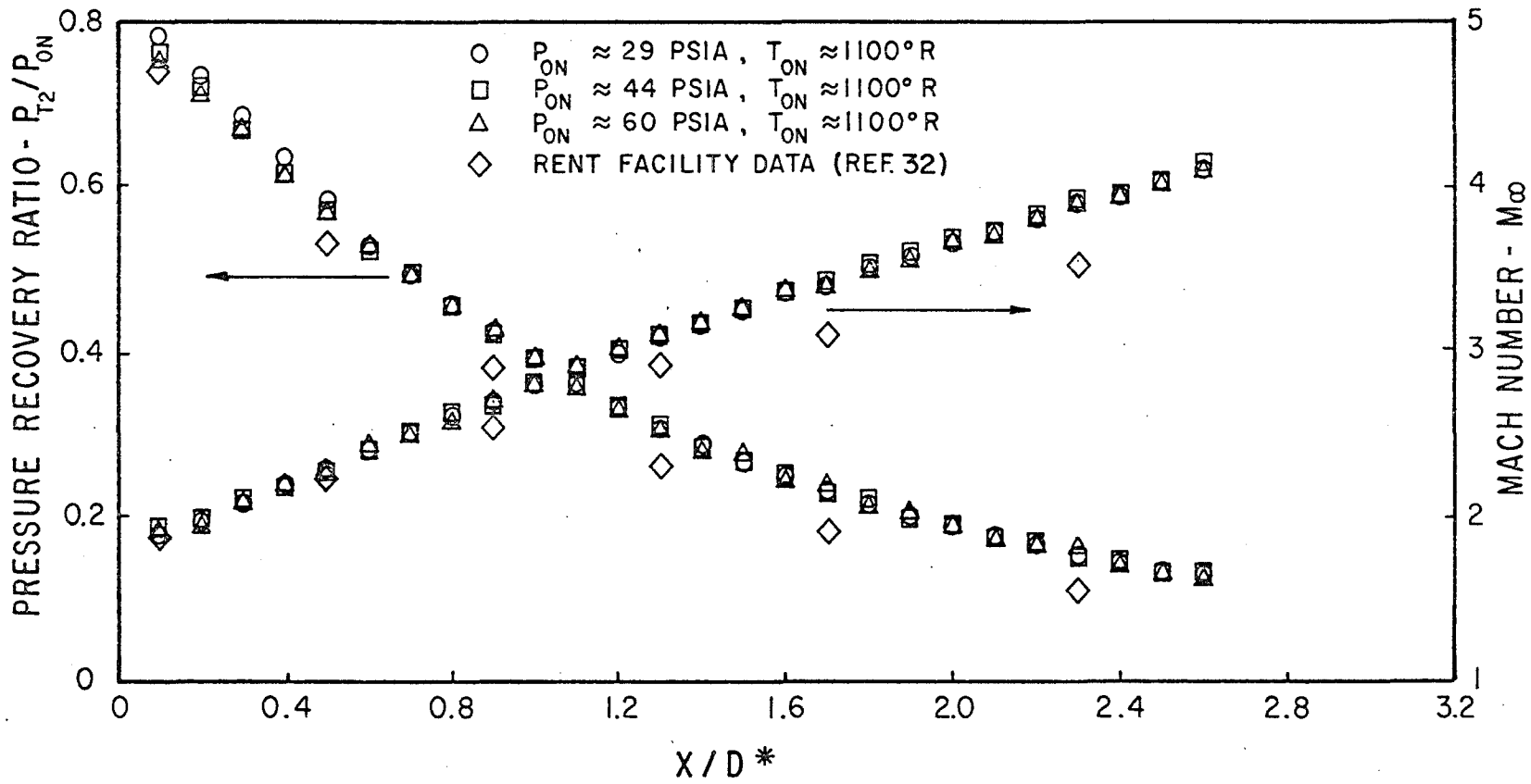


Figure 36. Axial Distribution of Pitot Pressure and Mach Number of Flared Nozzle

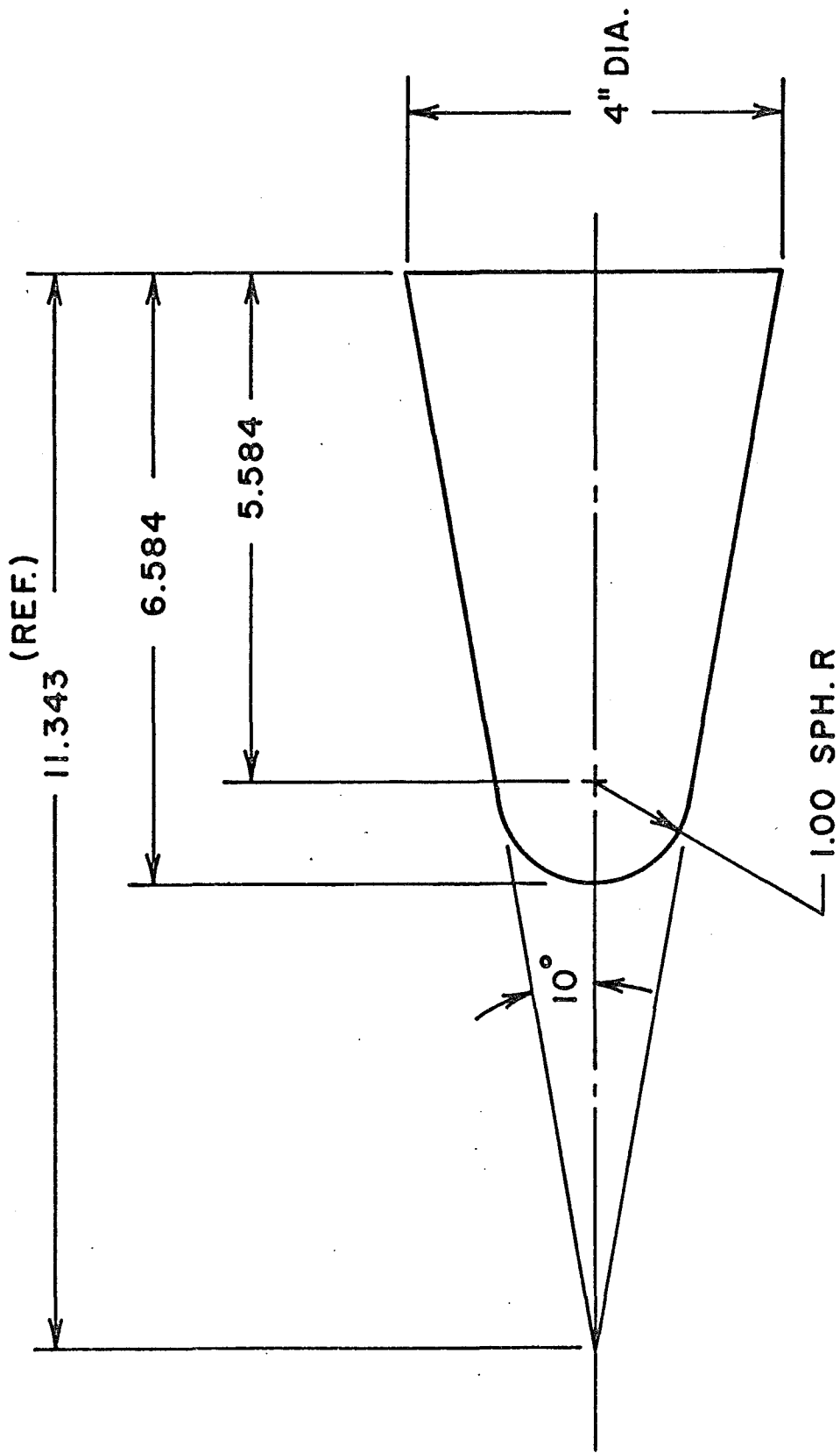
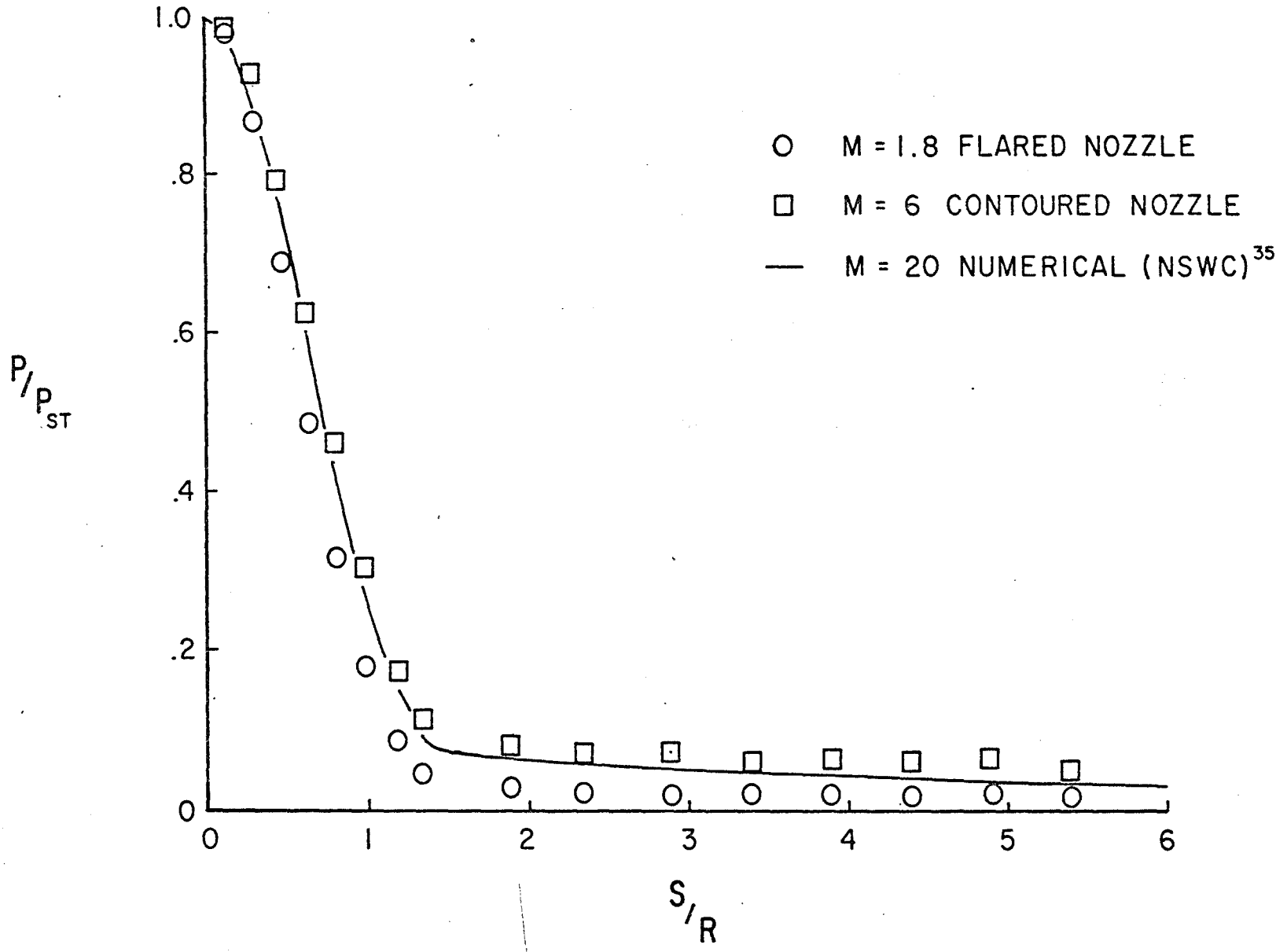


Figure 37. Model Geometry



88

Figure 38. Pressure Distribution, $P_{T_2} = 22$ psia, $T_0 = 1100^\circ R$

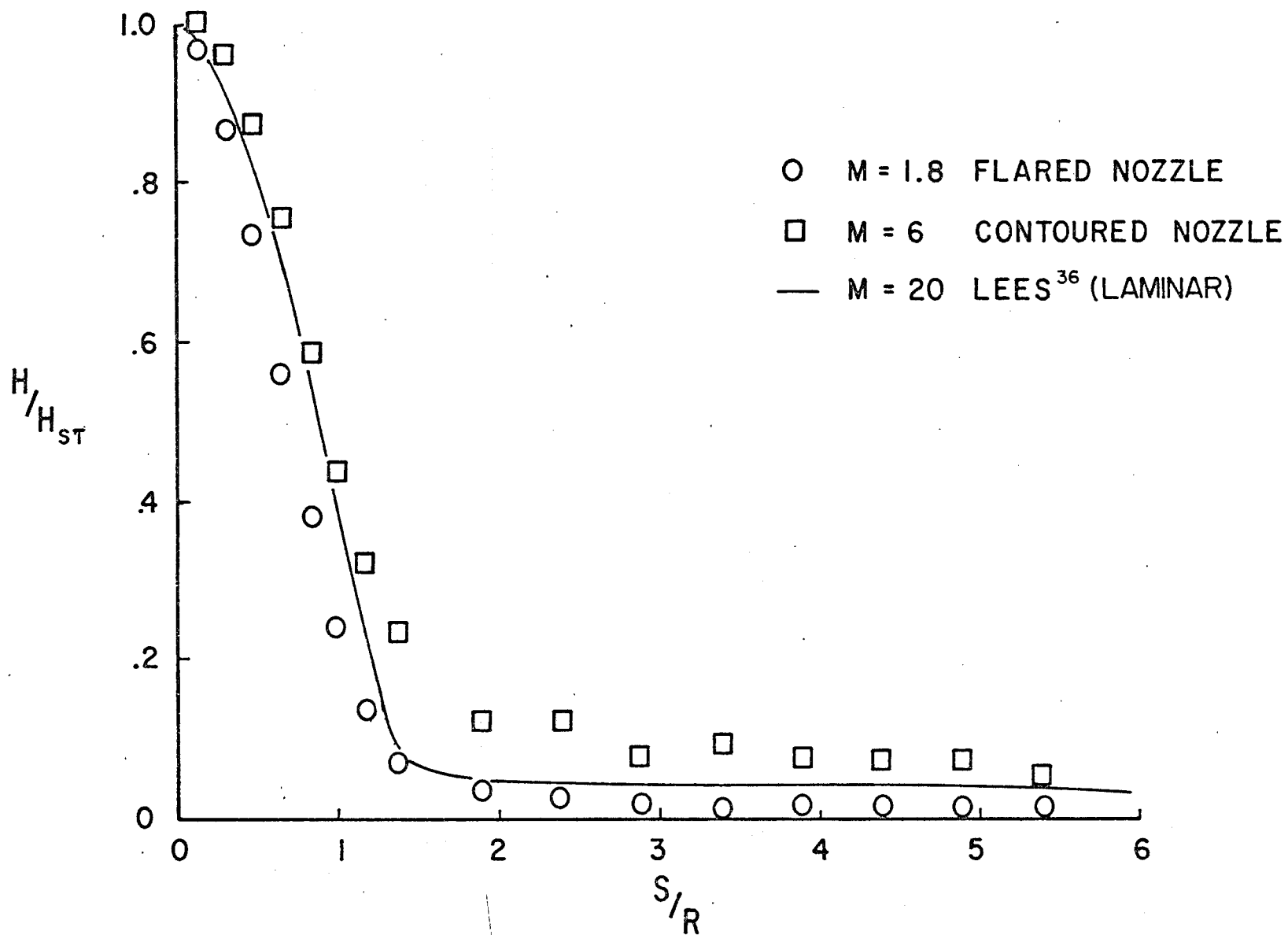


Figure 39a. Heat Transfer Coefficient Distribution, $P_{T_2} = 22$ psia,
 $T_0 = 1100^\circ\text{R}$

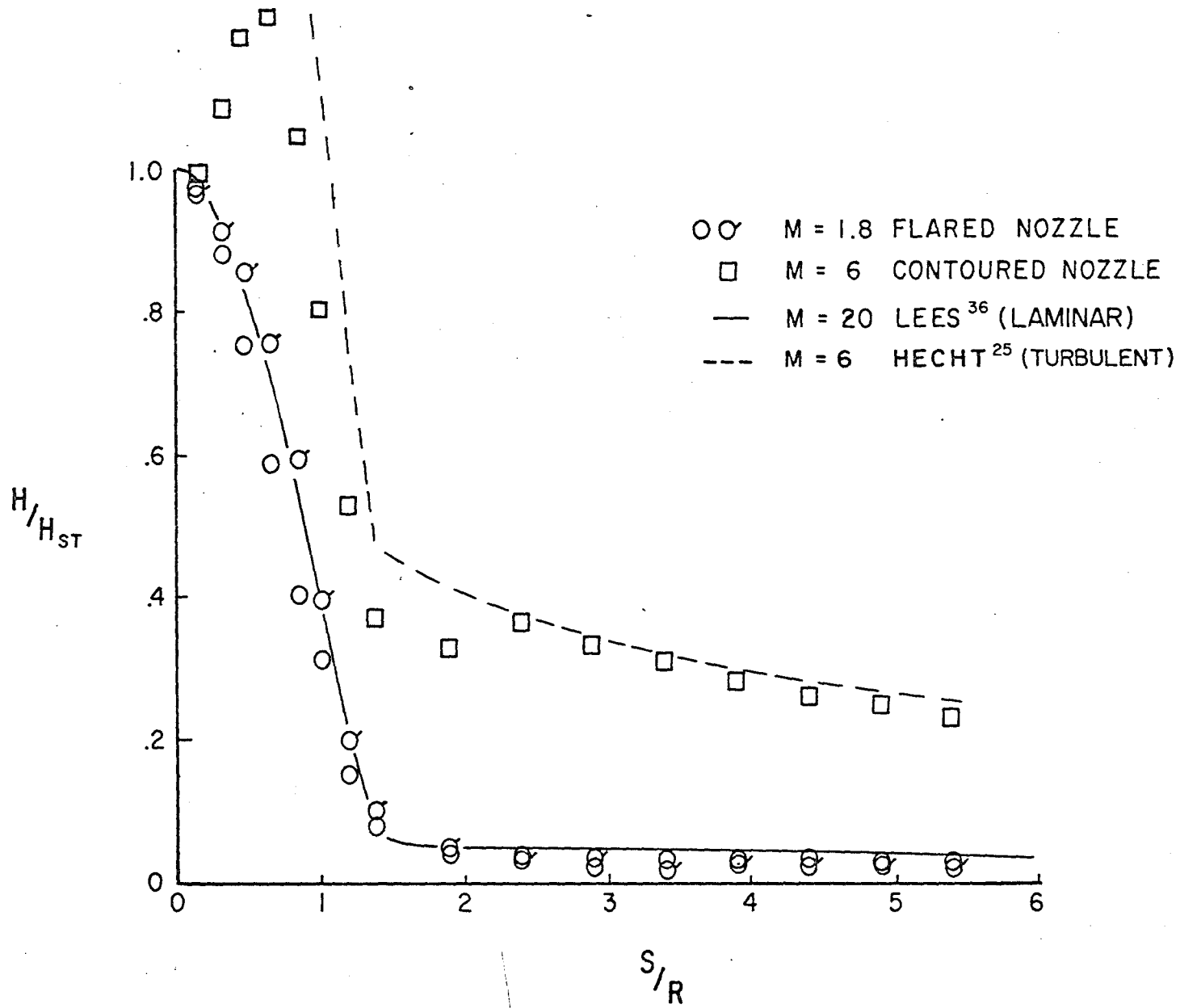


Figure 39b. Heat Transfer Coefficient Distribution, $P_{T_2} = 50$ psia,
 $T_0 = 1100^\circ R$

SIDE PROFILE VIEWS OF ABLATED CAMPHOR MODELS
(10 second intervals)

$P_{T_2} = 22$ PSIA
 $T_0 = 1100$ °R

$P_{T_2} = 33$ PSIA
 $T_0 = 1100$ °R

$P_{T_2} = 44$ PSIA
 $T_0 = 1100$ °R

71

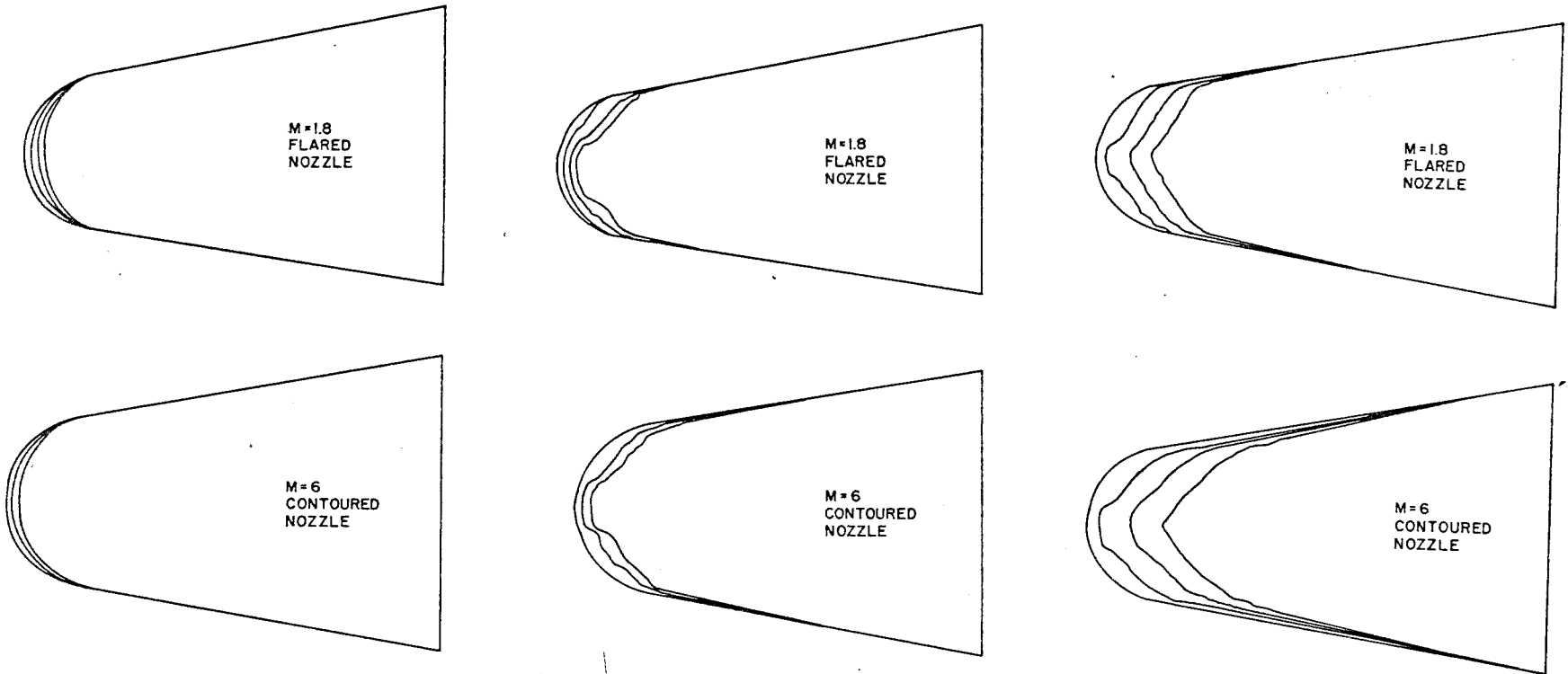
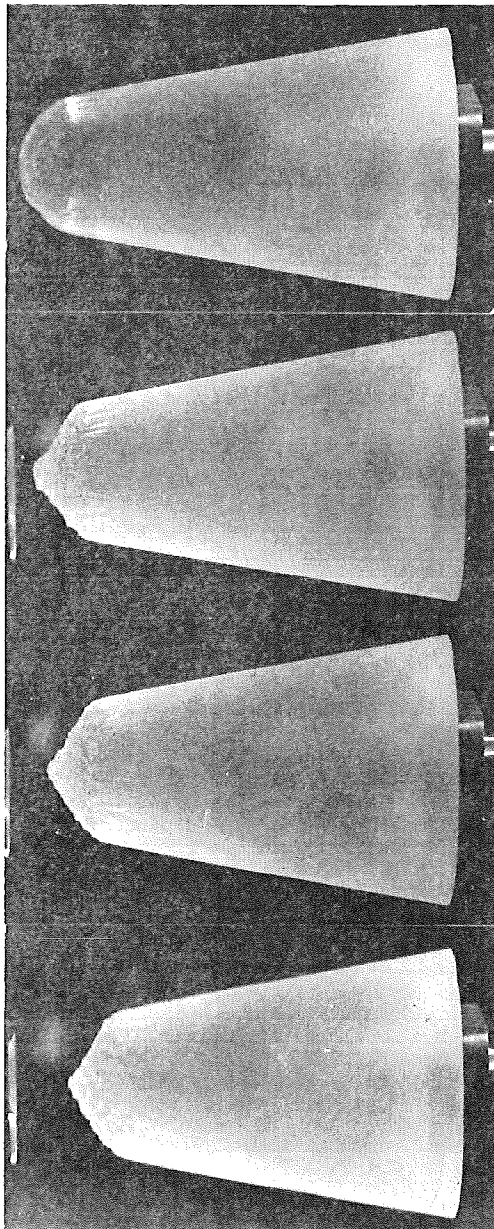


Figure 40. Side Profile Views of Ablated Camphor Models

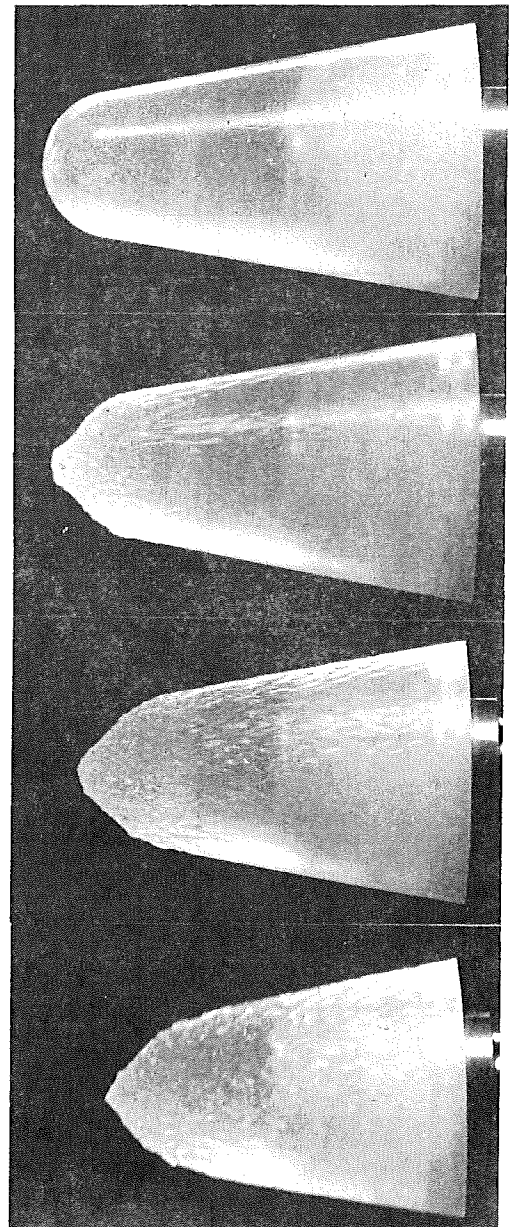
CAMPHOR ABLATION

$P_{T_2} = 44$ PSIA, $T_0 = 1100$ °R

**M = 1.8
FLARED NOZZLE**



**M=6
NOZZLE**



**TIME
(sec)**

0

10

20

30

Figure 41. Photographs of Camphor Ablation

REFERENCES

1. L. M. Mack, "Transition and Laminar Instability", JPL publication 77-15, May 1977 (NASA-CP-153203).
2. D. C. Wilcox and R. M. Traci, "A Complete Model of Turbulence", AIAA paper No. 75-351, San Diego, California, 1976.
3. S. R. Pate, "Dominance of Radiated Aerodynamic Noise on Boundary Layer Transition in Supersonic-Hypersonic Wind Tunnels, Theory and Application", AEDC-TR-77-107, March 1978.
4. M. V. Morkovin, "Instability, Transition to Turbulence and Predictability", AGARDograph No. 236 (May 1977).
5. K. F. Stetson, "Boundary Layer Transition on Blunt Bodies with Highly Cooled Boundary Layers", IAS Report No. 59-36 (Jan 1959).
6. K. F. Stetson, "Effect of Bluntness and Angle of Attack on Boundary Layer Transition on Cones and Biconic Configurations", AIAA preprint 79-0269 (Jan 1979).
7. K. F. Stetson and G. H. Rushton, "Shock Tunnel Investigation of Boundary Layer Transition at $M = 5.5$ ", AIAA Journal, Vol. 5, pp. 899-906 (May 1967).
8. A. W. Fiore and C. H. Law, "Aerodynamic Calibration of the Aerospace Research Laboratories $M = 6$ High Reynolds Number Facility", ARL-TR-75-0028 Feb. 1975.
9. Test Facilities Handbook (Tenth Edition), Von Karman Gas Dynamics Facility, Vol. 3, Arnold Engineering Development Center, May 1974.
10. J. F. Muir and A. A. Trujillo, "Effects of Nose Bluntness and Free Stream Unit Reynolds Number on Slender Cone Transition at Hypersonic Speeds", Proceeding of the Boundary Layer Transition Workshop, Vol. III, 20 Dec 1971, Aerospace Report No. TOR-0172 (S2816)-5.
11. P. Krogmann, "An Experimental Study of Boundary Layer Transition on a Slender Cone at Mach 5", AGARD Symposium on Laminar-Turbulent Transition, Technical University of Denmark, Copenhagen, Denmark, 2-4 May 1977.
12. V. DiCristina, "Three-Dimensional Laminar Boundary Layer Transition on a Sharp 8° Cone at Mach 10", AIAA Journal, Vol. 8, pp. 852-856, (May 1970).
13. F. K. Moore, "Laminar Boundary Layer on a Circular Cone in Supersonic Flow at Small Angle of Attack", NACA TN 2521 (Oct 1951).

REFERENCES (CONTINUED)

14. J. B. Anders, P. C. Stainback, and I. E. Beckwith, "A New Technique for Reducing Test Section Noise in Supersonic Wind Tunnels", AIAA Preprint No. 78-817 (April 1978).
15. P. F. Brinich, "Effect of Leading-Edge Geometry on Boundary Layer Transition at Mach 3.1", NACA TN 3659 (March 1956).
16. W. E. Moeckel, "Some Effects of Bluntness on Boundary Layer Transition and Heat Transfer at Supersonic Speeds", NACA Report 1312 (1957).
17. E. J. Softley, "Boundary Layer Transition on Hypersonic Blunt, Slender Cones", AIAA Paper No. 69-705 (June 1969).
18. K. F. Stetson, "Boundary Layer Transition on Blunt Bodies with Highly Cooled Boundary Layers", J.A.S. Vol. 27, pp. 81-91 (Feb 1960).
19. A. D. Anderson, "Interim Report, Passive Nosedip Technology (PANT) Program, Vol. X, Appendix, Boundary Layer Transition on Nosedips with Rough Surfaces, SAMSO-TR-74-86 (Jan 1975).
20. A. Demetriades, "Nosedip Transition Experimentation Program, Final Report, Vol II", SAMSO-TR-76-120 (July 1977).
21. A. M. Berkowitz, C. L. Kyriss, and A. Martellucci, "Boundary Layer Transition Flight Test Observations", AIAA Paper No. 77-125 (Jan. 1977).
22. R. L. Wright and E. V. Zoby, "Flight Boundary Layer Transition Measurements on a Slender Cone at Mach 20", AIAA Paper No. 77-719 (June 1977).
23. D. V. Maddalon and A. Henderson, Jr., "Boundary Layer Transition at Hypersonic Mach Numbers", AIAA Paper No. 67-130 (Jan 1967).
24. N. R. Rotta, "Effects of Nose Bluntness on the Boundary Layer Characteristics of Conical Bodies at Hypersonic Speeds", NYU-AA-66-66 (Nov 1966).
25. A. M. Hecht and D. E. Nestler, "A Three-Dimensional Boundary Layer Computer Program for Sphere-Cone Type Reentry Vehicles, Vol. 1, Engineering Analysis and Code Description", AFFDL-TR-78-67 (June 1978).
26. R. H. Rogers, "Boundary Layer Development in Supersonic Shear Flow", Boundary Layer Research Meeting of the AGARD Fluid Dynamics Panel, London, England, AGARD Report No. 269 (April 25-29, 1960).

REFERENCES (CONCLUDED)

27. J. C. Adams, Jr., W. R. Martindale, A. W. Mayne, Jr., and E. O. Marchand, "Real Gas Scale Effects on Shuttle Orbiter Laminar Boundary Layer Parameters", *Journal of Spacecraft and Rockets*, Vol. 14, pp. 273-279 (May 1977).
28. C. L. Merkle, "Stability and Transition in Boundary Layers on Reentry Vehicle Nosedips", AFOSR-TR-76-1107 (June 1976).
29. A. Martellucci, private communication.
30. J. M. Kendall, unpublished paper (1971).
31. J. L. Potter, "The Unit Reynolds Number Effect on Boundary Layer Transition", Dissertation submitted to Vanderbilt University (May 1974).
32. Edmund, G. Brown-Edwards, "Calibration Data for the 10138F Flared Nozzle of the RENT Test Leg", AFFDL TM-75-145-FXE (August 1975).
33. G. M. Gregorek and J. D. Lee, "Design Performance and Operational Characteristics of the ARL Twenty-Inch Hypersonic Wind Tunnel", ARL 62-392 (August 1962).
34. G. M. Gregorek, "Initial Calibrations and Performance of the ARL Twenty-Inch Hypersonic Wind Tunnel", ARL 62-393 (August 1962).
35. A. M. Morrison, J. M. Solomon, M. Ciment, and R. E. Ferguson, "Handbook of Inviscid Sphere-Cone Flow Fields and Pressure Distributions, Vol. I", NSWC/WOL/TR 75-45, 1 December 1975.
36. L. Lees, "Laminar Heat Transfer Over Blunt-Nosed Bodies at Hypersonic Flight Speeds", *Jet Propulsion*, Volume 26, No. 4, (April 1956) pp. 259-269.
37. A. L. Laganelli and A. Martellucci, "The Effect of Mass Addition Around a Blunt Nose on Flow Properties and Vehicle Performance", GE TIS 75SD250, (November 1972).